Delft University of Technology

Faculty of Aerospace Engineering

Master of Science Thesis – May 28th 2015

Temperature effects on an acoustic emission based structural health monitoring system – Applied to composite materials –

Alexandru Vărgălui


TECHNISCHE UNIVERSITEIT DELFT
MDCCCXLII

Temperature effects on an acoustic emission based structural health monitoring system
– Applied to composite materials –

Master of Science Thesis

For obtaining the degree of Master of Science in Aerospace Engineering
at Delft University of Technology

Alexandru Vargalui

May 28th 2015

Faculty of Aerospace Engineering – Delft University of Technology

Delft University of Technology

Faculty of Aerospace Engineering

Department of Aerospace Structures and Materials

Structural Integrity & Composites Chair

Graduation committee

Dated: 28-05-2015

Chair holder:

Prof.dr.ir. R. Benedictus

Committee members:

Dr. M.J. Martinez

Dr.ir. D. Zarouchas

Dr. C. Kassapoglou

“Real revolution starts at learning”

T. McIlrath - Musician

Abstract / Summary

Acoustic Emission (AE) based structural health monitoring systems have the potential to assess the state of metallic / composite structures and detect damage in real time as it grows. This is done by monitoring the Lamb waves that occur due to the release of energy and the specific boundary conditions. Environmental and Operational Conditions (EOC) have a significant effect on the wave propagation phenomena, potentially influencing their ability to detect and localize damage.

This study sought to extend past research done on metallic structures and was focused on understanding the effects of temperature on the propagation of ultrasonic Lamb waves in composite materials using analytical, numerical and experimental tools. Two test specimens were used, one hybrid laminate with glass and carbon fibre epoxy layers and a sandwich panel with a 2 mm foam. Three temperatures steps of -40, 25 and 70°C were used.

An analytical MATLAB code was used to generate dispersion curves for the hybrid material at the previously mentioned temperature steps. Next, the experimental setups were modelled in an FEM ABAQUS CAE environment. Three 5 cycle Hanning windows, with frequencies of 150, 300 and 400 kHz, were used to excite a piezoelectric actuator. The response was then picked up using 3 piezoelectric sensors located at angles of 0, 45 and 90° with respect to the actuator. Finally, the experimental tests were performed and the results were compared with those of the FEM model and the dispersion curves. The comparison was performed using the signals received by the 3 sensors. Preliminary experimental results showed that the maximum change in speed due to temperature variation was 7% for the laminate and 12% for the sandwich panel. The results have also been verified using the FE models.

Acknowledgements

I would like to take some time to thank all of the people which helped me on my journey towards the completion of this thesis. Their support was always appreciated and it certainly helped me improve the quality of my work.

First of all, I would like to thank my supervisor, Dr. Marcias Martinez, who was always there to advise me and support me whenever I needed some guidance. I would also like to thank my second supervisor, Dr.ir. Dimitrios Zarouchas, for sharing his experience within the field of Acoustic Emission systems with me and for always being there to answer my questions.

Many aspects of this thesis would certainly have taken longer to complete without the help of the people here at the Aerospace Faculty. I would like to thank the Aerospace Structures and Materials Laboratory staff for their assistance with the experimental side of my work. Furthermore, I would like to thank Patricia Martinez Bueno and Maurice Boon for taking time from their own work and helping me learn about vacuum infusion and the AE system used in this thesis.

I would also like to thank my friends both for taking part in discussions related to my thesis and for taking my mind off of it once in a while. Last but not least, I would like to thank my parents for their unconditional support through-out my life and for giving me the opportunity to pursue the education that lead to this work.

Abbreviations

AE – Acoustic Emission

BC – Boundary Condition

CBM – Condition Based Maintenance

CF – Carbon Fibre

CFRP – Carbon Fibre Reinforced Plastic

CM – Condition Monitoring

DP – Damage Prognosis

EOC – Environmental and Operational Conditions

FEM – Finite Element Method

GF – Glass Fibre

GM – Global Matrix

GWSHM – Guided Wave Structural Health Monitoring

NDE – Non-Destructive Evaluation

SHM – Structural Health Monitoring

SPC – Statistical Process Control

TOA – Time of Arrival

TOF – Time of Flight

TDOA – Time Difference of Arrival

TM – Transfer matrix

UD – Unidirectional

Vpp – Peak-to-peak Voltage

Frequently used symbols

A_0 – Fundamental anti-symmetric Lamb wave mode

S_0 – Fundamental symmetric Lamb wave mode

c_p – Phase velocity

c_g – Group velocity

λ – Wavelength

ω – Angular frequency

k – Wavenumber

T^* – Temperature degradation factor

T_g – Glass transition temperature

d_{ij} – Piezoelectric coupling matrix

ε^T – Free electric permittivity tensor

E_1 – Longitudinal modulus

E_2 – Transverse modulus

ν_{12} – Poisson's ratio

G_{12} – In-plane shear modulus

γ_{12} – Shear strain

Table of Contents

List of figures

List of tables

1 Introduction

Aircraft structures are subjected to high loads, fatigue cycles and they operate in a range of -60 to 80° C. In addition, because of the influence of weight on fuel economy, lightweight structures are needed in order to keep flying at a reasonable cost. In order to accommodate these operating conditions while also maintaining the structural integrity of the aircraft, several design philosophies have been employed: safe-life, fail-safe and damage tolerant. Modern aircraft are designed according to all three approaches [1]. With the damage tolerant method, structures are designed to withstand damage up to a certain size while undergoing regular inspections. Determination of the inspection interval is done by first determining the number of load cycles that it takes for the crack to grow to a detectable level and also the number of cycles in which the crack grows to a critical level. The number of cycles needed for the crack to grow from a detectable level to the critical level is ΔN. The inspection interval is then set to $\Delta N/2$ [2] in order to allow for more than 1 chance of discovering the crack. This process is outlined in Figure 1-1. This approach gives enough chances to find the damage and repair it. Most of the structural components on an aircraft have to go through this process leading to high maintenance costs and significant downtime of the plane. This process is mostly applicable to commercial aircraft and it is based on the regulations imposed by organisations such as the Federal Aviation Administration (FAA) [3] and the European Aviation Safety Agency (EASA) [4].

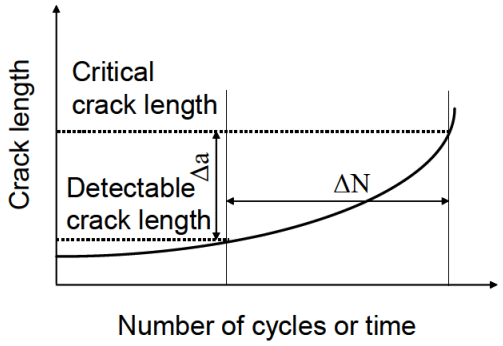

Figure 1-1: Determination of crack propagation life in damage tolerant design [2]

Another aspect to take into consideration is the increasing use of composite materials in the new generation of commercial aircraft. Boeing was the first to build a composite fuselage and wing (Boeing 787), about 50% of the structure, and Airbus was not far behind with the A-350, with its all-composite fuselage and wings [5]. Although these materials do provide improved performances, they also introduce some new problems like their susceptibility to impact damage [6], more failure modes [5] and different maintenance procedures.

Most of the current structural maintenance is done in a time-based mode as the one described earlier. There is a growing need to move to the more cost-effective Condition Based Maintenance (CBM). This concept requires a sensing system that monitors the structure and reports to the operator if any damage occurs [7]. Any maintenance is performed only when needed.

Acoustic emission (AE) based systems have been shown to have the potential to inspect impact damage [8] and study the fracture behaviour of composite materials [9]. One difficulty this system has is that the waves used to inspect the structure are sensitive to Environmental and Operational Conditions (EOC), which vary considerably during the life of an aircraft structure. The influence of these factors must be determined if Structural Health Monitoring (SHM) systems are to be installed on an aircraft. Temperature and load were found to be the factors with the greatest impact on the propagation of waves [10] [11].

1.1 Research problem

AE based systems are among the most promising SHM tools. Gagar *et al.* [12] have shown that AE signals can be recorded in complex structures such as a wing-box and that this technique can be used to localize damage occurring during the life of the structure. However, the system is not yet ready for commercial application in the aerospace industry, as there are still some challenges left to overcome [7].

One of the main issues that require further investigation is the effect of Environmental and Operational Conditions (EOCs) on the propagation of guided Lamb waves. The propagation of these waves depends on the material they are propagating through. Thus, any change in the properties of the medium will affect the features of the waves. It is well known that external factors such as temperature and loading can alter the mechanical properties of materials. Therefore, it is important that the effect of these EOCs is taken into account in SHM systems based on Lamb waves.

Most research in this area has been focused on active SHM systems that use guided Lamb waves and has mostly looked at metallic structures. Composite structures have received less attention due to their anisotropic nature and inherently more complicated wave propagation mechanisms. However, due to the increasing use of composite materials in the aerospace industry and the benefits that a reliable SHM system would provide, the effects of EOC in anisotropic media must be thoroughly understood.

1.2 Research objective and research questions

Considering the facts presented in the introduction and the current state of research on the topic of temperature effects on the propagation of guided Lamb waves in anisotropic materials, the objective of the research project can be formulated as:

> *To understand how temperature affects the propagation of guided Lamb waves in anisotropic materials by modelling the behaviour both analytically and with Finite Element Modelling (FEM) simulations while performing experimental verifications.*

Based on the previous objective, the main research question can be formulated as follows:

> *How and to what extent does temperature affect the propagation of AE signals in anisotropic materials?*

In order to answer the main research question, several sub questions must first be posed:

1. Can we develop a thorough understanding of the physics governing the propagation of Lamb waves in anisotropic materials influenced by the effects of temperature?

2. How do analytical results and FEM simulations of guided Lamb waves propagating in anisotropic materials compare with the experimentally obtained results?

3. How do these effects influence the results given by an AE based SHM system?

1.3 Research approach

In order to answer the main research question, a methodology consisting of analytical modelling, FEM modelling and an extended experimental campaign was chosen. The overview of the tasks that were performed is shown in Figure 1-2.

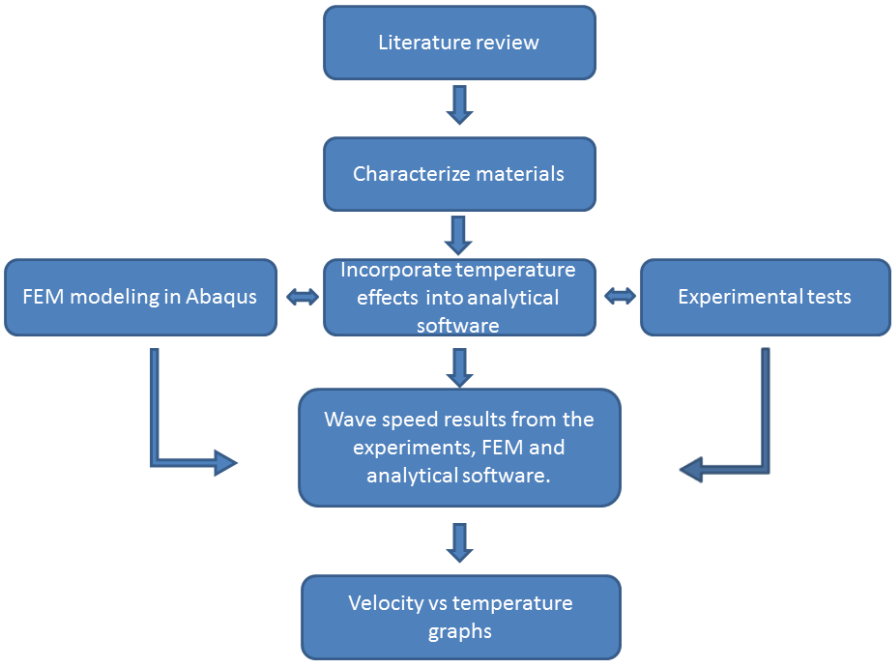

Figure 1-2: Work plan

The first step was to perform a literature review on the current state of research in the field of temperature effects on the propagation of AE signals in anisotropic materials. In the second step, the approach developed by Pant *et al.* [13] was used to characterize a composite material with the following layup: [±45° glass fibre, 0° carbon fibre, ±45° glass fibre]. During this step, some tensile tests were performed on the materials in order to obtain the elastic properties required for modelling. This was done according to the ASTM D 3039 – 08 and D 3518 – 94 standards. In the third step, temperature effects were incorporated into the model developed by Pant based on methods found in the literature. Also, FEM models were built in the ABAQUS CAE [14] environment taking into account the same conditions as for the experimental tests. In the fourth step the model and the analytical work were verified through experiments. The experiments were performed on two plates: one laminate with the previously mentioned layup and one sandwich panel with a foam core and face sheets with the same hybrid layup. The composite plates with the bonded sensors were exposed to temperatures ranging from -40° C to 70°C in 3 steps. At each temperature one of the piezoelectric sensors was used to actuate a signal and the response registered by the other sensors was recorded and analysed. The results of the experiments and the modelling were then compared.

2 Literature study

2.1 Structural health monitoring

This chapter focuses on SHM in general. Section 2.1.1 presents a short background, Section 2.1.2 gives an overview of the most important monitoring techniques and Section 2.1.3 presents the concept of guided waves. Section 2.1.4 highlights the AE technique, Section 2.1.5 gives a short presentation to the localization procedure and Section 2.1.6 gives an introduction to piezoelectric materials.

2.1.1 Background

Looking back at the early days of commercial aviation, the need for determining the true operational conditions of an aircraft structures was realized after a series of crashes of the de Havilland Comet aircraft between 1952 and 1954 [15]. Over time, airworthiness authorities set new regulations that subjected aircraft to more intensive inspection [2], especially ageing aircraft which were entering the second half of their operational life. Even with the more stringent maintenance conditions, there were still cases were unique repair solutions applied to certain aircraft led to major accidents such as the Japan Airlines B-747 in 1985 or China Airlines B-747 in 2001.

Currently, each aircraft has its own maintenance programme, usually comprising so called A, B, C and D checks. The first two are performed more often and require between a night and a few days while the last two are more intensive. The D check is the most comprehensive, requiring around 2 months to complete. It is done every 5 years and it consists on taking the entire aircraft apart. All of these checks cost money but they also create a lot of downtime that in turn ends up creating a financial burden on the operator. Due to these issues there is a need for a CBM approach for which SHM is a corner stone of this programme.

SAE International created a guideline on how to implement SHM technologies in which SHM is defined as "the process of acquiring and analysing data from on-board sensors to evaluate the health of a structure" [16].

Adams [17] describes health monitoring as "the scientific process of non-destructively identifying four characteristics related to the fitness of an engineered component (or system) as it operates:

- the operational and environmental loads that act on the component (or system)
- the mechanical damage that is caused by that loading
- the growth of damage as the component (or system) operates
- the future performance of the component (or system) as damage accumulates."

Boller and Meyendorf [2] define SHM as "the integration of sensing and possibly also actuation devices to allow the loading and damaging conditions of a structure to be recorded, analysed, localized and predicted in a way that non-destructive testing becomes an integral part of the structure".

The two major aspects of SHM that are mentioned in the previous definitions are: load monitoring and damage monitoring. In addition, the health monitoring techniques should be non-destructive, ideally implemented in an automated manner [17] and should function while the structure is under operating conditions.

Despite the fact that a lot of research and development has been done in the SHM field, no application has matured to the point where it can be called a true commercial product [18]. According to Farrar and Worden [7], significant developments in this area will most likely require multi-disciplinary research efforts between different fields. The authors also believe that the problem of SHM will not be solved in the near future and that it will require small steps over a long period of time.

SHM is closely related to four other disciplines that are used for damage identification: condition monitoring (CM), non-destructive evaluation (NDE), statistical process control (SPC), and damage prognosis (DP).

CM is very similar to SHM and it mainly addresses damage identification in rotating machinery, such as pumps, electric motors, internal combustion engines by monitoring certain parameters during the operation of the machinery (vibration, temperature etc.) [19].

According to the American Society of Nondestructive Testing (ASNT) "NDE is the examination of an object with technology that does not affect the object's future usefulness." This examination is usually performed when the object under investigation is not operational and the main goal is to characterize damage that has been previously located. NDE is a well-established field that is widely used in many engineering branches such as: aerospace, civil, mechanical, electrical etc. Common NDE techniques include: ultrasonic, liquid penetrant, magnetic-particle, eddy-current, acoustic emission, thermography [20].

SPC is a process based approach that uses sensors to monitor changes in a process, changes that can also result from structural damage [7]. SPC generally refers to the application of statistical tools to processes in order to improve the quality of products and services [21], although it has also been used for damage detection purposes [22].

DP refers to the process of predicting the remaining operational life of a system by evaluating the current damage state, estimating the future loading conditions and by running simulations [23].

2.1.2 Structural health monitoring techniques

SHM techniques can generally be divided into two categories [1]: active and passive approaches. In the active approach, an external input is applied to the structure and the response is monitored, while the passive method "listens" for any perturbations caused by occurring damage. An overview of the most used techniques is presented in this section.

Vibration and modal analysis is a passive SHM approach that identifies damage by measuring modifications of physical parameters such as mass, stiffness or damping. The work done by Cawley and Adams [24] was the first to use natural frequencies for damage detection in structures. Other studies, such as the ones done by Robinson *et al.* [25] and Manson *et al.* [26] [27] [28] had some success in detecting damage on aircraft structures using vibration-based data. The main disadvantage of this method is that any defects that are parallel to the loading direction are reliably detectable only at very large sizes, at least 10% of the inspected area according to [29] and [30].

Another passive SHM method relates the energy of impact events with damage severity. Piezoelectric sensors are used to detect the features of the vibrations induced by these impact events, which are then used to determine the energy and subsequently the damage. Although NDT is still required to confirm the results, the inspection time is reduced significantly [31].

Comparative vacuum monitoring is a passive technique developed by Structural Monitoring Systems in Perth/Australia [2]. A two chamber-system of thin channels is introduced into a silicon-based sensor that is placed on a crack prone location. A vacuum is created in one of the chambers. If a crack appears beneath the evacuated chamber, pressure will increase, thus signalling the presence of the crack. This method has shown promising results in tests done in laboratories as well as in operational environments [32] [33]. The main drawback of this method is that the structure requires some mechanical treatment when placing the sensors [34] and there are possible issues with corrosion of the material blocking the sensors [35].

Another SHM method is based on guided Lamb waves. These waves have the ability to travel relatively large distances, thus making them useful for a fast evaluation of a structure's health [36]. Transducers are used to pick up the response of the structure to the initial excitation and based on this response faults or damage can be detected. The main issue with this method is the highly dispersive nature of the waves and the complicated physics behind them [6]. SHM based on Lamb waves can be either active or passive. In the active approach, a transducer is used to provide the initial excitation. The passive approach uses the sensors to monitor the structure and to detect any guided waves that occur due to fracture phenomena in the material.

2.1.3 Guided waves

Guided waves are structural waves that propagate through bounded media. There are various types of guided waves as described in [37]. Guided waves that result from stress/strain boundary conditions and propagate on the surface of a material are known as surface waves.

A large number of the structural elements used in the aerospace industry are 2D plate-like structures. The waves that propagate through this kind of structures are known as Lamb waves. Lamb waves are guided waves that are bounded by two surfaces and they are formed by the superposition of reflections of longitudinal P waves and shear waves from the two surfaces [38]. By looking at the distribution of displacements, two types of Lamb waves can be recognized: the symmetric modes S_0, S_1, S_2, … S_n and the antisymmetric modes A_0, A_1, A_2, … A_n . The symmetric modes mostly consist of in plane displacements while the antisymmetric modes consist of out-of-plane displacements. Although theoretically there are an infinite number of modes, in most of the surveyed literature, only the S_0 and A_0 modes are used, as can be seen in the work done by Bottai *et al.* [39], Giurgiutiu [40] and other papers presented in this study. This is mainly due to the fact that higher modes are more difficult to activate and interpret in practice [41]. These modes play an important role in the damage identification process. The A_0 mode enables detection of delaminations, transverse cracks and layer separation in composite materials especially near the surface [42] [43], while the S_0 mode enables the detection of cracks at greater depths [44]. The illustration of these two modes can be seen in Figure 2-1 and Figure 2-2.

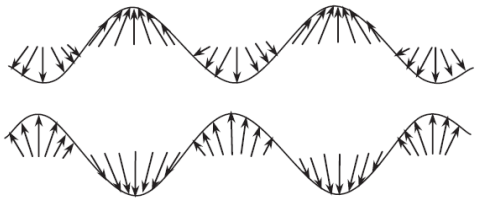

Figure 2-1: Illustration of symmetric Lamb wave mode [44]

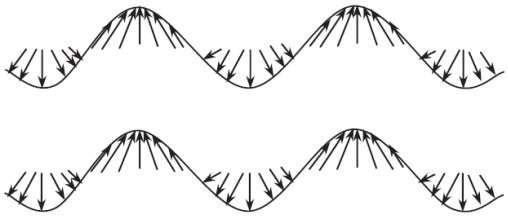

Figure 2-2: Illustration of anti-symmetric lamb wave mode [44]

When it comes to damage detection, Lamb waves have a few advantages compared to other elastic waves [45]:

- they have a relatively low attenuation
- specific modes can be chosen
- the presence of flaws modifies the propagation of the waves enabling control of a whole surface with just a few sensors

An important phenomenon that affects the detection of damage using elastic waves in general, even more so when using Lamb waves, is dispersion [38]. The main characteristic of elastic wave dispersion is the dependence between the wave velocity and the excitation frequency. In consequence a wave packet propagating over a large distance tends to increase in length and change its shape, resulting in errors. In active approaches applying a narrow band, also known as a Hanning window, can be used to minimize this problem.

Waves are generally characterized by the following different properties. The wavenumber k refers to the spatial frequency of the perturbation. The wavelength λ is a measure of the spatial period of the perturbations and these are related mathematically as shown in Eq. 2.1 [38]:

$$\lambda = \frac{2\pi}{k} \tag{2.1}$$

Waves travelling at different speeds can form a group wave. This happens in materials where the wave speed is dependent on the frequency, the amplitude or the propagation direction. This phenomenon can be seen in anisotropic materials where waves travel at different speeds in different directions. The result is a strong wave, which propagates with a speed known as the group velocity, c_g.

$$c_g = \frac{d\omega}{dk} \tag{2.2}$$

The phase velocity, c_p, is the speed of the individual frequency components and is calculated with:

$$c_p = \frac{\omega}{k} \tag{2.3}$$

where $\boldsymbol{\omega}$ is the angular frequency.

The group and phase velocities are often used to characterize the dispersive behaviour of Lamb waves in different materials. The velocities are plotted as functions of the product between the frequency of the signal and the thickness of the material as can be seen in Figure 2-3.

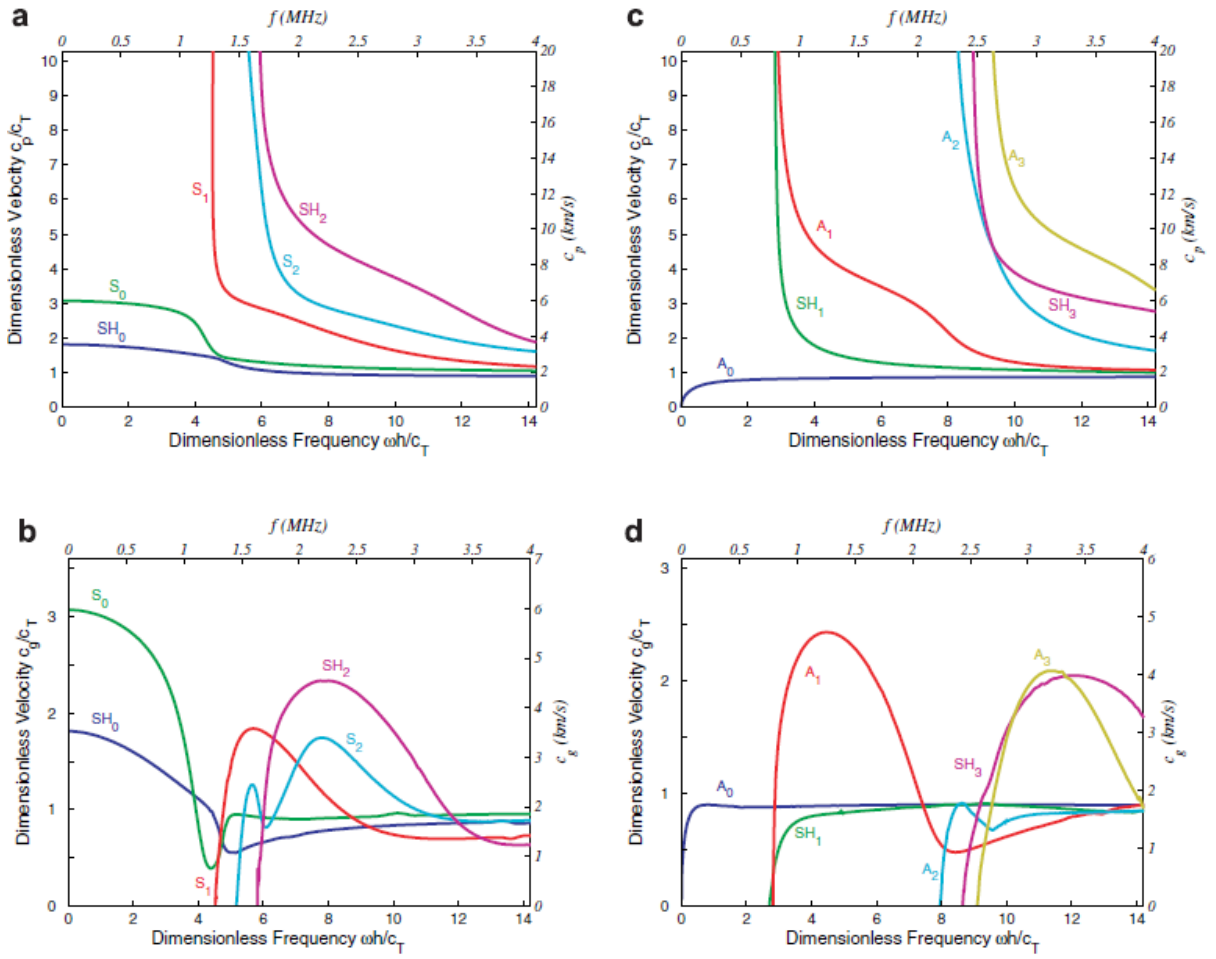

Figure 2-3: Examples of dispersion curves: a)phase velocity of symmetric modes, b)group velocity of symmetric modes, c)phase velocity of anti-symmetric modes , d)group velocity of anti-symmetric modes [46]

2.1.4 Structural health monitoring based on acoustic emission

An acoustic emission is described as a series of transient stress waves emitted by material defects under the effects of an external load. The waves are a result of the elastic energy released due to local stress redistribution [47]. Their typical frequency range is between 10 kHz and 1 MHz.

Acoustic emission monitoring is a passive technique because it identifies damage or defects that occur while the structure is subjected to operational loads. It is often used to detect failure at a very early stage, long before the structure would fail. Common sources of acoustic emissions are: crack initiation, crack growth, slip and dislocation movements or phase transformations in metals and matrix cracking, fibre breakage and de-bonding in composites [48].

An important advantage of this method is that the structure can be observed during the entire load history with just a few sensors and without disrupting the loading of the structure. The sensors are calibrated to detect strong signals that are above a certain threshold [49]. If this trigger level is reached, the signal is recorded and presented to the operator for further evaluation. The sensors are attached to the surface and do not require re-locating.

A disadvantage of acoustic emission testing is the fact that tests are not reproducible. Also, the signals that need to be detected are very small. Thus, more sensitive sensors are required in addition to amplifiers. This means that ambient noise, attenuation of signals and low signal-to-noise ratio can become an issue. This is a common problem of both active and passive Lamb wave systems.

The amplitude of the emission is directly related to the magnitude and the velocity of the event that produced it. This means that larger signals are produced by cracks that propagate instantaneously than by cracks which slowly propagate over the same distance [48]. The detection and conversion of the elastic waves to electrical signals form the basis of acoustic emission testing. The interpretation of these signals gives information regarding the location as well as the severity of the damage.

A typical AE system includes: a sensor, preamplifier, filter and storage equipment (such as a personal computer). An illustration of this setup is shown in Figure 2-4.

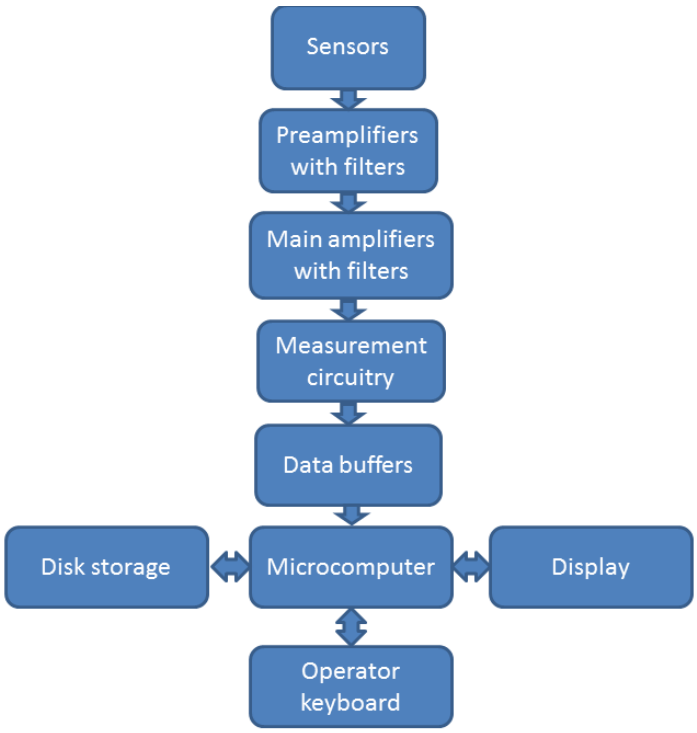

Figure 2-4: Typical AE system setup [50]

The sensors respond to the dynamic motion caused by the event and convert the mechanical movement into an electrical signal. These sensors are most often made from piezoelectric materials due to their intrinsic property of converting mechanical loads to electric signals and vice-versa. The preamplifier then boosts the signal strength. Next, the signal goes through a bandpass filter in order to eliminate the low and high frequencies associated with the signals. Once this is done, the signal is sent to the acoustic system mainframe and eventually to a computer for analysis and storage. The most common AE system is the so called "hit driven" system. During periods of inactivity it lies in a dormant state and when a signal is detected, the hit is recorded and the data is stored.

A very large number of articles on the subject of AE SHM can be found in literature. The articles in this literature review were mentioned because their results highlight the potential of AE to become a reliable SHM method.

SHM systems based on acoustic emissions have received a lot of attention in the past decades. Leone *et al.* [51] investigated acoustic emission as a method for detecting damage initiation and progression, identifying the location of the damage and anticipating ultimate fracture in notched honeycomb sandwich panels. Post-test signal processing was used and the results were compared with other inspection techniques. The results showed excellent correlation between the emission of acoustic waves and the corresponding failure initiation at the crack tips. Furthermore, the location of any occurring damage was clearly identified even though a constant wave speed was assumed and wave dispersion was ignored. This result was attributed to the near quasi-isotropic nature of the face sheets and the relatively large size of the structure. The authors conclude that the AE method can provide reliable and real time information on the state of a structure when all of the variable settings are properly selected.

Kundu *et al.* [52] demonstrated the possibility of locating the point of impact in a composite plate using acoustic emission data. The experiments consisted of dropping steel and ping-pong balls on a graphite-epoxy plate and recording acoustic signals using transducers that were adhesively bonded to the plate. This was done by using the time of arrival of the ultrasonic signals and by taking into account the directionality of the wave speed in anisotropic materials. The authors also showed that significant errors were introduced if the wave speed was assumed to be constant.

Aggelis *et al.* [53] looked at the efficiency of acoustic emission and ultrasonic transmission as a structural health monitoring tool. Cross-ply laminates were fabricated and tested under load controlled tension. Two AE sensors were attached on the same side of the specimen in order to monitor the structure. The results showed that the increase in load led to an increase in the number of hits registered by the sensors. The authors reasoned that the strong correlation between the applied load and the number of hits could be used as an indicator of the load that

had been applied to the material. The results also showed that the specific parameters that were measured could be used to understand the damage mechanisms. The acoustic energy emitted by delaminations was lower than that related to matrix cracking events in the tested material [54].

Fu *et al.* [55] investigated a fibre optic acoustic emission sensor and its application in structural health monitoring. The tests consisted of specimens made out of CFRP materials and had sensors both attached to the surface and embedded inside the composite material. Pencil lead break tests and three point-bending tests were used in order to produce AE events. The results showed that both the sensors were capable of detecting elastic waves released by the occurring damage and their specific energy. The authors conclude that the fibre optic acoustic emission sensor has potential advantages for SHM of composite structures.

Baldwin and Vizzini [56] developed an acoustic emission crack detection sensor system based on Fibre-Bragg grating for the structural health monitoring of composite structures. The sensors were tested in both a surface attached configuration and an embedded configuration using pencil lead break tests and tensile loading tests. The results showed that the system was able to detect the AE events in both configurations. The authors conclude by mentioning that great care was taken to isolate the sensors from strain and temperature variations, thus making the system impractical for real world applications until the challenge of environmental conditions could be overcome.

The general consensus in the analysed literature is that AE based SHM systems can be a useful tool in assessing the damage state of a structure and further research should be carried out in order to bring the method closer to consistent real world application.

2.1.4.1 Signal features

Because the electrical signal is generated by the fracture mechanism, it is useful to look at the signal parameters in order to learn more about the characteristics of the physical phenomena. The following parameters are the most widely used and their definitions are extracted from ISO 12716 2001:

1. Hit: a signal that exceeds the threshold and causes the system channel to accumulate data related to the actual wave and its features. It is frequently used to show the AE activity with counted number for a period (rate) or accumulated numbers. In Figure 2-5, one waveform corresponds to one hit.
2. Count / ring-down count / emission count: the number of times within the time window, where one signal exceeds a previously set threshold. In Figure 2-5 seven counts are observed. It should be noted that the numbers of counts depend strongly on the set threshold level, the operating frequency and the sampling rate

3. Amplitude: a peak voltage of the signal waveform is usually assigned. Amplitudes are expressed in a decibel scale instead of linear scale where 1 µV at the sensor is defined as 0 dB AE.
4. Duration: a time interval between the triggered time of one AE signal and the time of disappearance below the trigger level.
5. Rise time: a time interval between the triggering time of the signal and the time of the peak amplitude.
6. Energy: definitions of energy are different in AE system suppliers, but it is generally defined as the measured area under the rectified signal envelope.

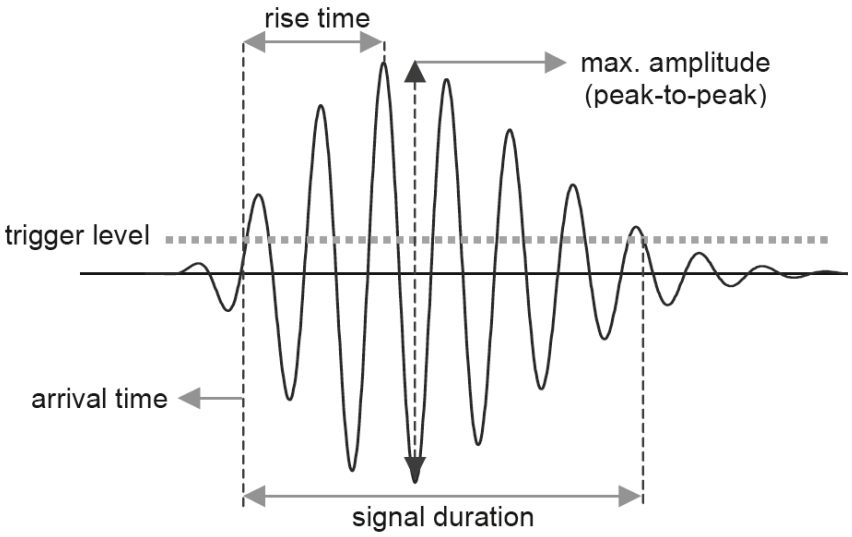

Figure 2-5: Typical AE signal features [57]

The intensity of an AE signal gets lower as the distance from the source increases. This is due to the process of attenuation. The reduction in the amplitude of the waveform is expressed by the logarithm of the ratio between the original and attenuated magnitudes. It is commonly measured in decibels and can be described by the following equation [58]:

$$A = 20log_{10}\left(\frac{a}{a_0}\right) \tag{2.4}$$

The three main causes of attenuation are: geometric spreading, material damping and wave scattering. The effects of attenuation on an AE signal can be measured using a Hsu-Nielson Source [48]. It consists of a mechanical pencil with either a 0.3 or 0.5 mm 2H lead that is passed through a cone-shaped Teflon shoe. The lead is placed in contact with the surface at a 30-degree angle and pressure is exerted until it breaks. Once that happens, a small local deformation that is relieved in the form of a stress wave occurs. This process is similar to that of the AE signal produced by a crack.

2.1.5 Localization considerations

The main purpose of a SHM system is to provide information regarding the location of any damage that occurs in a structure. In the case of AE based system, a common method of locating acoustic sources is Geiger's method, an example of the Gauss-Newton algorithm for solving nonlinear problems. The method was developed by a Swiss scientist of the same name with the purpose of finding the epicentres of earthquakes. Its implementation requires three steps [59]:

- establishing arrival time functions.
- data preparation.
- solving a system of simultaneous equations.

The first step is directly related to the subject of this work due to the fact that the arrival times are determined by the velocity of the Lamb waves, which in turn are affected by EOC such as temperature. An example of an arrival time function is given in the following equation:

$$f_i(x) = f_i(x, y, z, t) = t + \frac{1}{v_i}\sqrt{(x_i - x)^2 + (y_i - y)^2 + (z_i - z)^2} \tag{2.5}$$

where:

- x, y, z are the coordinates of an AE event.
- t is the origin time of the event.
- x_i, y_i, z_i are the coordinates of the i-th sensor.
- v_i is the velocity of the wave.

These functions may be more complicated than the one shown above, allowing more complex velocity models to be built. Using these time functions in conjunction with first-degree Taylor expansions, a system of equations is setup. Next a "guess" solution is defined and an iterative process is used to converge to the solution that matches the observed arrival times within a certain degree of accuracy set by the user. Analysing the previously mentioned equation, it is clear that any variation of the wave velocity will have an effect on the accuracy of the method.

Boon *et al.* [60] investigated the sensitivity of the Geiger localization algorithm to wave speed changes due to temperature and load in an aluminium plate. This was done by first defining a wave velocity function based on experimental results. Using this function, the time differences of arrival were calculated and then inserted into the localization program. The error of the location analysis was then calculated using the following equation:

$$error(T, F) = \sqrt{(x_0\ T, F\ - x_C\ T, F\ )^2 + (y_0(T, F) - y_0(T, F))^2} \tag{2.6}$$

The authors' results showed that when the AE event occurred in the area enclosed by the array of sensors, the error due to the effects of temperature and load was at most 1 cm from the actual location [60]. The results also showed that the error increased when the distance between the sensors was increased.

2.1.6 Piezoelectric transducers

A transducer is a general name for any sensor or actuator. Piezoelectric transducers are often used in Guided Wave Structural Health Monitoring (GWSHM) because they are lightweight and easy to apply [61]. They are also advantageous because they function both as a transducer/actuator and as a sensor of guided Lamb waves. They are made out of ceramic materials which exhibit a property called "piezoelectricity".

Piezoelectricity is a property of certain crystalline materials. When they are subjected to mechanical pressure, the crystalline structure produces a voltage that is proportional to the applied pressure. This phenomenon works both ways: an applied electric field will produce dimensional changes in the material. Pierre and Jacques Curie discovered piezoelectricity at the end of the 19^{th} century.

Piezoelectric ceramics have a pervoskite crystal structure, very close to cubic. In the corners of the cube we have large divalent metals ions (such as Pb), in the centres of the cubes faces there are oxygen ions and close to the centre of the cube there is a small tetravalent metal ion (such as Ti). Under a certain temperature, the Ti ion is slightly closer to one of the cubes edges thus producing positive and negative charges at opposing faces. This temperature is called the Curie temperature. Once this is reached, complete depolarization occurs.

After it is manufactured, a piezoelectric material has electric dipoles oriented in random directions. Any applied electric field would generate responses that eventually cancel out. In order to obtain the desired macroscopic response, the dipoles are aligned with one another through a process called poling.

Poling consists first of heating a piezoelectric material above its Curie temperature. Afterwards, a strong electrical field is applied and maintained while the material is cooled. As a result, the dipoles will be permanently aligned with the direction of the field. Now, if the poled ceramic is maintained below its Curie temperature and is subjected to a small electric field, the dipoles will expand along the poling axis and contract perpendicular to it (the opposite can also happen if the sign of the electric field is reversed.

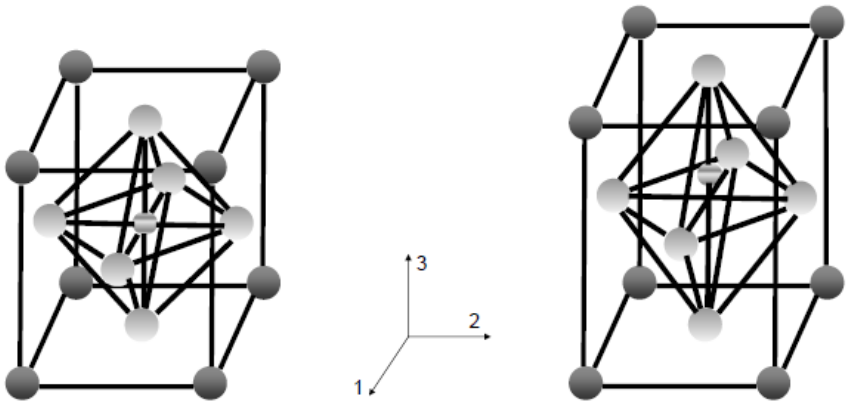

(a) Above Curie temperature. (b) Below Curie temperature.

Figure 2-6: Crystal structure of piezoelectric materials

The behavior of piezoelectric materials is governed by the linear constitutive relations, which relate four variables to each other: stress, strain, electric field and electric displacement. The standard form of these equations is [62]:

$$\begin{aligned} S_{ij} &= s^E_{ijkl} T_{kl} + d_{ijk} E_k \\ D_i &= \varepsilon^T_{ik} E_k + d_{kli} T_k \end{aligned} \tag{2.7}$$

where

- S is the symmetric second order strain tensor.
- s^E is the symmetric fourth order short-circuit compliance tensor.
- T is the symmetric second order stress tensor.
- d is the piezoelectric coupling tensor.
- E is the electric field vector.
- D is the electric displacement vector.
- ε^T is the symmetric second order free electric permittivity tensor.

"Short-circuit" indicates a condition of zero electric field and the term "free" indicates a condition of zero stress.

The piezoelectric transducers used in SHM are generally polarized along the thickness direction. Due to this fact, the actuation and measurement of Lamb waves will have the same sensitivity in the in plane directions of the plate. After polarization, the piezoelectric coupling matrix has the following form:

$$d_{ij} = \begin{bmatrix} 0 & 0 & 0 & 0 & d_{15} & 0 \\ 0 & 0 & 0 & d_{24} & 0 & 0 \\ d_{31} & d_{32} & d_{33} & 0 & 0 & 0 \end{bmatrix} \tag{2.8}$$

The constants in this matrix are provided by the manufacturer of the piezoelectric transducer.

The transducers are usually bonded to the structure of interest. This means that the glue could affect the sensing or actuation process when temperature variations are present. A study performed by Raghavan *et al.* [63] showed that the Epotek 353ND bonding agent does not degrade under thermal variations and that it can be used in the experiments described in this study.

It should be noted that the properties of piezoelectric materials are also temperature dependent [64] but this effect is not within the scope of this thesis and will not be investigated.

2.2 Waves in anisotropic media

2.2.1 Introduction

The acoustic emission system presented in the previous pages relies on the detection and analysis of the waves travelling in the material. It is important to understand the physics of this process and the factors that influence it. In consequence, this chapter is focused on the state-of-research on how the propagation of waves in anisotropic materials is affected by temperature.

Due to the increasing use of composite materials in the design of structures, there has been an increase of attention to the problem of elastic wave propagation in anisotropic materials. Due to their nature, these materials present many wave phenomena that are not observed in isotropic materials, such as [37]: directional dependence of wave speed, a difference between the directions of the phase and group velocity, three different wave speeds instead of two.

Section 2.2.2 presents the state-of-research on wave propagation in anisotropic media exposed to temperature variations. Section 2.2.3 presents methods for modelling the effects identified in Section 2.2.2.

2.2.2 Effects of temperature on the propagation of waves through anisotropic media

The study of how wave speeds change with temperature can be defined as thermo-elasticity. Sharma *et al.* [65] was among the first to analytically study the effect of temperature on guided waves. The theory added a term for the effect of temperature in the thermo-elastic constitution equations. Lee *et al.* [66] performed experiments on the effect of temperature change on an aluminium plate. He found that the effect was so important that it changed the signal even more

than when damage was introduced and analysed with a SHM system. Furthermore, Dodson [67] investigated analyticaly how dispersion curves change with temperature over a range of frequencies. In a later work, Dodson and Inman [68] extended the dispersion curve theory of Horace Lamb and included both thermo-elastic effects as well as a temperature dependent Young's modulus.

The previous studies were performed on isotropic materials, but they highlight the importance of performing similar research on anisotropic materials, whose mechanical behaviour is even more complex. In the following paragraphs, the work done by several authors on this subject will be presented and the methods they used will be highlighted.

Verma [69] performed a purely analytical study on the propagation of waves in layered anisotropic media in generalized thermoelasticity. The equations determined in this work can be used to model the thermo-elastic effects of temperature variation on any anisotropic material. This study did not take into account the changes in material properties that are associated with temperature variations.

Torres and Fritzen [70] took a different approach and only took into account the change in material properties. An experimental investigation was also performed on a CFRP plate and a glass composite laminate. The displacement fields were approximated using polynomial equations. The tests were conducted in a temperature-controlled oven and the temperature was raised in steps up to 60 $\pm$ 2°C. For the first plate, they found that an increase in temperature causes a right time-shift of the dynamic response, as can be seen in Figure 2-7 while a decrease in temperature causes a left shift.

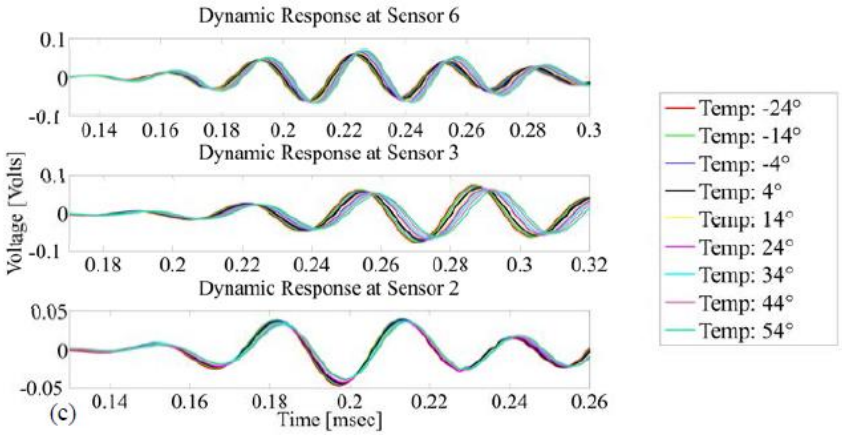

Figure 2-7: Temperature effects on wave directionality [70]

The authors reasoned that the time-shifts are the result of both thermal expansion and changes in the wave velocities with temperature but did not present an analysis of the separate contributions. In the case of the glass fibre laminate, the influence of temperature on the mode amplitude was studied. A change in amplitudes for a given frequency and orientation of the

sensor can be observed in Figure 2-8. The authors explain that this effect is due to the changing ratio of displacement and stress amplitudes with respect to the frequency and angular orientation for a particular mode along the plate thickness. The same effect on the dynamic response signals was found as for the CFRP plate. The effect of temperature increase on the capacitance value of the piezoelectric sensors was not taken into account.

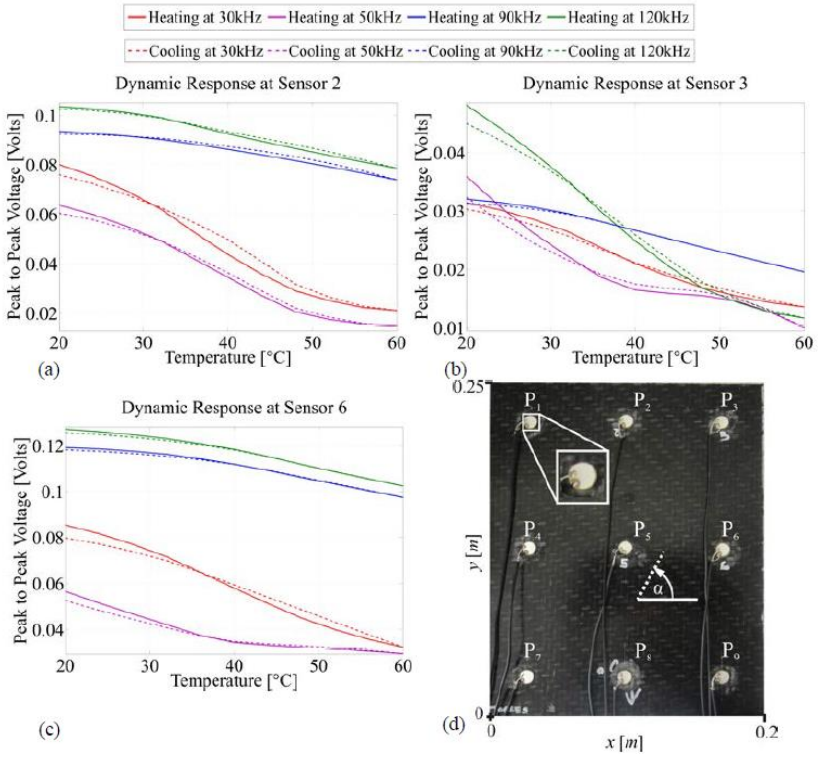

Figure 2-8: Temperature Gradient Effect on Peak-to-Peak Amplitudes of A_0: (a) Sensor 2, (b) Sensor 3, (c) Sensor 6 and (d) Experimental setup [70]

A different method of modelling the thermal effects was used by Kudela *et al.* [71]. A 36-node spectral plate element [72] developed specifically for modelling thermal effects was used. Two fields were considered, with temperatures ranging from 5°C to 50°C and 20°C to 60°C respectively. The dependence of the Young's modulus on temperature was used to incorporate the thermal effect in the mode. The plate was excited by a central transmitter and an array of 12 sensors was used to capture the signals. Their findings are in agreement with those of Torres and Fritzen, with a right time-shift as well as a small increase in amplitude being observed, as can be seen in Figure 2-9.

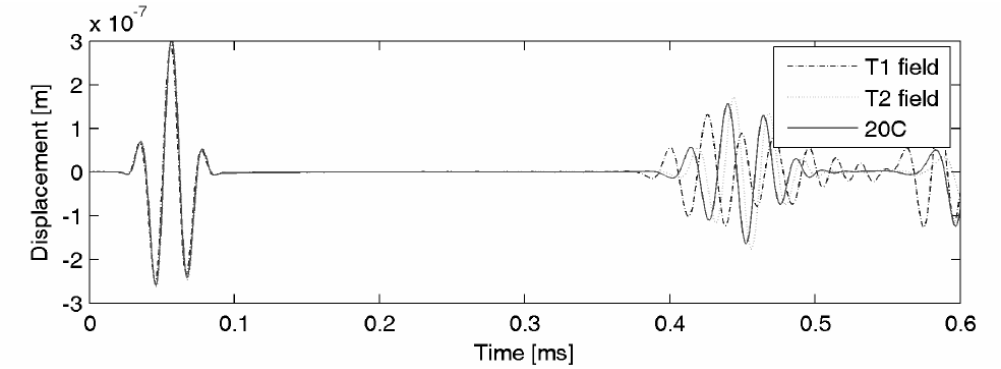

Figure 2-9: Signals registered for different temperature fields [11]

A different approach was used by Park and Jun [73], who investigated the effects of temperature variation on a guided wave damage detection system in composite plates. The thermal effects were modelled using a phase shift parameter that accounted for the change in wave speed and an amplitude ratio that accounted for the change in amplitude. No modelling of the wave propagation phenomena was done. The specimens were made out of graphite-epoxy and were tested in both undamaged and damaged states at different temperatures in order to evaluate the capability of the system to detect damage under varying conditions. The effect of the temperature variation on the waveform of one of the specimens can be seen in Figure 2-10. The authors also introduced a method of compensating for the temperature difference. Their findings indicated that the temperature effect on the damage index can be greater than the damage effect and that temperature-compensation must be used when applying baseline-based damage detection methods.

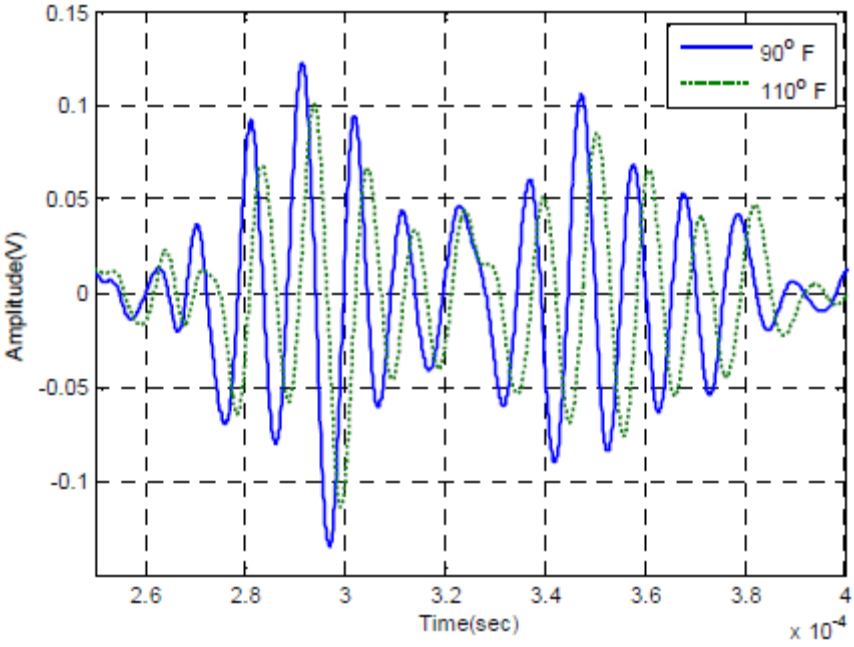

Figure 2-10: Waveform changes due to temperature variation [74]

As opposed to the previous works, Salamone *et al.* [75] took a more detailed approach and investigated the effects of temperature on the PZT actuator and sensors, the transducer/plate bond layer as well as the effect on the plate itself. A pitch-catch method was used, with an actuator exciting ultrasonic guided waves that were picked up by a similar piezoelectric transducer. The primary effect of the temperature variation was a change in the pitch-catch response amplitude of around 40% at the extremes of the range as can be seen in Figure 2-11. A change in the phase velocity was also encountered and the results were in agreement with previous works. Thermo-elastic effects were not taken into account in this work.

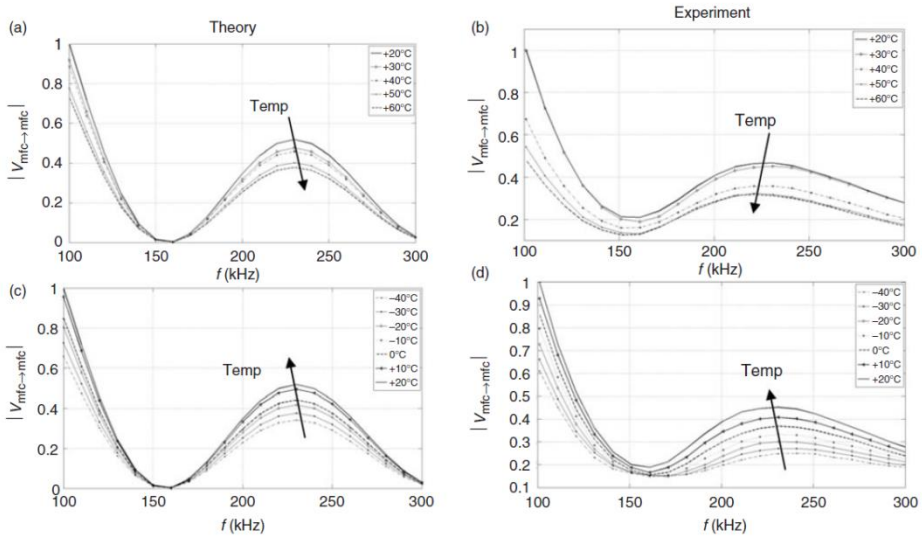

Figure 2-11: Pitch-catch response to S_0 Lamb mode [75]

Thermo-elastic effects were taken into account by Kumar and Kansal [76] who derived the constitutive relations and field equations for anisotropic generalized thermoelastic diffusion for a particular case of anisotropic, transverse isotropy. Unidirectional composite materials are an example of this case. They observed that temperature affected many of the parameters of wave propagation such as: phase velocity, attenuation coefficient and the amplitudes of the displacements. This study was done only analyticaly and was not verified through experiments. Also, the effect of temperature on the material properties was not included.

Schubert *et al.* [77] proposed an approach for compensating the environmental effects on active Lamb wave base SHM systems. As part of their study, they also looked at the effect of temperature on CFRP plates. Piezoelectric sensors were bonded to the plate and measurements were taken both before and after the plate was damaged. The authors found that the signal became less reconstructable during conditioning but once the damage was introduced it was easily identifiable. The compensation method was also found to produce good results, although in some cases it did not perform as well as intended. The authors concluded that the most significant errors come from wave interference, which is more likely to happen in more complex structures.

Chronopoulos *et al.* [78] studied the thermal effects on acoustic wave propagation in aerospace composite structures. They used a Wave Finite Element Method to calculate the temperature dependent wave dispersion characteristics of a composite panel and then performed experiments in order to validate their findings. The authors found that temperature has a significant influence on propagation of acoustic waves in composite panels, especially on the phase velocity of the flexural wave.

From the analysed literature, the dominant effect of temperature variations was a change in the mechanical properties of the materials. Other effects included the change in properties of the PZT elements and the effect of temperature on the bond line between plate and PZT elements. However, these effects are beyond the scope of this study.

2.2.3 Modelling temperature effects

The previous section outlined the main effects of temperature variation on the propagation of waves through anisotropic materials. In this section, some brief modelling considerations are presented.

According to [79], mainly the matrix dominated properties of a polymeric composite are influenced by varying temperatures. Properties that are affected include: transverse stiffness and shear stiffness. These properties are present in the equations of motion so they will affect wave propagation. The effect on the fibres will generally be smaller [80]. This also applies to the

typical temperature range that an aircraft structure is exposed to [75]. Consequently, it is useful to see how this change in properties as a function of temperature can be modelled.

The general approach found in literature is to apply a degradation factor to the affected property. This degradation factor is calculated through empirical equations based on the glass transition temperature T_g of the resin. Examples of such approaches include the ones developed by Van Krevelen and Hoftyzer [81], Chamis [82] or Tsai [83]. The latter method is presented here because it also includes the small effect on the fibre properties.

Tsai [83] proposed an adimensional temperature T^* that is used to empirically fit the matrix and fibre stiffness data as a function of temperature.

$$T^* = \frac{T_g - T}{T_g - T_{rm}} \tag{2.9}$$

where

- T_g is the glass transition temperature of the resin
- T is the operating temperature
- T_{rm} is the room temperature

The material properties are then determined from the properties at room temperature and the adimensional temperature.

$$E_m = E_m^0 (T^*)^{0.5} \tag{2.10}$$

$$G_m = G_m^0 (T^*)^{0.5} \tag{2.11}$$

$$E_f = E_f^0 (T^*)^{0.04} \tag{2.12}$$

2.3 Analysis of the literature study and conclusions

SHM systems that use guided waves are affected by changes in temperature. The signal changes can be even more significant than those due to damage in some cases. The most important effect of these temperature changes is on the material properties of the constituents, which are temperature dependent. In composite materials, the most significantly affected are the matrix dominated properties, such as: transverse modulus and shear modulus. Any change in these properties leads to a change in the mode wave speeds.

The reviewed literature suggests that even though there has been some research into the subject of temperature effects on AE based SHM systems, further work is needed in order to develop a thorough understanding into certain areas such as: quantifying the effects on the wave speeds and comparing them to other sources of uncertainty for localization algorithms, such as the directional dependence of the phase and group velocities. Furthermore, to the author's knowledge, the temperature degradation model presented in this report has not been used for such an analysis.

This thesis sought to fill these voids by comparing analytical, FEM and experimental results for the group velocity of the S_0 mode for two specimens, a hybrid laminate and a sandwich panel. These results were put into perspective by comparing the variation due to thermal effects with the variation due to the directional dependence and with errors related to the trigger level.

3 Manufacturing and testing procedures

As mentioned in the introduction, the goal of this work was to investigate the effects of temperature on the propagation of ultrasonic waves through composite materials. Thus, two specimens were manufactured for the temperature tests: a hybrid laminate made out of glass and carbon fibres and a sandwich panel with hybrid face sheets and a foam core. Several other laminates were also manufactured for the mechanical tests. This chapter presents the manufacturing process of the sandwich and the monolithic and hybrid laminates as well as the testing methodology that was used. Section 3.1 highlights the reasons for choosing these particular materials. Section 3.2 discusses the manufacturing of the monolithic and hybrid laminates. Section 3.3 describes the testing methodology and also presents the results of the tests. Section 3.4 shows the manufacturing process of the sandwich panel.

3.1 Introduction

The panels used in this work were based on the preliminary design of a solar powered UAV developed by Group 4 in the 2012-2013 Design and Synthesis Exercise [84]. The "Dragonfly", shown in Figure 3-1, features front and back wings made of sandwich panels with the following layup: $[(\pm 45^0)_{GF}$ / $90^0{}_{CF}$ / $(\pm 45^0)_{GF}]$ face sheets and a 20 mm thick foam core. In the beginning, it was intended to perform the tests on this structure, however, due to limitations regarding the frequency range of the piezoelectric transducers that were available, it was decided to use a thinner foam of 2mm, which was used in the design of the fuselage.

Figure 3-1: The Dragonfly UAV [84]

3.2 Manufacturing test samples

The face sheets of the sandwich panel were designed using UDO® CST 300/300 unidirectional carbon fibre produced by SGL group [85] and HexForce® 7581 glass fibre weave from Hexcel [86]. The data sheets of these materials, provided in the appendix, do not contain the material properties that are needed in order to model the behaviour of the sandwich panel. Thus, it was decided to manufacture test samples in order to determine the following mechanical properties: E_1, E_2, G_{12} and ν_{12}. In the case of the glass fibre weave, experimental results were eventually obtained from the supplier, however it was decided to manufacture samples for this material as well in order to gain experience with the manufacturing process and to double check the values. The following test samples were manufactured: $[0_5]$, $[90_7]$ laminates using UDCF layers and $[(0/90)_9]$, $[(\pm 45)_8]$ using GF weave layers. All laminates were 300 mm by 300 mm. The number of layers was selected in order to have a laminate thickness consistent with the ASTM 3039 – 08 and D 3518 – 94 standards. A laminate with $\pm 45°$ layers of UDCF was also attempted but the infusion process failed due to difficulties associated with infusing thick UD laminates.

Vacuum infusion was the selected manufacturing process due to the positive results obtained by a previous master student working on the Dragonfly project using the same materials [87] and considering the facilities available in the ASM lab of the Faculty of Aerospace Engineering at Delft University of Technology. The Hexion® Epikote™ 04908 epoxy resin and Epicure™ 04908 curing agent [88] were selected due to their availability in the composites lab and because of the long pot life of the mixture (300 minutes). The long pot life was important especially for the infusion of the UD carbon fibre laminates which had an average infusion time of 2 hours. The manufacturing process is described in detail in the following paragraphs.

The manufacturing of the test samples was an iterative process. A few samples were manufactured for every laminate in order to find any unforseen issues and to set a standard production methodology. This final methodology is the one presented in this report.

The infusions were carried out using 3mm thick Al2024 plates as moulds. First the mould surface was cleaned thoroughly using Scotch Brite, PFQD and water. Tape was applied on the edges of the plate in the areas where tacky tape would be applied later on. Next, the Marbocote release agent [89] was applied using the instructions given by the supplier. Four layers were applied and each layer was left to dry for 15 minutes. In the meantime, the fibres were cut using the Gerber cutting machine available in the composites lab. This ensured that the plies were cut to the exact size that was needed and at the desired orientation.

Once the final layer of release agent had dried, tacky tape was applied on the edges of the mould and the fibres were stacked using a ruler to make sure the laminate is centred. Tape was applied to the corners in order to keep the fibres in place. A layer of perforated release foil was placed on

top. This was done in order to prevent the flow mesh from sticking to the laminate and to facilitate the infusion through the thickness. The release foil was cut to a slightly larger size than the laminate and about 10 cm longer in the infusion direction so it could also be placed between the flow mesh and the mould. Next the flow mesh was applied. The size of the flow mesh was different depending on the material that was being infused. A shorter mesh was used for the carbon fibre laminate in order to provide a longer infusion time. A short infusion time would leave dry spots on the side facing the mould because the through the thickness infusion takes place very slowly.

The mesh was extended 10 cm towards the edge of the plate where the inlet tube was located. The inlet was connected to a spiral tube which provided a path of less resistance for the resin. On the outlet side of the laminate, 3 layers of peel ply were used to connect the fibres and the vacuum source. This was done to provide and even distribution of the vacuum through the laminate. A piece of bleeder was wrapped around the outlet tube and place on top of another layer of bleeder material that was also used to ensure an even distribution of the vacuum. A close view of the inlet and outlet setups can be seen in Figure 3-2 a) and b). Once everything was set in place using tape, the vacuum bag was applied. The bag was cut to a size about 50% larger than the mould in order to make pleats. The purpose of these pleats was to provide extra material once the vacuum was applied, otherwise the vacuum bag would stretch and bend the plate and could even fail to come into contact with the laminate in the corners and create runners (a path of lower resistance for the resin).

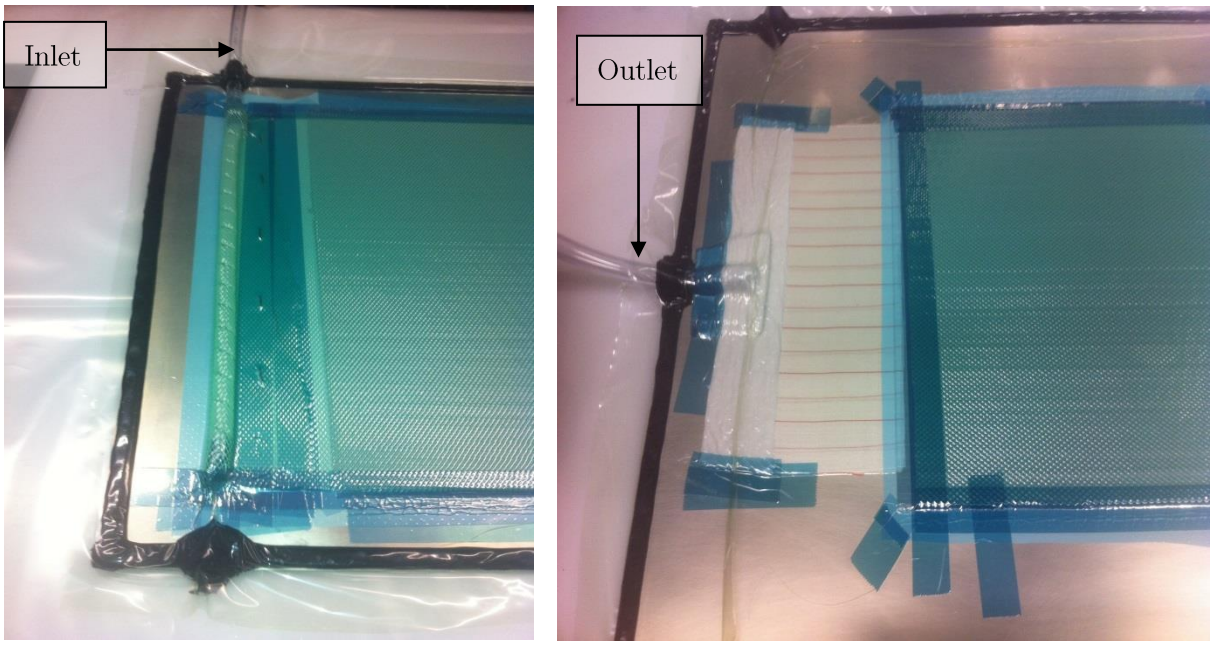

Figure 3-2: a) Inlet setup **b)outlet setup**

After placing the vacuum bag, the inlet tube was clamped and the outlet tube was connected to the vacuum pump. A vacuum of 800 mbar was first applied and the vacuum bag was manually adjusted to avoid creases in the laminate area. Once this was done, the vacuum was set to 50 mbar, a standard value for vacuum infusions. At this point, a leak test was performed. The valve between the vacuum pump and the catch pot was closed and the vacuum was checked after 15 minutes. Generally, a loss of vacuum of over 1 mbar/minute is considered unacceptable. In that case, the bond between the vacuum bag and the tacky tape is checked all around the mould. In the case of the laminates that were manufactured the loss of vacuum was between 0 and 5 mbar in 15 minutes, well within the acceptable range.

After the leak test was performed, the resin was mixed. The amount of resin needed for the infusion was determined using an Excel sheet provided by the technicians of the ASM lab. The mixing ratio of 100:30 indicated by the manufacturer was followed as closely as possible using a digital scale that had a precision of 0.1 g, well within the margin of error mentioned in the data sheet of the resin. The mixture was then placed in a degassing chamber in order to remove the air bubbles which were inevitably caught inside the resin during the mixing. The degassing was performed at a vacuum of 3 to 5 mbar for 30 minutes.

Once the degassing was done, the infusion was performed. After the resin had infused the laminate, the inlet was clamped and the whole ensemble was left to sit for 22 hours in order to reach an equilibrium that ensured an even spread of the resin through the laminate. After the 22 hours had passed, the resin was partly cured so the tubes were cut and the mould was placed in an oven and post-cured for 6 hours at 80^0C. An infused laminate ready for the post-curing process can be seen in Figure 3-3.

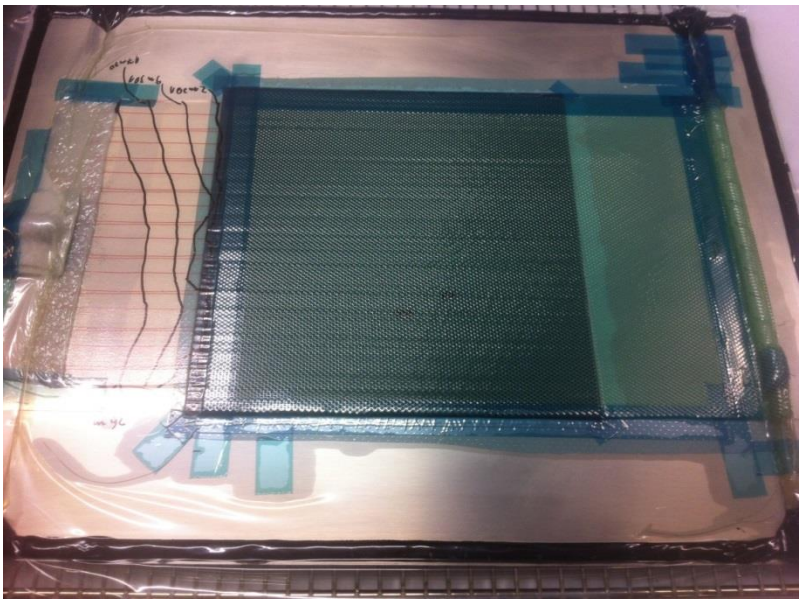

Figure 3-3: Infused UDCF laminate

After being removed from the oven, the laminate was demoulded and kept in a storage area in the composites lab. The lab maintains a fairly constant climate of 20 to 23^0 C and humidity between 30 and 50 percent. This procedure was followed for all of the tested samples.

3.3 Testing material properties

3.3.1 Procedure and standards

Once all of the panels were manufactured, the test samples could be prepared. First, the panels were cut into small rectangular pieces, with dimensions provided by the ASTM standards. The cutting was done using a Carat Wet Diamond cutter because it provided the highest precision cutting and the best quality among the options available in the ASM lab.

Next, all of the samples were weighed and measured and the relevant information was catalogued. Paper tabs were applied to the edges of the samples using fast curing acrylic glue in order to provide a good load introduction mechanism. Finally, the samples were instrumented with strain gauges. Before bonding the tabs and the strain gauges, the specimens were prepared by degreasing the surface using acetone, sanding and final cleaning. Figure 3-4 shows an example of a CF test sample, instrumented with a strain gauge and ready for testing.

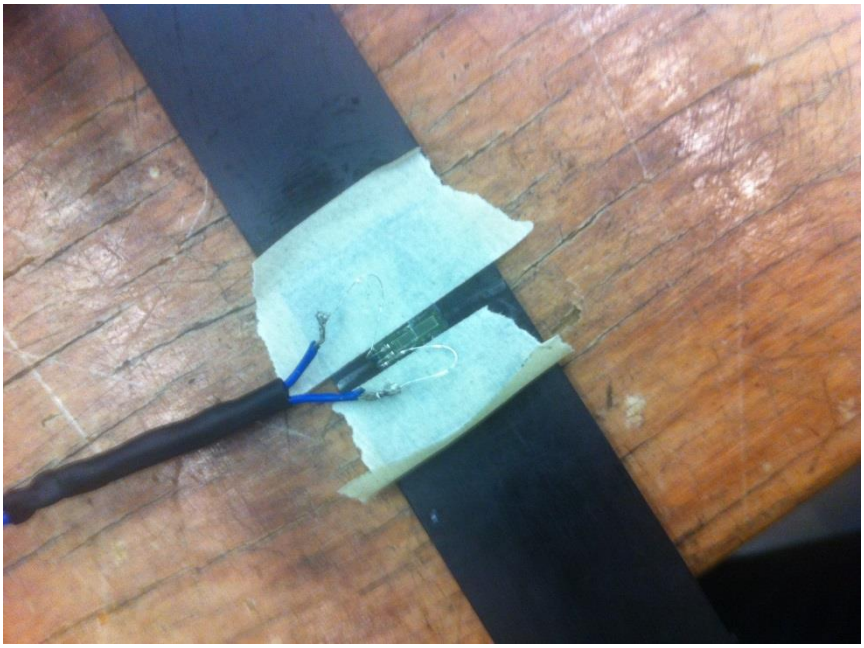

Figure 3-4: CF test sample instrumented with a strain gauge

The Young's modulus in the longitudinal (E_1) and transverse (E_2) directions and the Poisson's ratio (ν_{12}) were determined by following the ASTM D 3039 – 08 standard test method for Tensile Properties of Polymer Matrix Composite Materials [90]. The following formulas were used:

$$E_{1/2} = \frac{\Delta\sigma}{\Delta\varepsilon_{1/2}} \tag{3.1}$$

$$\nu_{12} = -\frac{\Delta\varepsilon_2}{\Delta\varepsilon_1} \tag{3.2}$$

where:

- $E_{1/2}$ – tensile modulus of elasticity in longitudinal (1) or transverse (2) direction.
- $\Delta\sigma$ – difference in applied tensile stress between two strain points.
- $\Delta\varepsilon_{1/2}$ – difference between two strain points in longitudinal (1) or transverse (2) direction (nominally 0.002 or 2000με).
- ν_{12} – Poisson's ratio.

The shear modulus test was performed by following the ASTM D 3518 – 94 standard test method for In-Plane Shear response of polymer matrix composite materials [91]. The following formulas were used:

$$\tau_{12_i} = \frac{P_i}{2A} \tag{3.3}$$

$$\gamma_{12_i} = \varepsilon_{x_i} - \varepsilon_{y_i} \tag{3.4}$$

$$G_{12} = \frac{\Delta\tau_{12}}{\Delta\gamma_{12}} \tag{3.5}$$

where:

- τ_{12} – shear stress at i-th data point.
- P_i – load at i-th data point.
- A – cross-sectional area of the sample.
- γ_{12_i} – shear strain at i-th data point.
- ε_{x_i} and ε_{y_i} – longitudinal and lateral normal strain at i-th data point.
- G_{12} – shear modulus of elasticity.

Further details regarding the ASTM standards can be found in the referenced documents.

The tests were performed using the Zwick 250 kN tensile and compression bench, located in the ASM lab hall. This machine was chosen because it is equipped with a high precision extensometer that was used to measure the longitudinal strain. The transverse strain was

measured using the previously mentioned strain gauges. The standard procedure for performing a test is described in the following paragraph.

The wires of the strain gauge were connected to a 4 channel Peekel Strain machine that was used to amplify the signal sent by the strain gauges. The Peekel strain machine was then connected to a computer equipped with software capable of controlling the Zwick machine and monitoring the results of the measurements. The sample was then placed in the hydraulic grips of the testing machine. The grips are equipped with a mechanism that facilitates easy alignment of the sample. Next, the load was applied and the strains of the sample were recorded. The test was stopped once the required strain level was achieved. An example of the test setup can be seen in Figure 3-5. It can also be observed in the figure that the specimen was slightly bent when placed in the grips. This was due to a small compressive load that is introduced by the grips once they are closed. In order to counter act this effect a preload value was set before the measurements began.

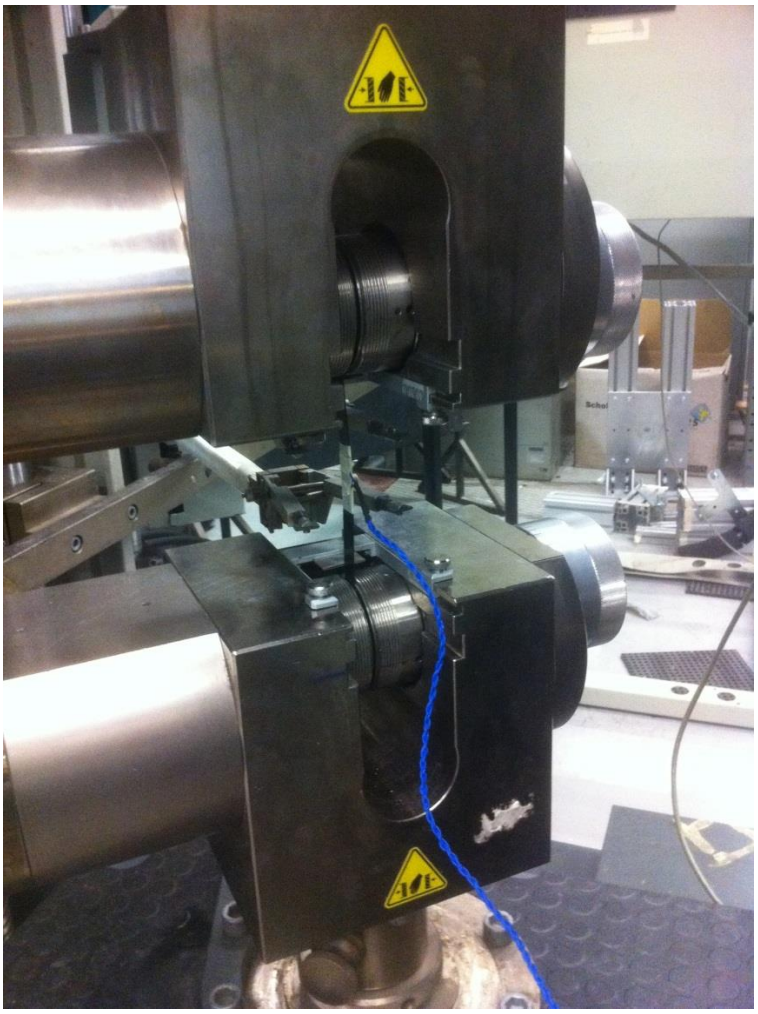

Figure 3-5: Zwick 250 kN bench with CF test sample

3.3.2 Specimen information

This section presents some relevant information regarding the test specimens. The samples were catalogued in the manner described in Table 3-1.

Table 3-1: Description of the sample ID's

ID	Description
CF_1_X	Carbon fibre samples used to test E_1 and ν_{12}
CF_2_X	Carbon fibre samples used to test E_2
GF_1_X	Glass fibre samples used to test E_1 and ν_{12}
GF_2_X	Glass fibre samples used to test E_2 and ν_{12}
GF_12_X	Glass fibre samples used to test G_{12}

The samples were manufactured as close to the ASTM standards as possible. The dimensions of the samples are presented in Table 3-2. The thickness value used in the calculations was measured in the middle of the samples, at the location where the stress values were calculated. In general, specimens manufactured through vacuum infusion have slight thickness variations between the sides of the laminate that are closer to the inlet and the outlet respectively. All of the dimensions were measured using calipers.

Table 3-2: Dimensions of the CF_1 samples

Sample	t_m [mm]	w [mm]	L [mm]
CF_1_1	0.94	15	251
CF_1_2	0.94	15.18	252
CF_1_3	0.98	15	249
CF_1_4	0.96	14.95	251

Table 3-3: Dimensions of the CF_2 samples

Sample	t_m [mm]	w [mm]	L [mm]
CF_2_1	1.84	25.3	174
CF_2_2	1.93	25.25	173
CF_2_3	1.9	25.23	174
CF_2_4	1.93	25.28	174
CF_2_5	1.86	25.12	174
CF_2_6	1.87	25.57	174
CF_2_7	1.83	25.4	175

Table 3-4: Dimensions of the GF_1 samples

Sample	t_m [mm]	w [mm]	L [mm]
GF_1_1	2.39	26.1	250.5
GF_1_2	2.4	25.6	249
GF_1_3	2.33	26	250
GF_1_4	2.38	26	250

Table 3-5: Dimensions of the GF_2 samples

Sample	t_m [mm]	w [mm]	L [mm]
GF_2_1	2.43	25.6	249
GF_2_2	2.43	25.5	249
GF_2_3	2.5	25.5	250
GF_2_4	2.41	25.6	248.5

Table 3-6: Dimensions of the GF_12 samples

Sample	t_m [mm]	w [mm]	L [mm]
GF_12_1	2.2	25.14	249
GF_12_2	2.17	25.19	249.5
GF_12_3	2.17	25.11	249
GF_12_4	2.13	25.27	250
GF_12_5	2.19	25.16	249
GF_12_6	2.16	25.17	248

3.3.3 Results

The results of the tests are documented in this section.

The experimental stress-strain curves for the CF-1 samples are shown in Figure 3-6 and Figure 3-7. The corresponding values are shown in Table 3-7.

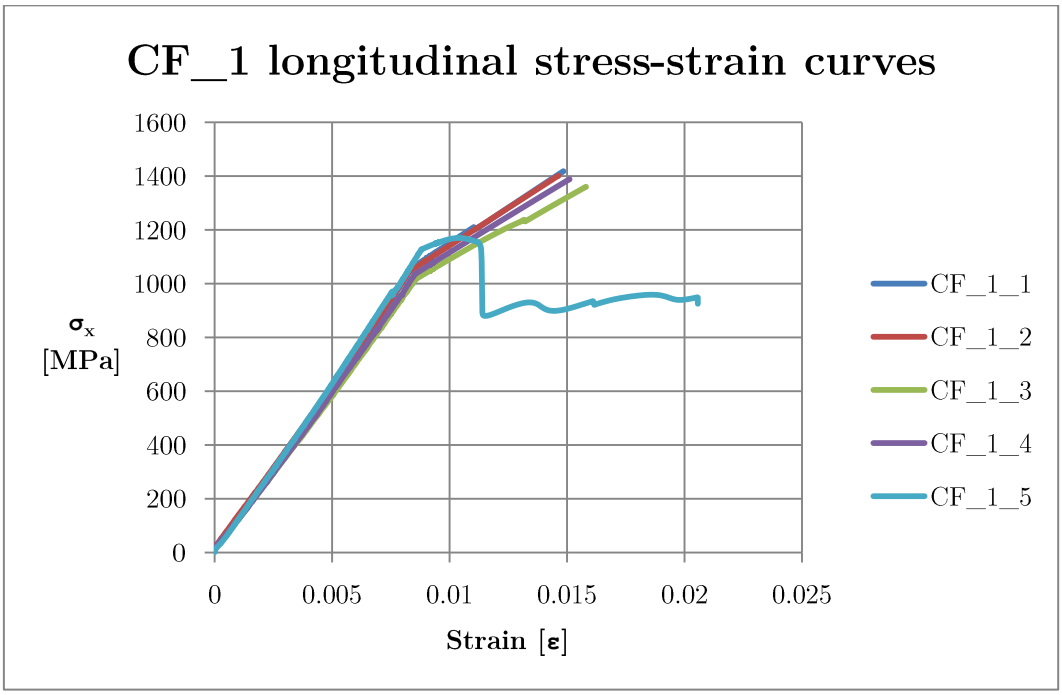

Figure 3-6: Experimental longitudinal stress-strain curves for the CF_1 samples

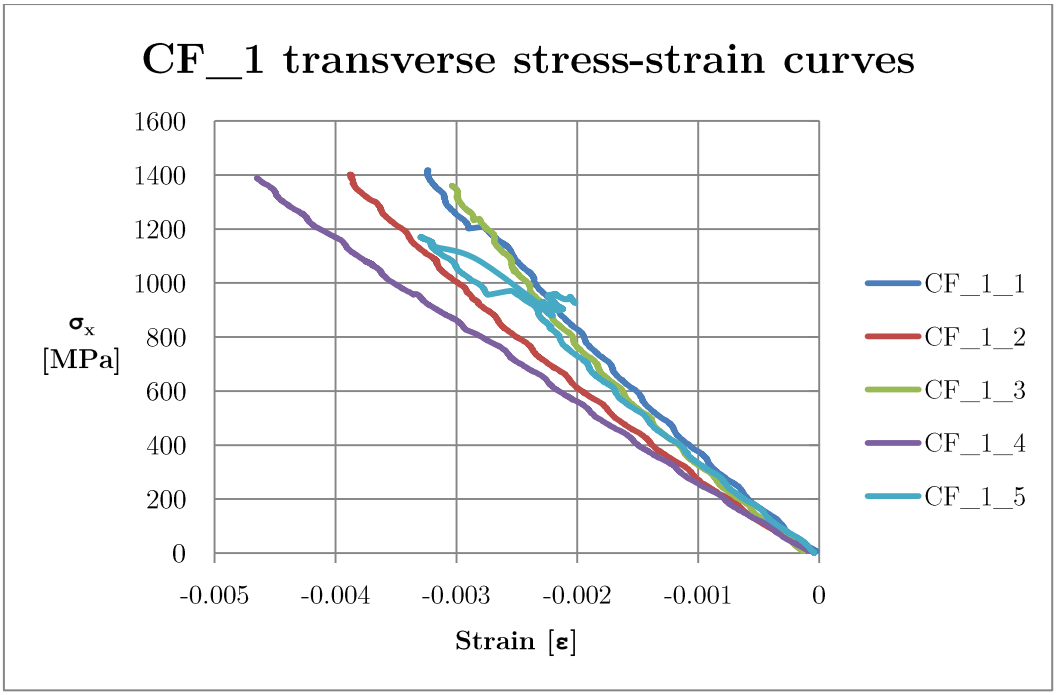

Figure 3-7: Experimental transverse stress-strain curves for the CF_1 samples

Table 3-7: CF_1 results

Sample CF_1_X	E_1 [GPa]	ν_{12}
CF_1_1	116.169	0.31
CF_1_2	118.73	0.37
CF_1_3	121.64	0.3
CF_1_4	114.82	0.41
CF_1_5	123.88	0.34
Average value	**119.05**	**0.34**
Standard deviation (σ)	**3.75**	**0.04**

As can be seen from the graphs, sample CF_1_5 failed before reaching the same load as the other samples. However, the modulus and the Poisson's ratio could still be calculated because the failure occurred after the strain level that was needed for the calculations, as described by the ASTM standard 3039-08.

The stress-strain curves of the CF_2 samples are shown in Figure 3-8 and the corresponding values are shown in

Table 3-8. The transverse stress-strain plots for the CF_2 samples were not included in this report due to the fact that the strains were very small and did not show any meaningful results.

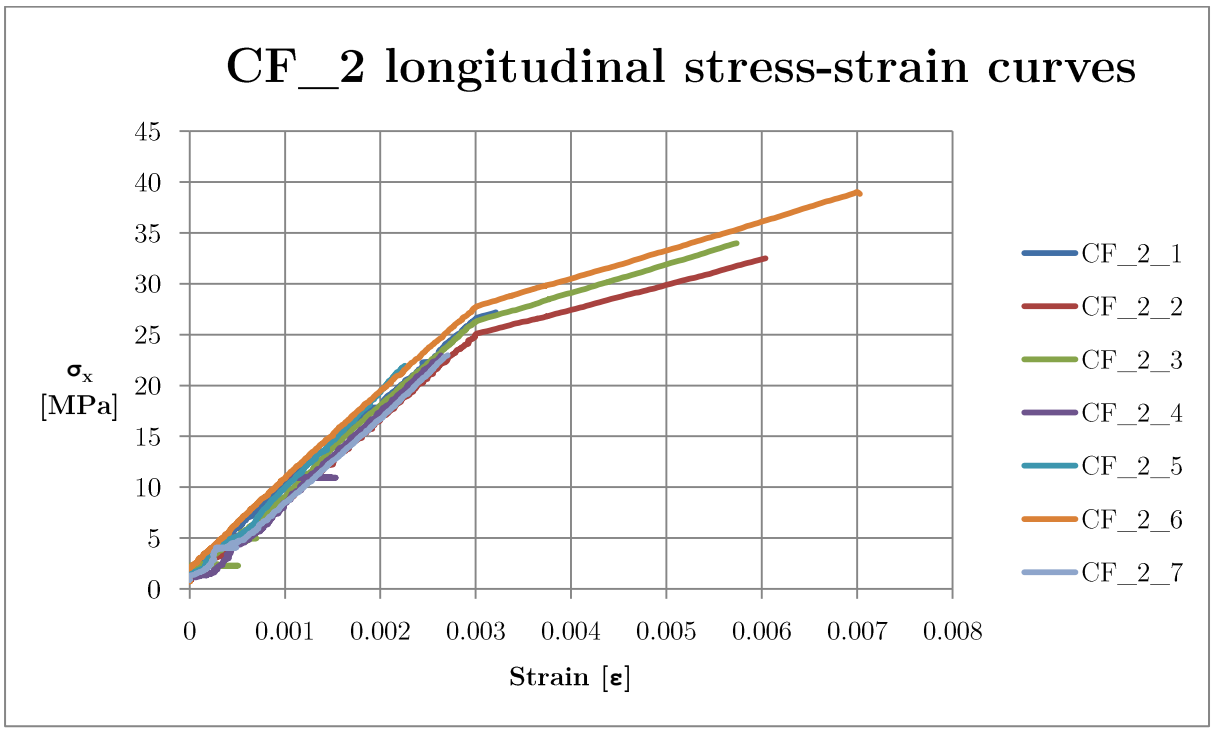

Figure 3-8: Experimental longitudinal stress-strain curves for the CF_2 samples

Table 3-8: CF_2 results

Sample CF_2_X	E_2 [GPa]
CF_2_1	8.14
CF_2_2	8.21
CF_2_3	8.6
CF_2_4	-
CF_2_5	-
CF_2_6	8.42
CF_2_7	-
Average value	**8.34**
Standard deviation (σ)	**0.2**

Due to premature failure of specimens CF_2_4, CF_2_5 and CF_2_7 the modulus of these samples could not be calculated. The other four samples showed consistent results.

The stress-strain curves of the GF_1 samples are shown in

Figure 3-9, while the relevant values are shown in Table 3-9.

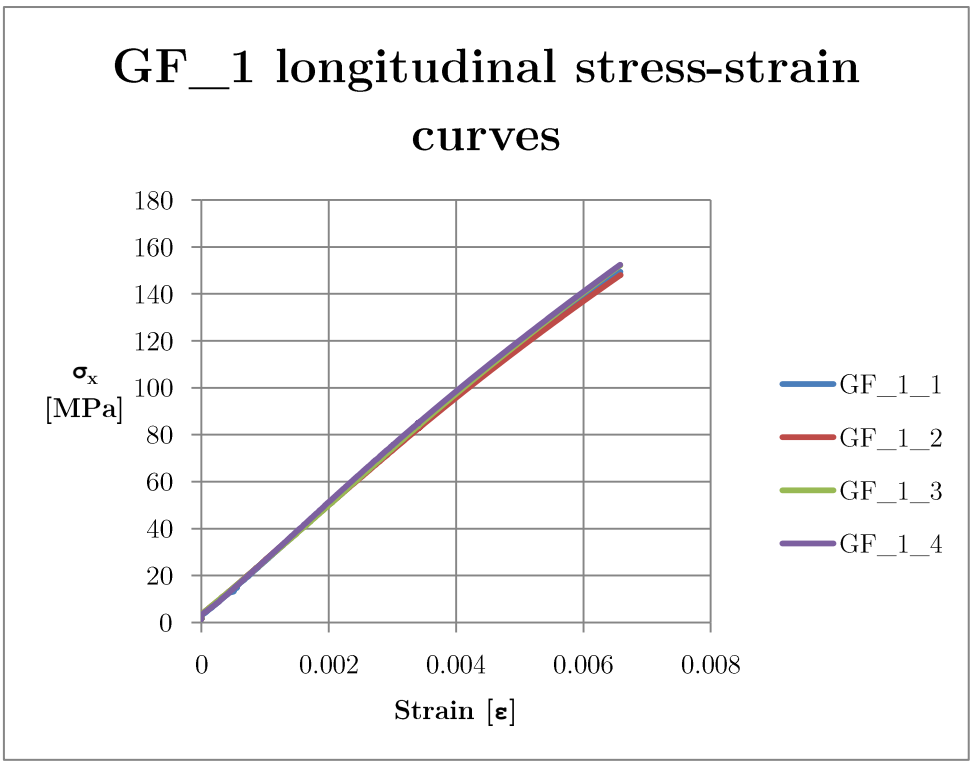

Figure 3-9: Experimental longitudinal stress-strain curves for the GF_1 samples

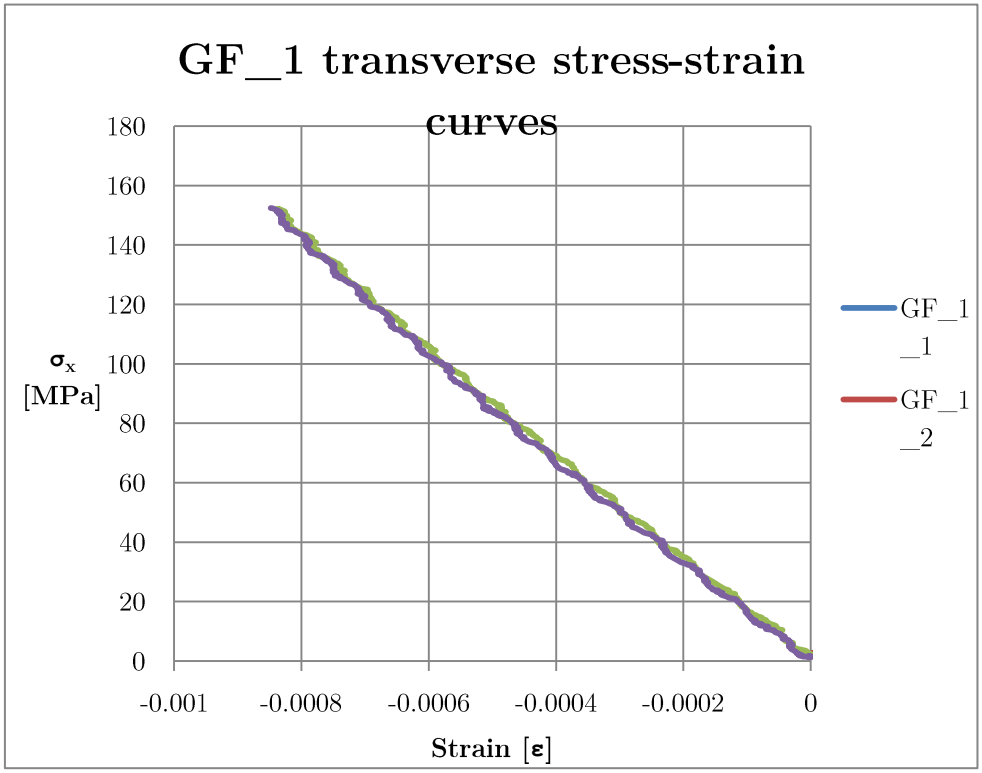

Figure 3-10: Experimental transverse stress-strain curves for the GF_1 samples

Table 3-9:GF_1 results

Sample GF_1_X	E_1 [GPa]	ν_{12}
GF_1_1	24.29	0.15
GF_1_2	23.29	0.145
GF_1_3	23.84	0.137
GF_1_4	24.5	0.147
Average value	**23.98**	**0.145**
Standard deviation (σ)	**0.46**	**0.005**

The stress-strain curves of the GF_2 samples are shown in Figure 3-11. Table 3-10 shows the values of the transverse modulus and the Poisson's ratio.

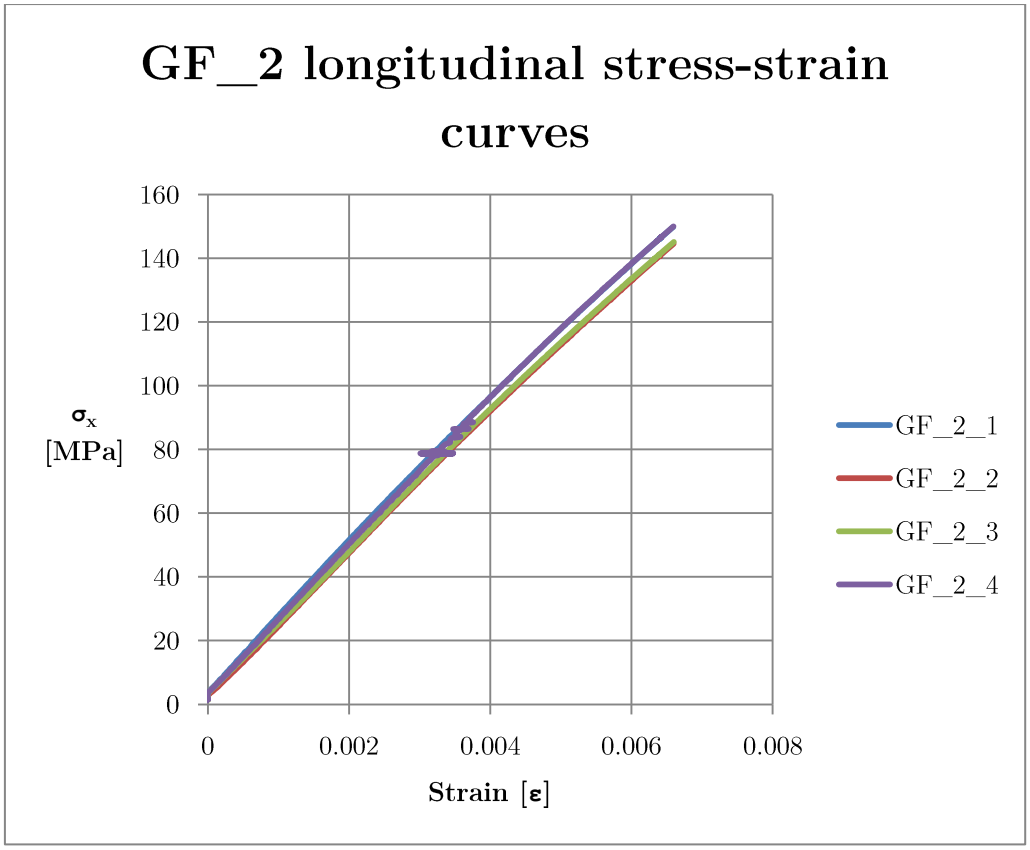

Figure 3-11: Experimental longitudinal stress-strain curves for GF_2 samples

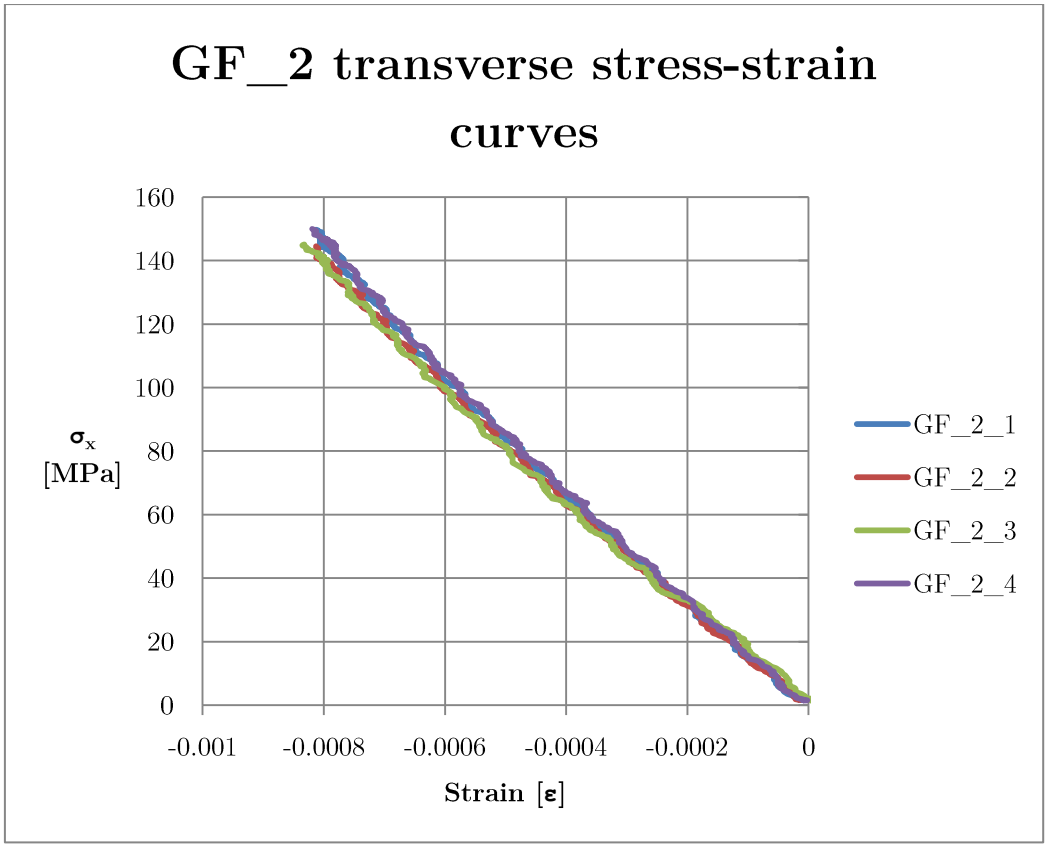

Figure 3-12: Experimental transverse stress-strain curves for GF_2 samples

Table 3-10: GF_2 results

Sample GF_2_X	E_2 [GPa]	ν_{12} [Unitless]
GF_2_1	23.32	0.134
GF_2_2	23.29	0.131
GF_2_3	22.86	0.13
GF_2_4	22.7	0.145
Average value	**23.04**	**0.135**
Standard deviation (σ)	**0.26**	**0.0048**

The results show a slight difference between the values of E_1 and E_2. This is to be expected due to the difference in fibre content between the warp and weft directions described in the material data sheet [92].

The stress-strain curve of the GF_12 samples is shown in Figure 3-13. It should be noted that this plot shows the relationship between the shear stress τ_{12} and the shear strain γ_{12}. The corresponding values of the shear modulus are shown in Table 3-11.

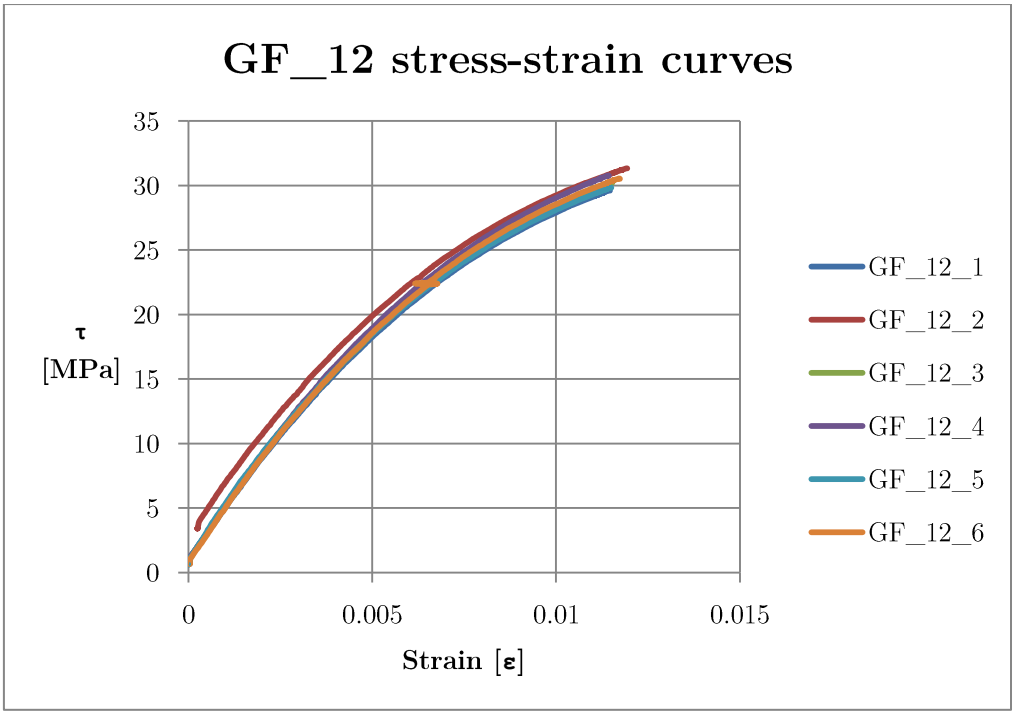

Figure 3-13: Experimental shear stress-strain curves for the GF_12 samples

Table 3-11: GF_12 results

Sample GF_12_X	G_{12} [GPa]
GF_12_1	3.46
GF_12_2	3.43
GF_12_3	3.51
GF_12_4	3.62
GF_12_5	3.5
GF_12_6	3.56
Average value	**3.52**
Standard deviation (σ)	**0.06**

A final overview of the values is shown in Table 3-12. These values were later used in the FEM models and the dispersion curve software. It should be mentioned that the G_{12} value of the CF layer and the G_{13} and G_{23} value of both CF and GF layers were not determined experimentally. As mentioned before, due to difficulties with manufacturing CF samples for the shear modulus test, this value was selected as an average value for this type of material (UDCF with epoxy resin). The $G_{13}$and G_{23} values were not determined experimentally due to lack of time and due to the fact that they do not have a significant influence on the propagation of the S_0 mode, as

shown in previous research by Arredondo *et al.* [70]. However, due to the fact that the FEM software needs these values to perform the calculations, the values were extracted from previous work done in this project [93].

Table 3-12: CF and GF laminae mechanical properties – mean values

Material	E_1 [GPa]	E_2 [GPa]	G_{12} [GPa]	G_{13} [GPa]	G_{23} [GPa]	ν_{12} [Unitless]
CF	119.05	8.342	4.5	2.24	2.51	0.34
GF	24	23	3.52	2.24	2.51	0.14

3.4 Manufacturing the sandwich panel

The manufacturing of the sandwich panel was done using a process similar to the one used in the case of the solid laminates. Some adjustments had to be made due to the fact that the closed-cell foam did not allow for through the thickness impregnation from one face sheet to the other. This section describes these adjustments and the reasoning behind them.

The main modification to the process was the addition of a layer of flow mesh at the bottom of the layup. This was done in order to make sure that the resin reaches the bottom face sheet as well as the top. Thus, two separate flow fronts were created.

A second adjustment was made in order to ensure that the flow fronts remained separate between the edge where the foam core ended and the bleeder layer located at the outlet. Using this technique, a good infusion on both sides was achieved.

The infusion layup, including the two adjustments previously mentioned, is illustrated in Figure 3-14 and Figure 3-15 with the help of the Ply Plot tool from ABAQUS CAE.

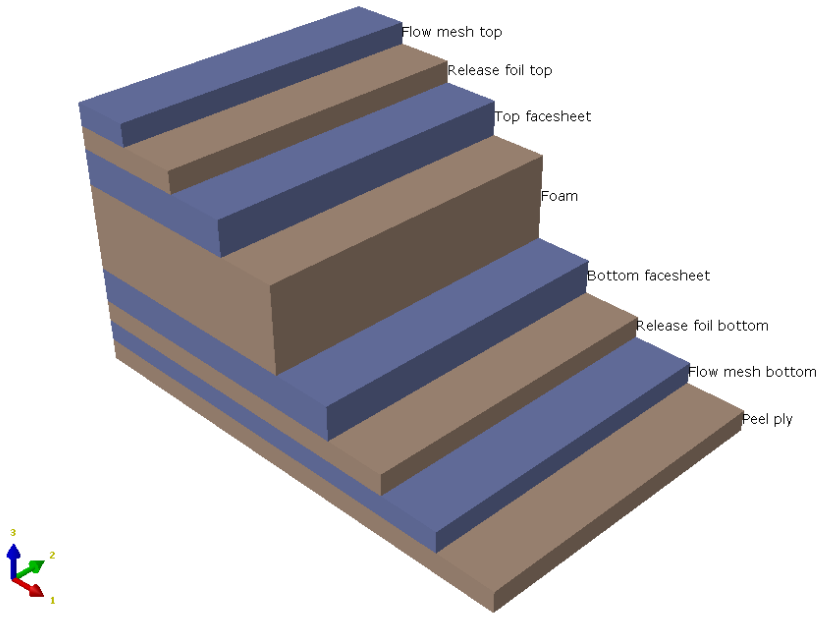

Figure 3-14: Infusion layup at the inlet side

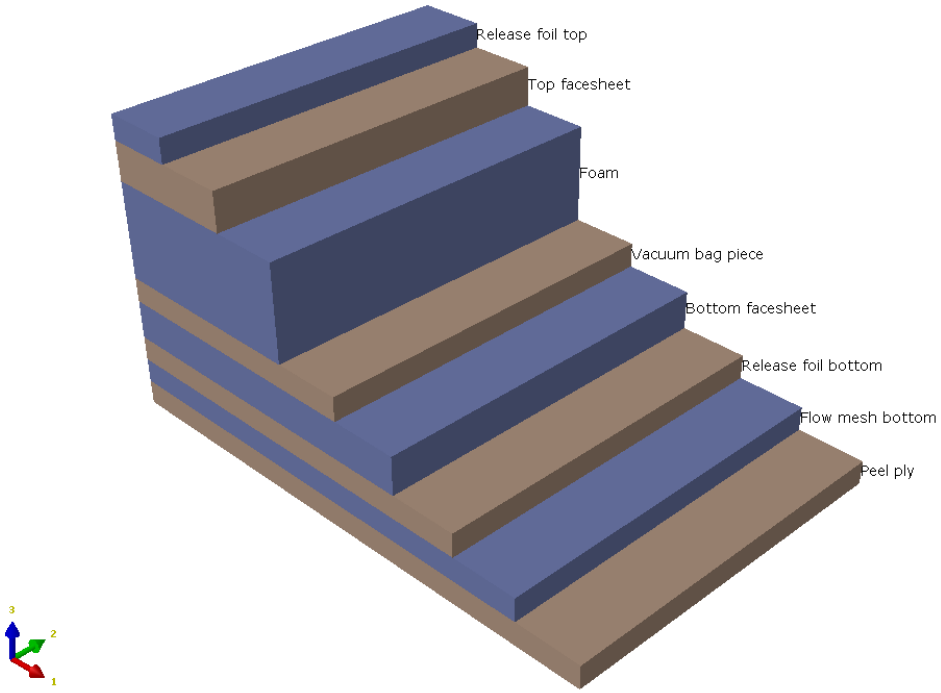

Figure 3-15: Infusion layup at the outlet side

4 Modelling considerations and experimental setup

As it was mentioned in the introduction, the work presented in this report was performed using a mix of analytical modelling in MATLAB, finite element simulations in ABAQUS/CAE and experiments performed in the laboratory. This chapter describes the setup of the simulations and the experimental tests. Section 4.1 describes the methodology of the work. Section 4.2 gives a short presentation of the analytical approach. Section 4.3 presents the FE models that were used, including any relevant information such as: boundary conditions, mesh size, time step, geometry etc. Section 4.4 describes the experimental setup and the process used to actuate and receive the signals.

4.1 Methodology

The velocity measurements were performed at 3 temperature steps: -40, 25 and 70° C. Previous work done by Boon *et al.* [60] showed that the wave speed changes linearly with temperature in aluminium plates. Thus, three steps were considered sufficient to investigate the trend in composite materials. The tests were performed on two different composite specimens: one hybrid laminate (layup :[±45° glass fibre, 0° carbon fibre, ±45° glass fibre]) and a sandwich panel consisting of two face sheets with the previously mentioned layup and a 2mm foam core (Rohacell 110A closed cell foam). The results from these tests were then compared with wave speeds predicted by FE models and, in the case of the hybrid laminate, with the results of the analytical method developed by Pant *et al.* [13].

Due to the specific conditions of the test (the panels had to be isolated in an environmental chamber), Lamb waves were generated using a piezoelectric transducer that was used so excite the specimens with a five cycle Hanning window [94]. The Hanning window was chosen due to its ability to focus the energy at the desired frequency and in order to prevent the excitation of higher modes. Three different frequencies of 150, 300 and 400 kHz were used in the tests. The window is mathematically described by the following equation:

$$H(t) = \frac{1}{2}\left[1 - \cos\left(\frac{2\pi f_{act} t}{n_c}\right)\right] \sin(2\pi f_{act} t) \tag{4.1}$$

where:

- f_{act} is the actuating frequency.
- t is the time.
- n_c is the number of cycles of the modulated sine wave.

The equation was implemented in a MATLAB code and used to generate data files which were then used as input for a wave generator. An example of a 5 cycle, 150 kHz Hanning window is shown in Figure 4-1.

Due to the anisotropy of the previously mentioned specimens, an array of piezoelectric sensors had to be used in order to show the difference in speed at different orientations. Thus, sensors were placed in the 0, 45 and 90° directions at a distance of 20 cm with respect to the source of the signal. Previous work done by Tsai [83] and Shen & Springer [95] found that, for FRP materials, fibre dominated properties are less sensitive to temperature changes than resin dominated properties.

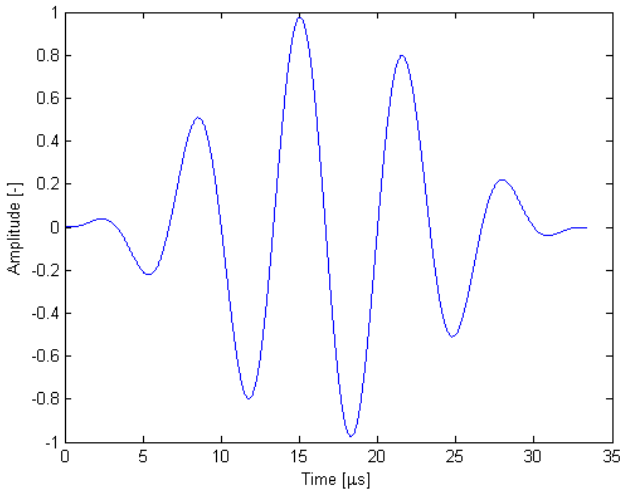

Figure 4-1: 5 cycle, 150 kHz Hanning Window

4.1.1 Threshold considerations

The AMSY-6 AE system uses a threshold approach to determine the Time Of Arrival (TOA) of a wave. This means that the user sets a value for the minimum threshold and if that value is surpassed at any point, the system records the hit and stores the subsequent transient recording of the signal. This approach does have some drawbacks however. If the threshold is set too low, the system may record unwanted signals that originate from the noise of the environment. If the threshold is set too high, the system may not start recording at the TOA but rather at a later time when packets of higher amplitudes hit the sensor.

Figure 4-2 shows the waveform of a Lamb wave propagating through a $[(0/90)_9]$ GFRP laminate. The threshold value used in this case was 0.1 mV. This value ensured that there were no false hits due to environmental noise. As can be seen from the figure, the amplitude of the signal is many times larger than the threshold value. Due to this fact, the TOA (indicated by the blue line) is quite accurate.

Figure 4-3 a) shows the waveform captured during one of the tests conducted on the sandwich panel. Due to the presence of the foam core the recorded signal is much weaker. The parallel lines showing the threshold value are clearly visible. The effect on the TOA can be better seen in Figure 4-3 b), which shows a close-up of the beginning of the signal. It can be seen that the recorded TOA is off by 3 µs from the actual TOA. In the case of this sandwich panel, this would amount to an error of around 300 m/s, an error that is of the same order of magnitude as the change due to temperature effects, as described in the results chapter.

It was therefore important to analyse each individual waveform in order to ensure the consistency of the results. Furthermore, it was important to set a standard point of measurement on the waveform in order to compare with the FEA results. All of the calculations were performed using the peak of the second wave packet. This was done due to the fact that the first wave packet is not clear in some cases due to the low amplitude of the signal.

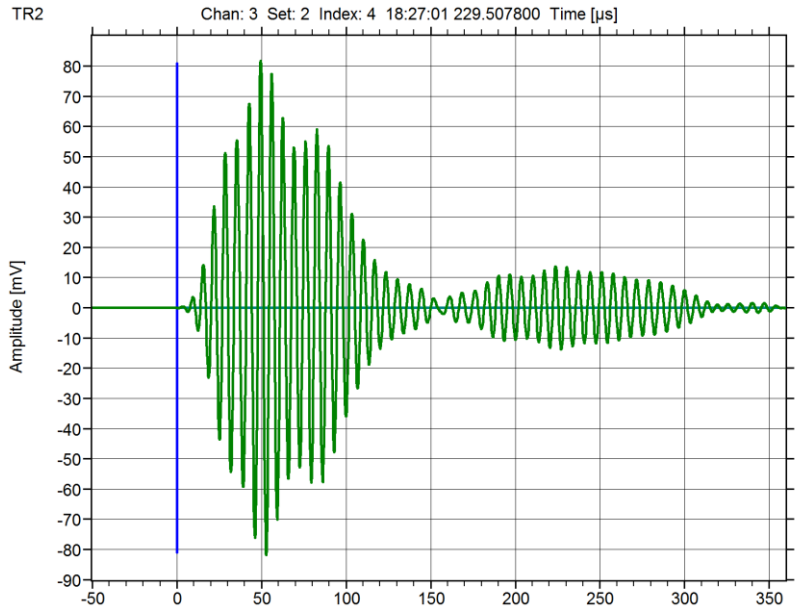

Figure 4-2: GF laminate waveform

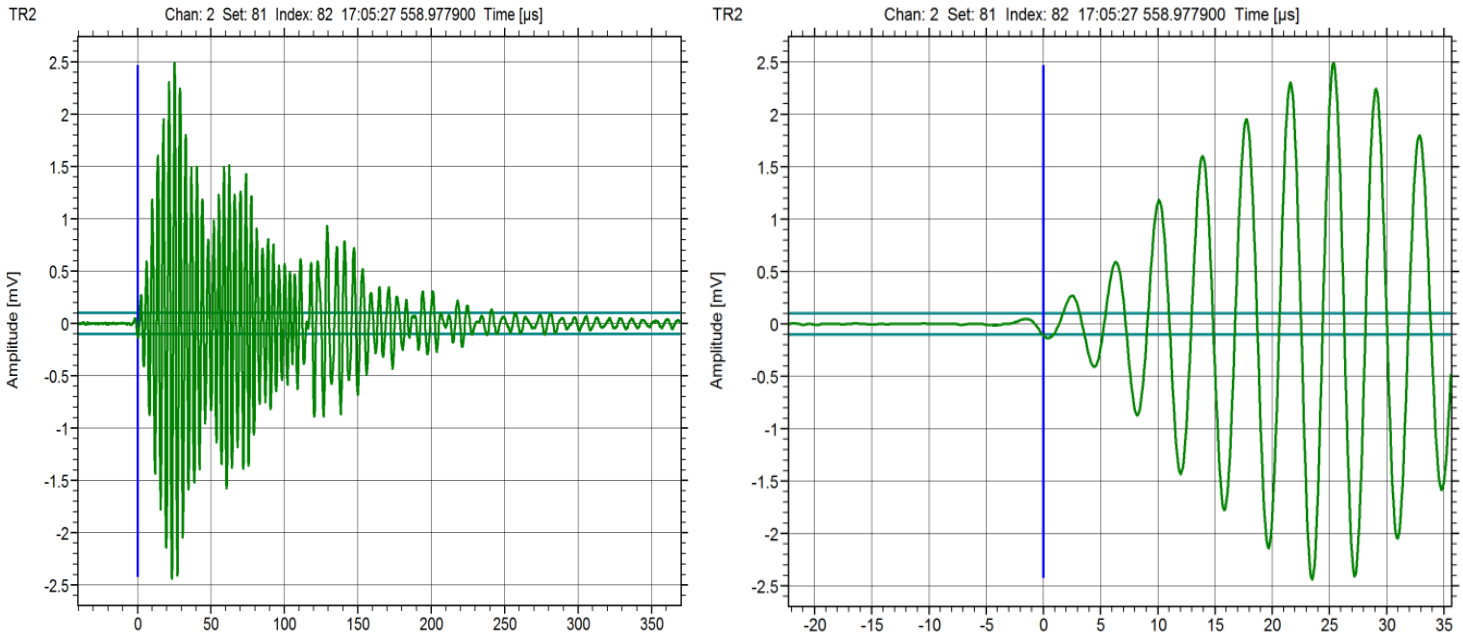

Figure 4-3: a)Sandwich panel waveform **b)Sandwich waveform close-up**

4.2 Analytical modelling

This section gives a short presentation of the method used to generate dispersion curves for the hybrid laminate. The approach presented here was derived by Pant *et al* [13]. For the full derivation of the equations, the reader is encouraged to see the referenced paper.

This method is based on the equations of linear 3D elasticity and uses a combination of two techniques to derive the Lamb wave equations: the partial wave technique and the Global Matrix approach. The partial wave technique assumes the superposition of three upward and three downward traveling waves. Due to the associated boundary conditions, the free surfaces reflect the waves and through interference of these reflections guided waves are formed.

The Global Matrix (GM) approach is used to assemble the equations derived for each of the n layers of the laminate. The method was first implemented by Randall [96] and has since become a standard method of modelling wave propagation phenomena in multilayered media due to its advantages over the alternative Transfer Matrix (TM) technique. The main advantage of the GM approach is that it is stable for large $frequency * thickness$ values. It is also advantageous due to the fact that the same matrix may be used for any kind of solution (response or modal, vacuum or solid half-spaces). Its main drawback is the computational load required to assemble and run the system of equations.

The derivation starts from the stress-strain relationship for a linear elastic anisotropic solid medium written in the tensor form:

$$\sigma_{ij} = c_{ijkl}\varepsilon_{kl} \tag{4.2}$$

$$\varepsilon_{ij} = s_{ijkl}\sigma_{kl} \tag{4.3}$$

After transforming each of the layers properties to a common global coordinate system and applying the previously mentioned methods, the whole problem is reduced to a matrix equation of the following form:

$$[Z]\{U\} = 0 \tag{4.4}$$

where:

- $[Z]$ is the Global Matrix.
- $\{U\}$ is the amplitude vector.

In order to find the Lamb wave dispersion curves, one must then solve:

$$|Z| = 0 \tag{4.5}$$

Due to the fact that the longitudinal and transverse velocities are coupled in the case of anisotropic materials, the Global Matrix has $6(n-1)$ equations and $6n$ unknowns. Thus, the equations need to be solved numerically in order to obtain the dispersion curves. This was also done by Pant *et al* as part of the same work using a MATLAB code based on the flow chart shown in Appendix A.

Using this code and the degradation factor approach presented in Section 2.2.3, the dispersion curves that were used in this study were generated. An example of the dispersion curves of the S_0 mode of a UDCF laminate for different temperatures is shown in Figure 4-4.

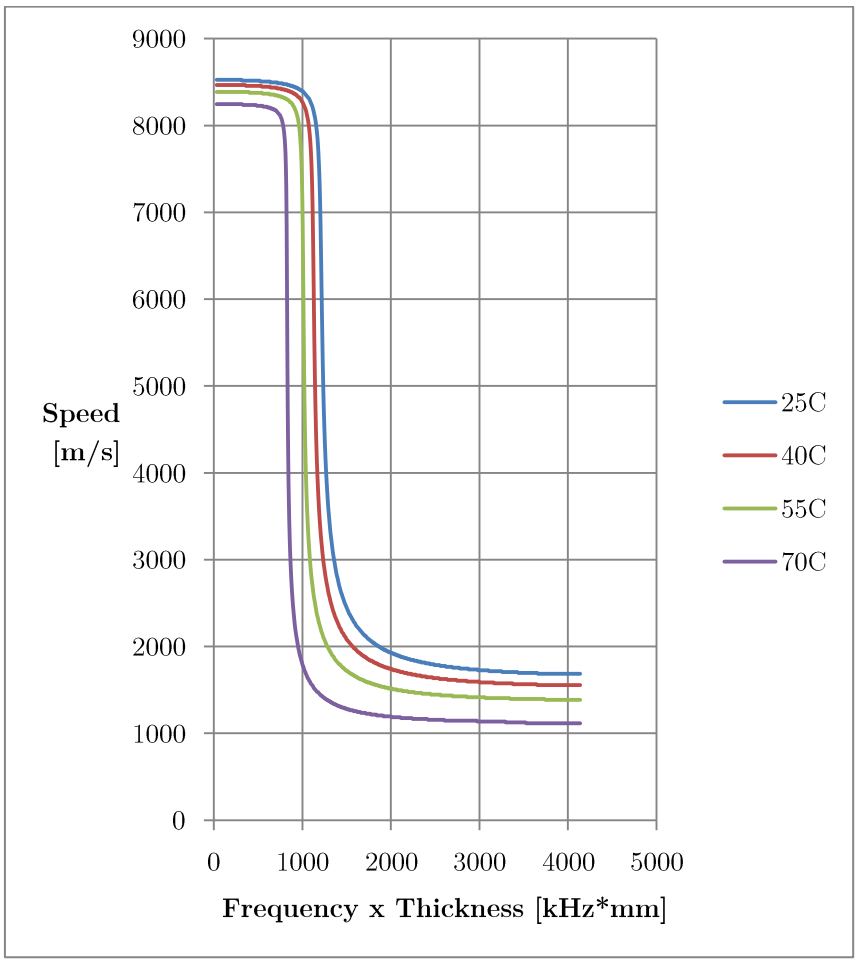

Figure 4-4: S_0 phase velocity dispersion curves for a UDCF laminate at different temperatures

4.2.1 Group velocity variation in the 45° direction

After initial comparisons between the analytical results and experimental data on several types of laminates with various degrees of anisotropy, it was found that there was a significant error for predicted speeds in the 45° direction, especially for the UDCF laminate.

The cause of this error was a phenomenon that occurs in anisotropic media. Due to the variation of the material properties the wave generated by a point source does not propagate in a circular shape. This means that there is a difference between the direction of the phase velocity (which is normal to the wave front) and the group velocity (which indicates the energy flow direction – it is the given by a straight line from the source to the wave front). This incompatibility, which is illustrated in Figure 4-5, is most evident in laminates with high degrees of anisotropy. It was found in the work done by Rhee *et al* [97] that the effect in quasi-isotropic laminates is much smaller.

Despite this error, the results for the 45° direction were still used because the focus of this work was the relative changes of the group velocity with temperature.

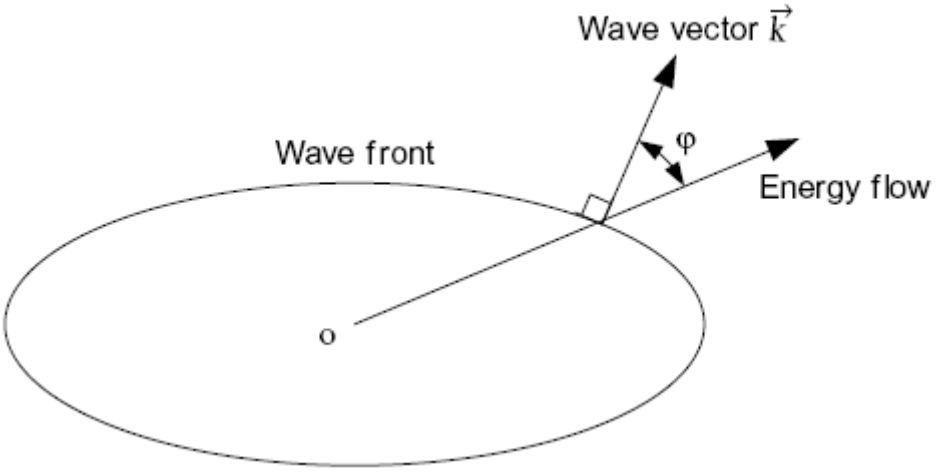

Figure 4-5: Difference between phase and group velocity directions

4.3 FE modelling

This section describes the FE models that were set up in order to verify the experimental results. Two models were constructed using the Abaqus/CAE® environment: one full model of the hybrid plate and one quarter model for the sandwich panel. The sandwich panel was modelled using symmetry boundary conditions due to the large amount of computational resources needed to run a full sandwich model. The analyses were performed on the cluster and on special computers with the following specifications: Intel® Xeon E5-1620 CPU with 8 cores and 64 GB of RAM.

4.3.1 Geometry

Hybrid model

The hybrid model consists of a square plate with sides of 300 mm and a thickness of approximately 0.86 mm. The sensors were placed at the locations shown in in order to achieve a distance of 200 mm between each sensor and the source of the signal.

Table 4-1: Sensor locations

Element	Coordinates (x;y) [mm]
Actuator	(50;50)
Sensor 0 direction	(250;50)
Sensor 45 direction	(141;141)
Sensor 90 direction	(50;250)

The hybrid model is shown in Figure 4-6 together with the array of sensors. The plies of the laminate are orientated with respect to the x direction.

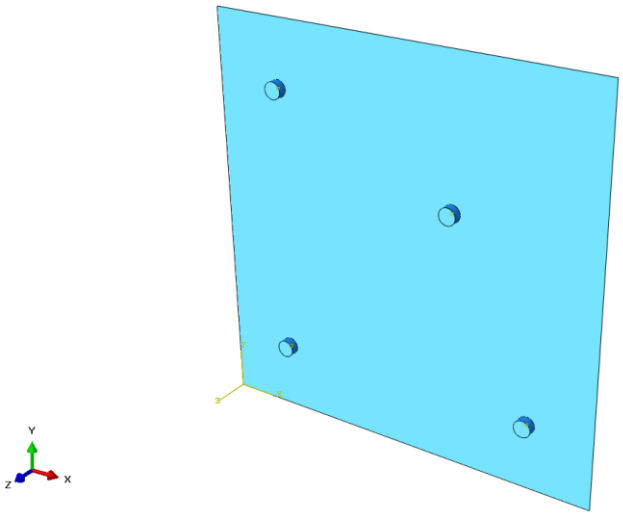

Figure 4-6: Final assembly of the hybrid model with piezoelectric elements

Sandwich model

The sandwich panel used in the test had a size of 600x600 mm^2 and a thickness of approximately 3.5 mm. In order to reduce the amount of computational resources needed to run the FE simulations of this model, only one quarter of the panel was modelled using appropriate symmetry conditions. The array of sensors was placed in the same way as for the hybrid model, with the added mention that only one quarter of the actuator and half of the sensors in the 0 and 90 directions were modelled due to the same symmetry conditions.

The computational power needed to run the quarter model for the higher frequencies of 300 and 400 kHz was still very large due to the factors mentioned in Section 4.3.4. Due to this fact, it was decided to further reduce the number of elements by modelling only a 220x220 mm^2 section of the panel and using special elements at the edges in order model infinite boundary conditions in order to avoid unwanted reflections. The symmetry boundary conditions were applied on the AB and AD edges that coincide with the directions of the x and y axes of the coordinate system shown in Figure 4-7, while the infinite boundaries were modelled on the BC and BD edges. The degrees of freedom that were suppressed are shown in Table 4-2.

Table 4-2: Symmetry boundary conditions

Edge	Symmetry	U_1	U_2	U_3	UR_1	UR_2	UR_3
AB	Y	0	-	-	-	0	0
AD	X	-	0	-	0	-	0

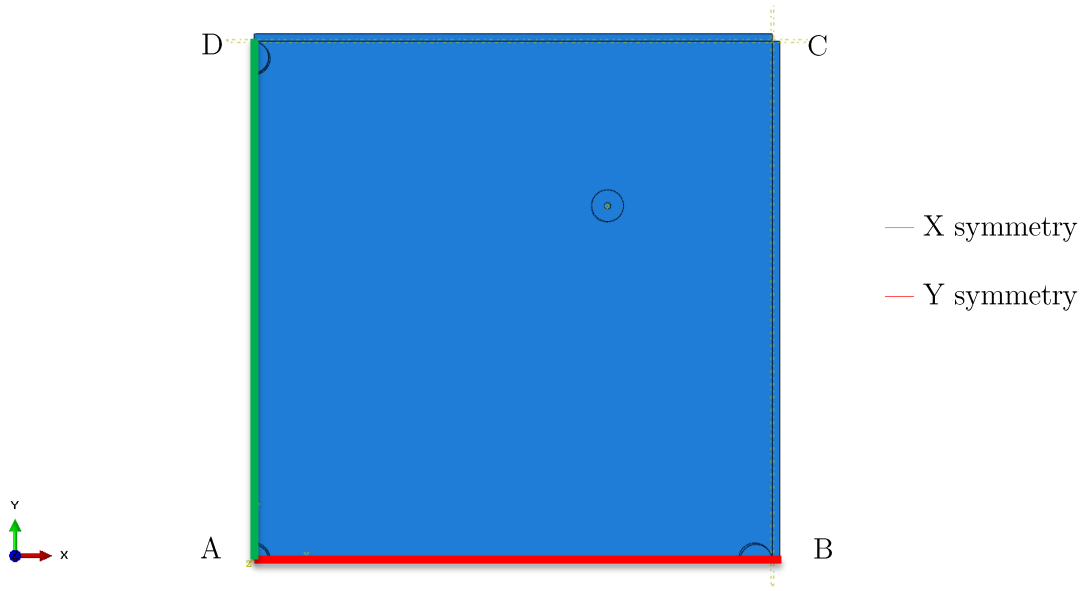

Figure 4-7: Final assembly of the sandwich model with piezoelectric elements and infinite BCs

The face sheets of the sandwich panel were modelled using the "Skin" feature in Abaqus/CAE. When the mesh was applied, the face sheets shared nodes with the top and bottom parts of the foam thus reducing the computational load of the analysis.

Piezoelectric transducers

Two types of sensors were used in this work, both manufactured by Vallen Systeme. They were modelled in Abaqus using only the piezoelectric part and had the following geometry: the VS 150-M sensors had a cylindrical shape with a diameter of 12.7 mm and a height of 6.35 mm, while the VS 900-M sensors had a ring shape with an outer diameter of 12.7 mm, inner diameter of 2.6 mm and a height of 3.8mm. A meshed model of a VS 150-M sensor can be seen in Figure 4-8.

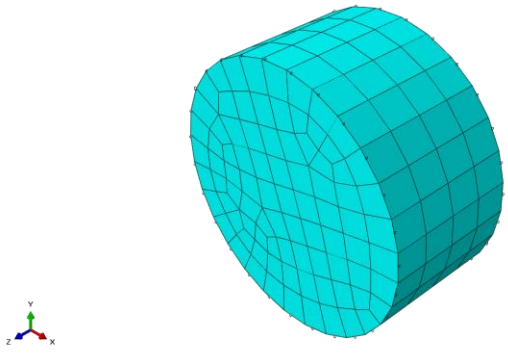

Figure 4-8: Meshed model of a 150-M piezoelectric element

The poling direction of the material was orientated along the z axis shown in the figure above.

4.3.2 Material properties

As mentioned before in Chapter 3, most of the material properties of the CF and GF layers were determined through experimental tests conducted according to ASTM standards. The overview of these material properties was already presented in Section 3.3.3. However, for the sake of clarity they are presented once more together with the predicted values for the -40 and 70° C temperature steps in Table 4-3 . These values were calculated using the temperature degradation factor mentioned in Section 2.2.3. The Poisson's ratios and the densities are not shown in this table due to the fact that they were assumed to remain constant.

Table 4-3: Material properties at different temperatures

	E_1 [GPa]			E_2 [GPa]			G_{12} [GPa]		
T [°C]	-40	25	70	-40	25	70	-40	25	70
CF	122.7	119	111.8	12.2	8.34	3.83	6.58	4.5	2.06
GF	24.74	24	22.55	23.71	23	21.61	5.75	3.93	1.8

Table 4-4: Material properties at different temperatures

	G_{13} [GPa]			G_{23} [GPa]		
T [°C]	-40	25	70	-40	25	70
CF	3.28	2.24	1.02	3.67	2.15	1.15
GF	3.28	2.24	1.02	3.67	2.15	1.15

In order to model the piezoelectric elements, a number of specific properties were required. The sensors were made using the NCE51 PZT material manufactured by Noliac Group [98]. The material properties listed in Table 4-5 were obtained from the material datasheet found in Appendix B. A short introduction to piezoelectric materials and the physical significance of the properties listed below was given in Section 2.1.6.

Table 4-5: Elastic stiffness matrix of the NCE 51 material

D_{ij} [10^{10} N/m^2]					
13.2	8.76	7.34	0	0	0
8.74	13.2	7.34	0	0	0
7.34	7.34	16.2	0	0	0
0	0	0	4.37	0	0
0	0	0	0	4.37	0
0	0	0	0	0	2.24

Table 4-6: Charge constant matrix of the NCE 51 material

d_{ij} [10^{-12} C/N]					
0	0	0	0	669	0
0	0	0	669	0	0
-208	-208	443	0	0	0

Table 4-7: Electrical permitivities

ε^T [10^{-8} F/m]	
ε_{11}^T	1.72
ε_{22}^T	1.72
ε_{33}^T	1.68

4.3.3 Analysis type and Boundary conditions

Several boundary conditions were necessary in order to model the wave propagation. Most of these are common between the two models. Simply supported conditions were applied to the two edges on which the specimens were standing on. Furthermore, in order to measure or apply a voltage difference to the piezoelectric elements, a zero electric potential boundary condition was applied on the bottom surface of each sensor. The sensors were connected to the upper surface of the plates using the Tie constraint within Abaqus, which assumes perfect contact between the two surfaces. All of these boundary conditions were applied in the Initial step.

Due to the fact that wave propagation is a time dependent process, a Dynamic/Implicit type analysis was chosen for the second step. The boundary condition for the actuation process was defined here. Using the data previously determined by the MATLAB code, Hanning windows of 150, 300 and 400 kHz and amplitude of 40 Vpp were applied to the upper surface of the actuator. The amplitude of the signal was determined by the maximum output that the wave generator and amplifier could provide. The waveforms of these Hanning windows, as they were implemented in the FE models, can be seen in Figure 4-9. The waveforms were plotted on the same graph in order to illustrate the difference between the 3 signals.

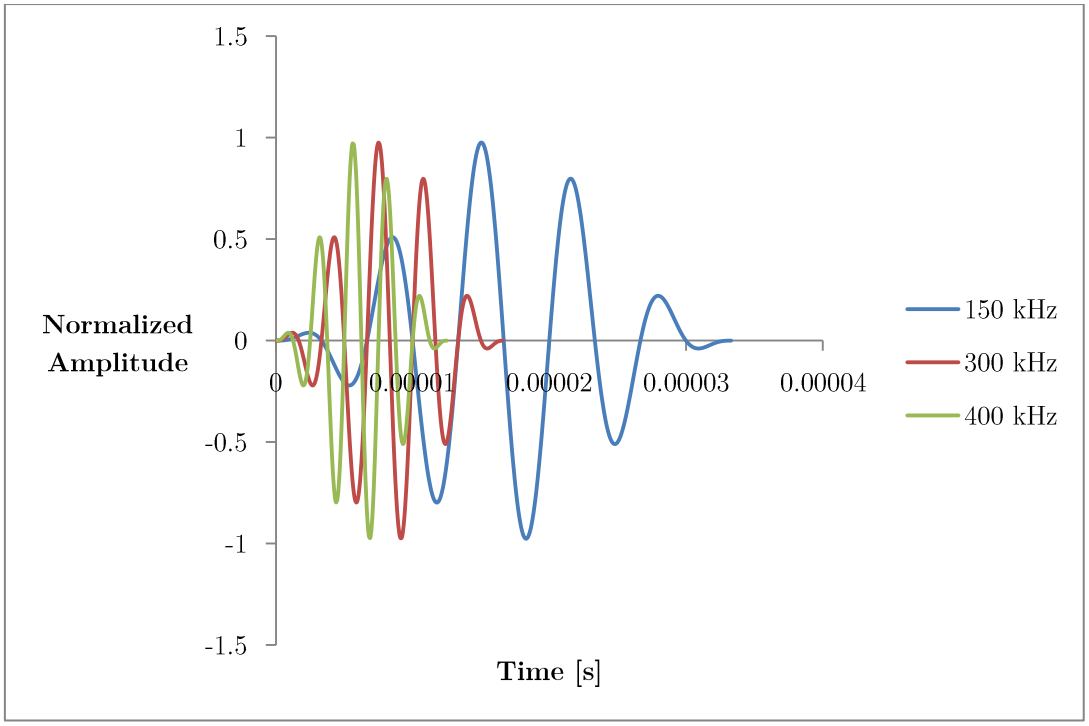

Figure 4-9: Hann window waveforms

4.3.4 Mesh size and time step considerations

All of the parts were meshed using rectangular elements of different types depending on their geometry and material properties. The hybrid laminate and the face sheets were modelled using the 4 node S4R shell elements with reduced integration (5 integration points) and hourglass control. The foam was modelled using the 8 node C3D8R solid elements with reduced integration and hourglass control. Finally, the piezoelectric transducers were modelled using the 8 node C3D8E elements and the infinite edges using CIN3D8 elements.

In order to ensure the stability of the analysis, certain restrictions had to be applied to the sizes of the elements and the time step of the analysis. Chen *et al.* [99] stated that 10 nodes per wavelength were sufficient to achieve a good spatial resolution and also found that a minimum of 20 points per cycle at the highest frequency must be used to ensure time stability. These two conditions can be expressed in the following equations:

$$L_e = \frac{v_p}{10 f_{max}} = \frac{\lambda_{min}}{10} \tag{4.6}$$

$$\Delta t = \frac{1}{20 f_{max}} \tag{4.7}$$

where:

- v_p is the minimum phase velocity of interest.
- f_{max} is the maximum actuating frequency.
- λ_{min} is the minimum wavelength.

Using these equations, the maximum sizes of the elements were calculated for each of the frequencies under investigation. The results and the final values used in the FE models are shown in Table 4-8.

Table 4-8: Element sizes and time steps of the analyses

Frequency [kHz]	Max element size [mm]	Used element size [mm]	Max time step [µs]	Used time step [µs]	Average run time [hours]	
					Hybrid	Sandwich
150	1.6	1	0.33	0.1	3	33
300	0.7	0.6	0.16	0.1	9	41
400	0.6	0.6	0.125	0.1	10	42

The time step was set at 0.1 µs for all of the analyses for convenience. The analyses in the case of the 150 kHz frequency were reasonable in computational load even with this time step, while 300 and 400 kHz cases required a maximum time step of 1.66 and 1.33 µs respectively. The maximum element size had the greatest influence on the computational load of the analyses.

4.4 Experimental setup

This section describes the experimental setup, all of the different systems that were used to and also provides a detailed description of the process used to perform the measurements.

4.4.1 Vallen AMSY—6 AE system [100]

The AMSY-6 is a multi-channel AE measurement system that consists of 8 parallel measurement channels and front end software used for post-processing of the measurements. A measurement channels consists of a sensors, a pre-amplifier and a channel of an ASIP-2 (acoustic signal processor). Through a combination of an analogue measurement section and a digital signal-processing unit, the system is able to extract and store AE signal features such as the ones mentioned in Section 2.1.4.1 (arrival time, peak amplitude, energy etc.). The system is also capable of storing the complete waveform of the signal which is very useful in light of the observations made in Section 4.1.1.

4.4.2 Acoustic emission sensors and pre-amplifiers

An AE system requires sensors that are capable of converting surface displacement into electrical signals. The sensors used by Vallen are manufactured out of piezoelectric materials due to their inherent physical property of generating an electric signal when a strain is applied. The AMSY-6

is capable of working with different sensors, designed for a wide range of applications. In the case of the work presented here, it was important to use sensors that could be operated within the previously mentioned range of -40 to 70° C. Thus, the VS-150 M and VS-900 M sensors were used. Both sensors have an operating temperature between -50 to 100.

AE pre-amplifiers are used as an intermediary between the sensors and ASIP-2 channel. Their purpose is to amplify the output of the sensor in order to match the input requirements of the channel, while also achieving the highest possible signal-to-noise ratio.

4.4.3 Environmental chamber

The system used to control the temperature of the specimens is shown Figure 4-10. It consisted of an environmental chamber constructed out of URSA XPS [101] extruded polystyrene and a temperature cycling unit manufactured by CTS [102]. The unit was connected to the chamber using two attachable tubes to ensure a good air flow. The plates were allowed to stabilize once the desired temperature was reached and the machine was turned off in order to minimize the noise that was detected by the sensors.

Figure 4-10: Environmental chamber and temperature cycling unit

4.4.4 Thermocouples

Due to the fact that the temperature cycling unit was not capable of measuring the temperature inside the climate chamber and the fact that the specimens took longer to reach the desired temperatures than the air flowing around them, three thermocouples were used in order to accurately monitor the plates. K type thermocouples were used due to their sensitivity and accuracy in the temperature range. They were connected to a Keithley data acquisition system which was in turn connected to a PC. A customizable software on the PC then converted the

electrical signal recorded by the acquisition system into temperatures. The thermocouples were placed as close as possible to the directions of interest (0, 45 and 90°). Measurements were taken every 30 seconds.

4.4.5 Signal generator and Amplifier

An Agilent 33500B Series waveform generator was used to actuate the Hanning window and an Agilent 33502A external amplifier was used to achieve a higher peak-to-peak voltage. This equipment was necessary because the AMSY-6 system does not have the capability of sending customized signals to the piezoelectric elements. The system does have a pulsing function, however only two actuation frequencies are available.

All of the previously mentioned systems can be seen in Figure 4-11 which shows the general setup of the experiment.

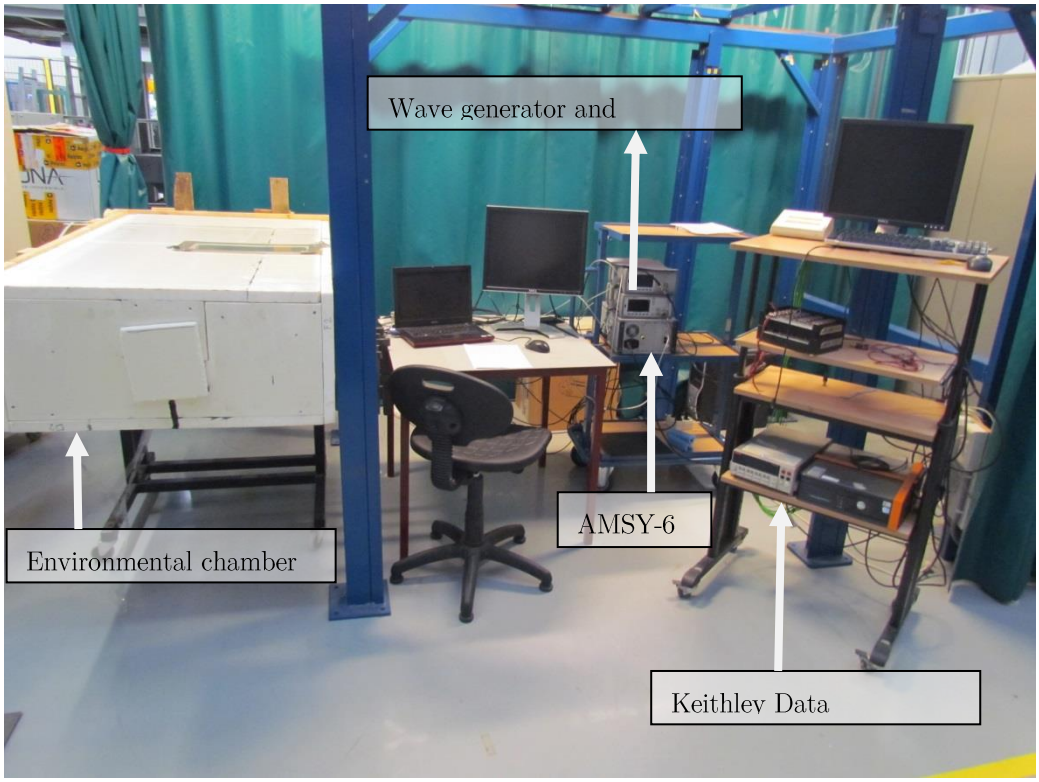

Figure 4-11: General test setup

4.4.6 *Bonding agent*

The bonding between the piezoelectric elements and the investigated specimens was very important. It was necessary to achieve a good bond quality while at the same time maintaining that quality through the temperature changes and also allowing an easy removal of the sensors to avoid damaging them. To this end, the Dow Corning® Epotek 734 flowable silicone adhesive sealant was used. The main advantages of this bonding agent are:

- stable from -65°C to +180° C.
- easy to apply and fairly easy to remove due to the fact that it cures to a tough, flexible rubber state.
- cures at room temperature.

4.4.7 *Measurement setup*

This section gives a detailed description of the standard procedure used for each measurement together with the standard settings used for the systems involved in the measurement.

Before bonding, the sensor positions were drawn as accurately as possible in order to ensure that the distance between them is close to 20 cm, the standard distance used in these tests. As mentioned before, 4 transducers were used: one used to actuate the signal and 3 used to measure the propagated signal (one for each of the 0, 45 and 90° directions). The sensor setup can be seen in Figure 4-12. The picture also shows the locations where the thermocouples were attached. The thermocouples were attached using two layers of tape due to the fact that electrically conductive materials interfere with the measurements.

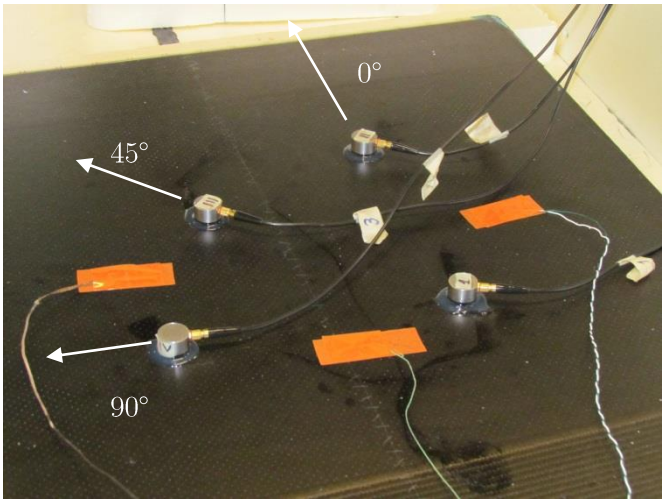

Figure 4-12: Sensors and thermocouples ready for testing

The settings used for the AMSY-6 AE system were:

- sampling rate of 10 MHz.
- maximum number of samples per set 4096.
- transient recording was enabled
- the threshold value was set to 40 dB while the average noise level was around 30 dB.
- the Duration Discrimination Time and the Rearm Time values were left as the default values for composite structures: 200μs and 0.4 ms respectively.
- 400 pre-trigger samples were recorded in order to facilitate the analysis of the waveforms that had a late TOA.

The settings used for the Agilent 33500B wave generator were:

- custom Arb. waveforms with frequencies of 150, 300 and 400 kHz generated using data files from the MATLAB code mentioned in Section 4.1.
- signal amplitude of 20 Vpp (maximum setting).
- sampling rate of 250 MHz (maximum setting).

The settings used for the Agilent 33502 amplifier were:

- DC coupling.
- impedance set to high.

The three sensors were connected to ports 2, 3 and 4 of the AMSY-6 system through the pre-amplifiers.

A splitter was used for the output of the wave generator. From here, one cable went to amplifier, which amplified the signal to 40 Vpp and then sent the signal to port 1 of the AE system, while the other cable went to the actuator. Through this method, the actuation time was precisely recorded.

All of the measurements were recorded on a laptop and post-processed using the VisualAE application that comes with the AE system.

5 Results

As mentioned before in Sections 1.3 and 4.1, the wave velocity measurements were performed on two types of specimens: a hybrid laminate and a sandwich panel with a foam core and face sheets with the same layup as the hybrid laminate. This chapter is focused on presenting the results of the experiments as well as the models. Section 5.1 shows the analytical, FEA and experimental results for the hybrid laminate. Section 5.2 shows the FEA and experimental results for the sandwich panel.

5.1 Hybrid wave velocities

In this section the results of the tests performed on the hybrid laminate are presented. The wave speeds from the experiment, FEA and analytical method are plotted on the same graph for the 150 kHz signal and the three directions of interest. The results for the 300 and 400 kHz signals are shown in Appendix C – Hybrid laminate 300 and 400 kHz resultsdue to the fact that they did not show any significant difference compared to the 150 kHz case.

5.1.1 Temperature dependence

Figure 5-1 shows the influence of temperature on the group velocity in the range of -40° C to 70° C in the 0 direction of the hybrid laminate, for a frequency of 150 kHz. The analytical results were obtained using the method derived by Pant [13], previously presented in Section 4.2, and using material properties determined using the approach described in Section 2.2.3. The FEM results were obtained by running individual simulations for each of the data points using the same adjusted material properties. The experimental values were obtained by taking the average of different measurements. For each temperature step, a signal was actuated and received every second.

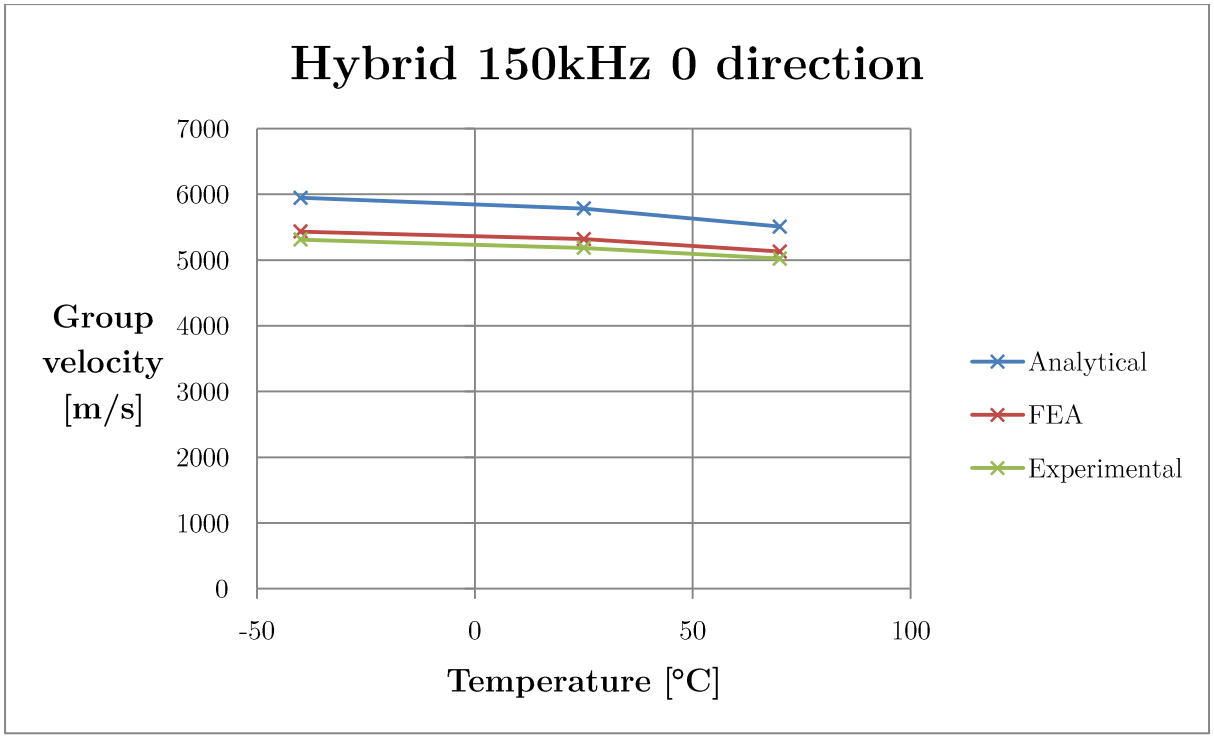

Figure 5-1: Velocity vs temperature graph for the 150 kHz signal in the 0 direction

Firstly, it can be observed is that there is a constant difference of around 10% between the results of the analytical method and the results of the experiments. This difference can be attributed to some of the assumptions that are made when setting up the equations. The method was designed to perform optimally for quasi-isotropic laminates. The hybrid laminate used in these tests is highly anisotropic: there is a significant difference between the stiffness of the 0, 45 and 90 directions. The 0 direction's stiffness comes mainly from the CF layer, the 45 direction's stiffness is given by the two GF weave layers, while the 90 direction is mostly resin.

The results of the FEA are much closer to those of the experiments, with a difference of around 3% at 25°C. This difference is well within the expected error of the measurements due to uncertainties such as: material properties, accuracy of the sensor positions.

The second observation that can be made is that the group velocity is linearly dependent on the temperature of the medium in which the waves are propagating. More precisely, the speed increases with decreasing temperature and decreases with increasing temperature. From a physical point of view this makes sense. By increasing the temperature, the volume of the polymeric matrix tends to increase leading to a slightly increased Time Of Flight (TOF). An example of how this effect can be observed is shown in Figure 5-2. The plot shows the transient response of the piezoelectric sensor corresponding to the 0 direction at temperatures of 25°C(blue) and 70°C(red) as predicted by the FEA. The difference between the TOF of the two signals is around 1.4 µs.

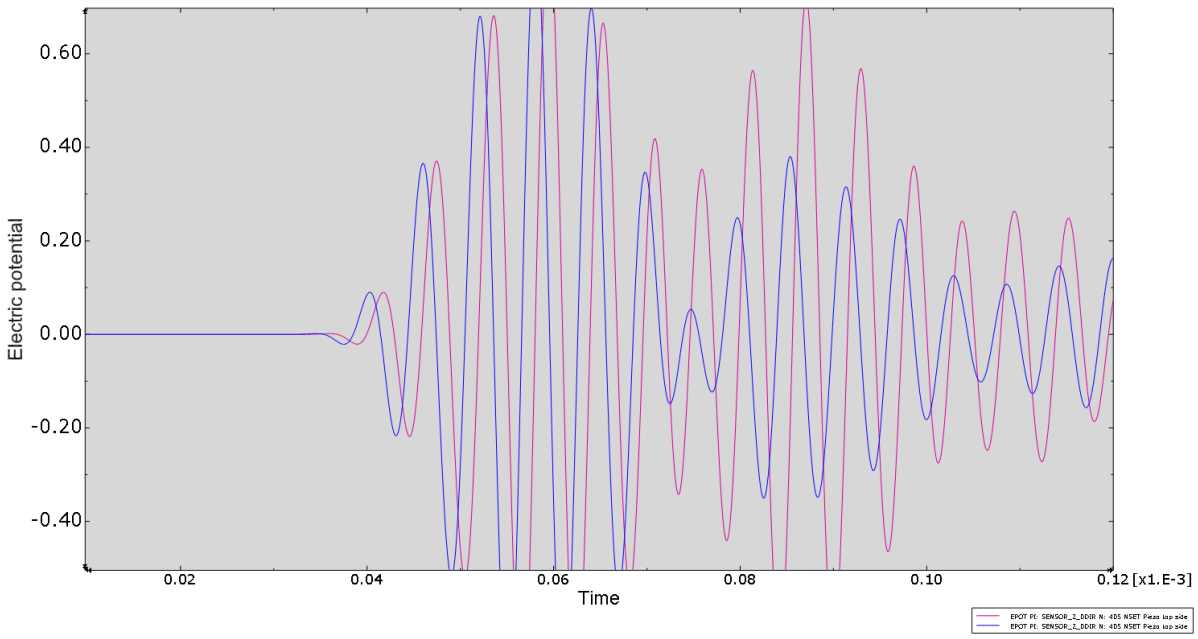

Figure 5-2: Hybrid laminate FEM waveforms at 25°C(blue) and 70°C(red)

The previously mentioned trend was captured by both the analytical approach and FEA with different degrees of accuracy. As can be seen in Figure 5-3, the analytical approach has a tendency to exaggerate the effects when compared to the FEA. The figure shows the wave velocity values normalized with respect to the 25°C temperature step and gives insight into the slopes of the curves shown in Figure 5-1. For example, we can see that at 70°C the experimental data showed a reduction of around 3% in the speed, while the FEA and analytical approach predicted drops of 3.5% and 5% respectively.

The results also indicated that both modelling techniques are slightly more accurate at lower temperatures, such as -40°C. This can be observed especially in the graphs for the 45 and 90 directions. The fact that this effect is present in both models suggests that the predicted values of the material properties for high temperatures are not as accurate as for lower temperatures. This can be attributed to the way the degradation factor is calculated using the glass transition temperature. The T_g of the resin used in this work was 82°C, while the highest temperature step was at 70°C.

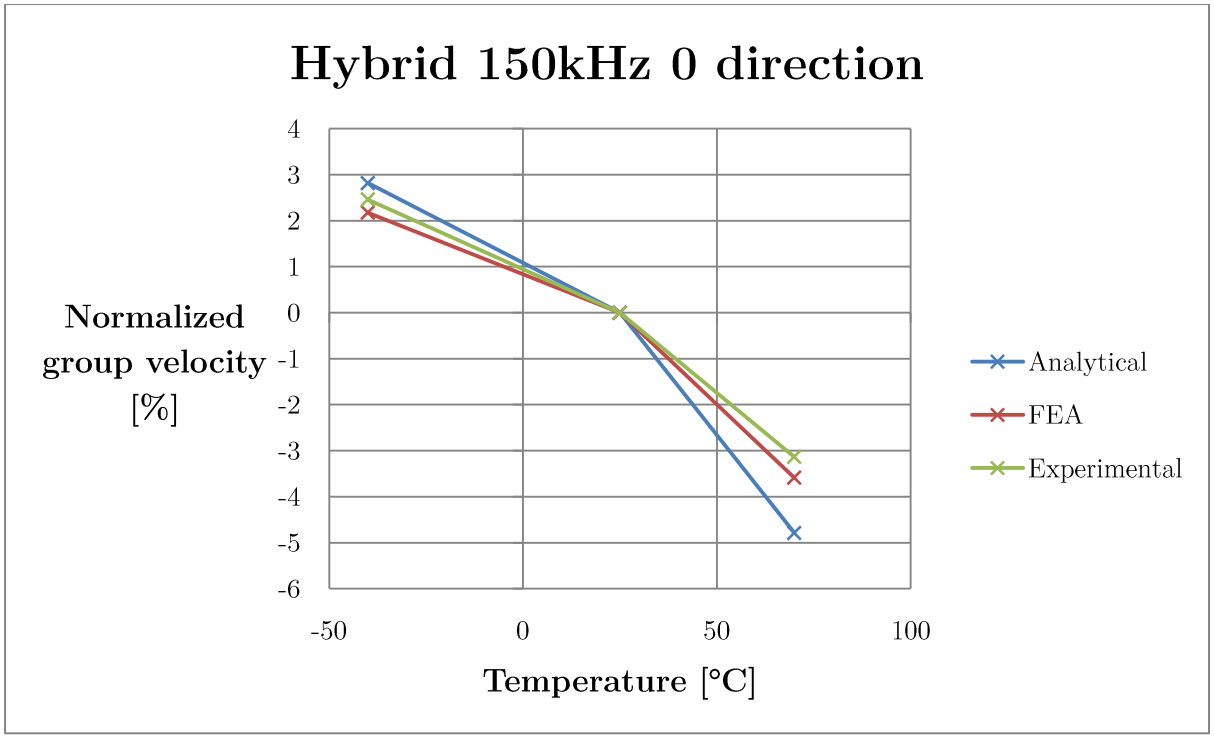

Figure 5-3: Velocity rate of change for the 150 kHz signal in the 0 direction

Figure 5-4 show similar results, this time for the 45° direction. As mentioned before in Section 4.2 the analytical model does not accurately predict the velocity due to the difference of direction between the phase velocity and the group velocity. In spite of this error, it is still interesting to look at the relative change of the speed due to temperature as this should not be influenced by the error as much.

From the two graphs we can see that there is a 5% increase in speed at -40°C in the experiment, while both models predict an increase of 6%. At 70°C, the experimental results showed a drop of around 5% while the FEA and the analytical model predicted drops of 8% and 12%. Once again the results at higher temperature show a larger deviation from the experimental values. This can be attributed to the same factors mentioned before with a larger effect due to the much lower stiffness of the GF layers.

All of the results are once again in line with the expected trend.

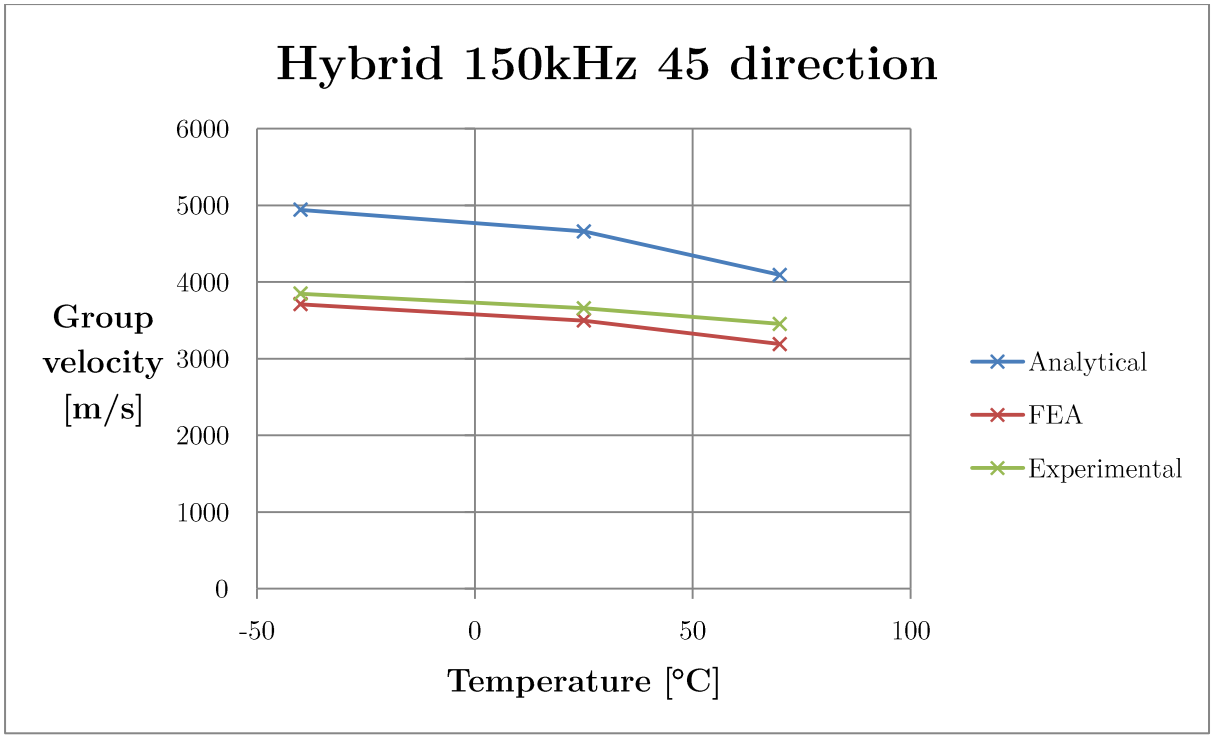

Figure 5-4: Velocity vs temperature graph for the 150 kHz signal in the 45 direction

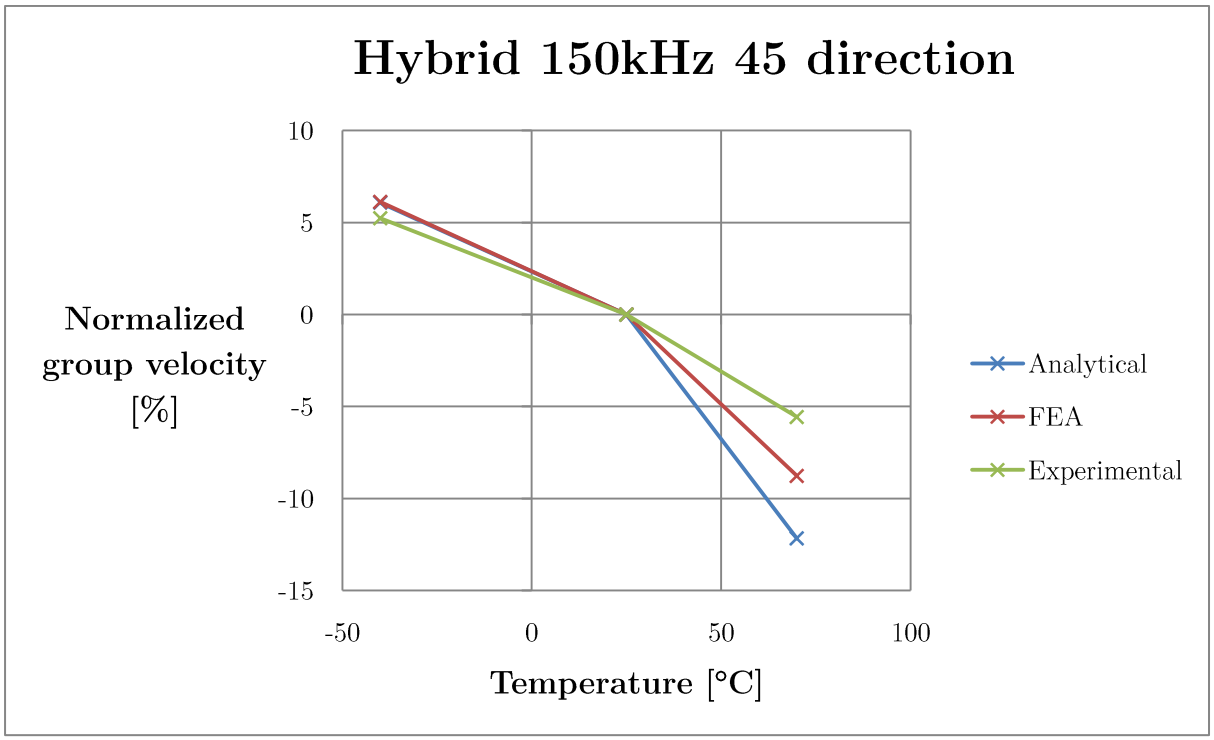

Figure 5-5: Velocity rate of change for the 150 kHz signal in the 45 direction

Finally, Figure 5-6 show the results for the 90° direction. Once again, the FEA results follow the experimental data quite closely, while the analytical exaggerates the effects of the temperature change even more, predicting a decrease in speed of 34% at 70°C as opposed to the 7% observed in the experiments. This suggests that the analytical method cannot reasonably predict the change in speed with temperature for orientations that have a much lower stiffness compared with the main direction of the laminate.

As mentioned at the beginning of this section, the 300 and 400 kHz cases showed similar results and trends and were therefore not reproduced here.

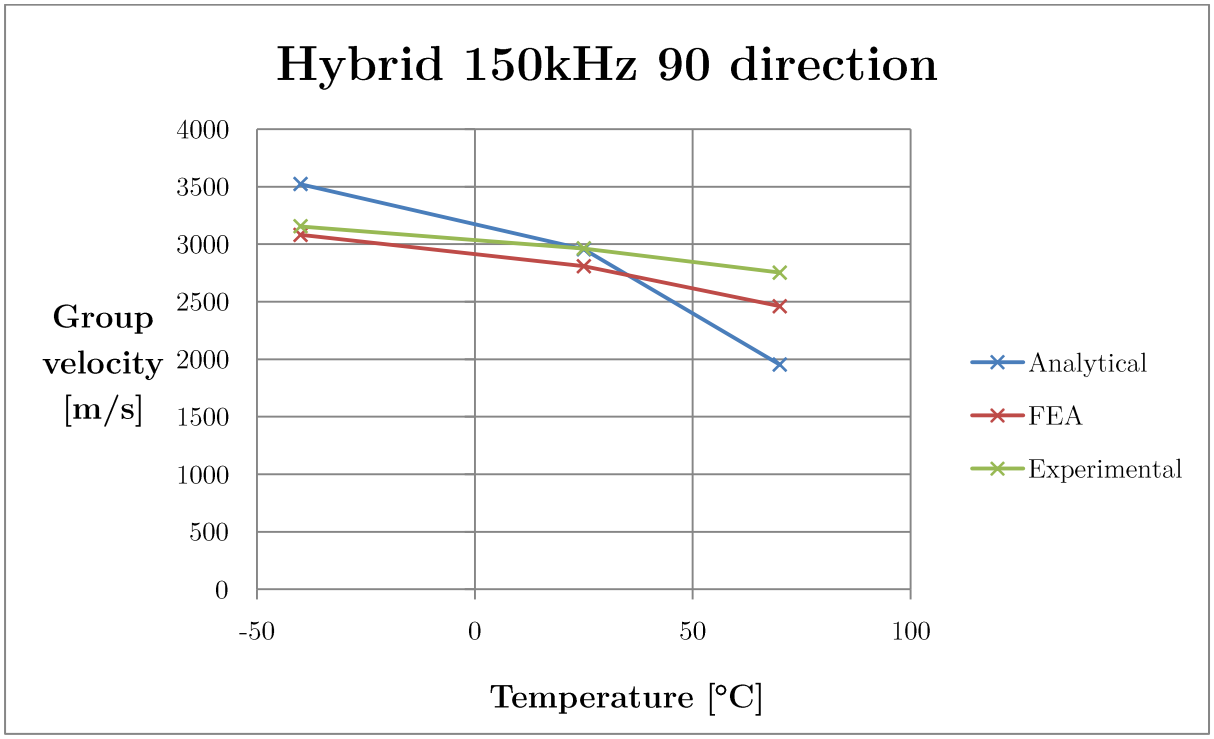

Figure 5-6: Velocity vs temperature graph for the 150 kHz signal in the 90 direction

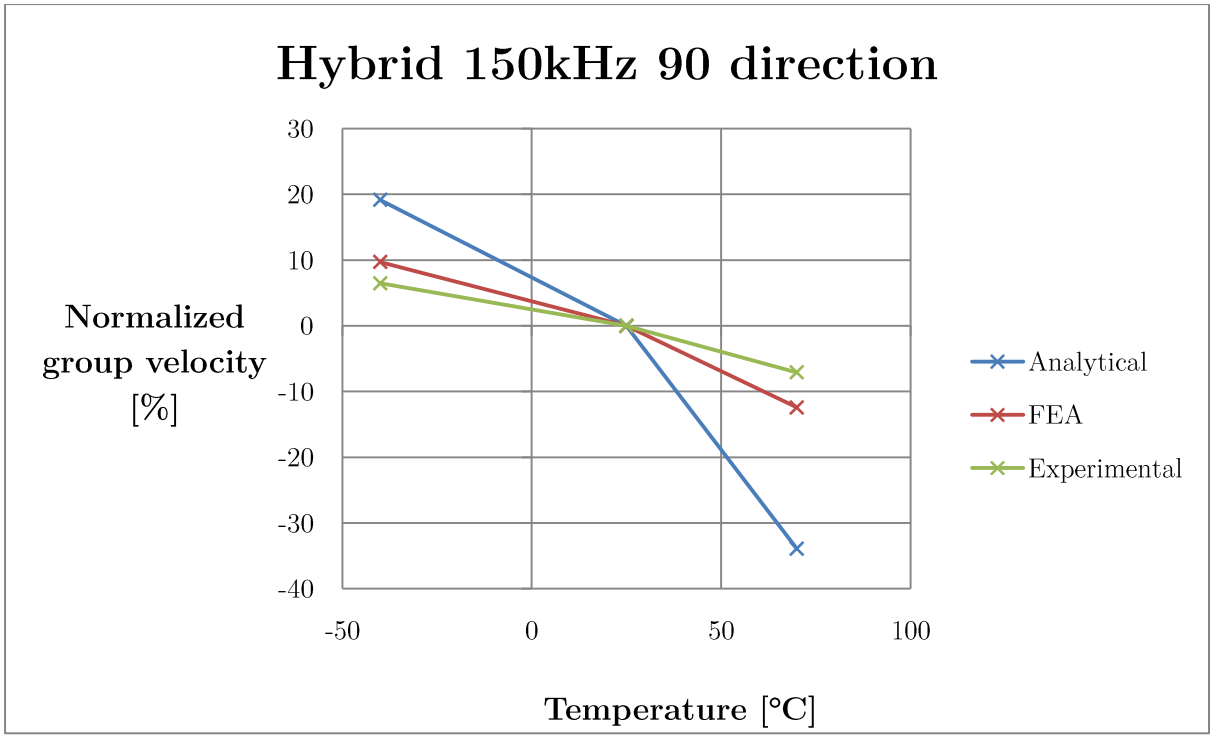

Figure 5-7: Velocity rate of change for the 150 kHz signal in the 90 direction

5.1.2 Directional dependence

In order to help put into perspective the results of the temperature dependency tests from a SHM point of view, the variation of the group velocity with respect to the material orientation is shown in Table 5-1 . Only the results of the 25°C case are shown.

Table 5-1: Experimental wave speeds 25° C case

	Speed [m/s]		
Frequency [kHz]	0°	45°	90°
150	5184	3657	2963
300	5277	3673	3084
400	5238	3629	3062

The experimental results show that there is a 42% drop in speed in the 45° direction and a 75% drop in speed in the 90° direction compared to the main direction of the laminate. These variations are significantly larger than the ones due to temperature changes. This difference can be observed in Figure 5-8, which shows the in plane displacements generated by a 150 kHz signal in the hybrid panel. As mentioned in Section 2.1.3, these in plane displacements correspond to the S_0 mode. The elliptical shape of the wave front makes it easy to see the difference in speed between the different directions.

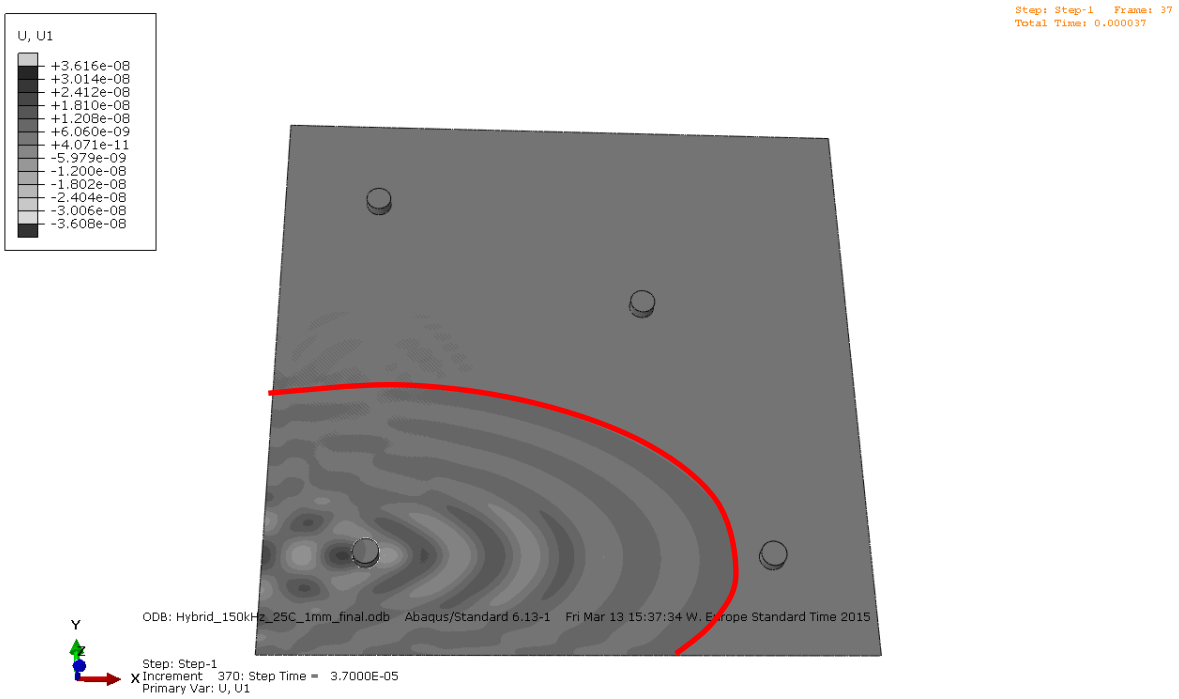

Figure 5-8: S_0 wave front

Similarly, the A_0 mode can be visualized by looking at the out-of-plane displacements. Figure 5-9 shows these displacements for the same case as before. It is clear that the wave front has an almost circular shape, which means that the group velocity of this mode remains fairly constant at different orientations. This is consistent with results found in literature, such as the ones from Arredondo & Fritzen [70].

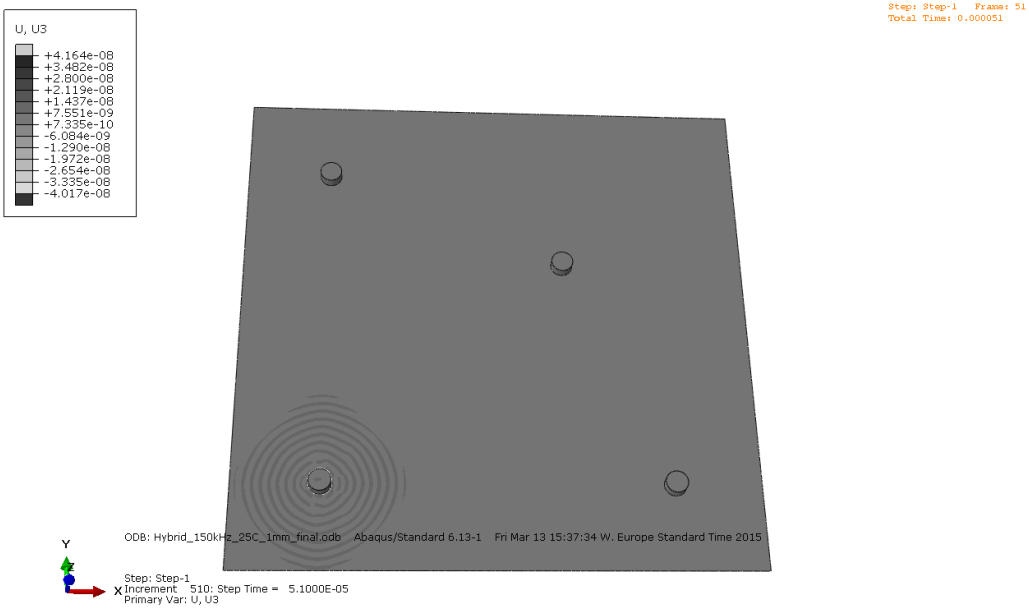

Figure 5-9: A_0 wave front

5.2 Sandwich wave velocities

In this section the results of the tests performed on the sandwich panel are presented. In this case only the results of the experiment and the FEA are compared. An attempt was made to use the same code to generate dispersion curves for the sandwich panel however the solution was unstable and did not give any meaningful results.

5.2.1 Temperature dependence

The results obtained using the sandwich panel generally follow the same trend that was observed in the case of the laminate: the velocity decreases with increasing temperature. There are also some differences that can be observed while analysing the graphs in this section.

The main observation that can be made is that there is 15 to 20% reduction in the group velocity due to the presence of the core. This is to be expected considering the lower mechanical properties of the core. The presence of the core also has a significant effect on the amplitude of the signals which tend to be around 20% lower than in the case of the laminate.

Figure 5-10 show a comparison of the experimental results and the FEM data for a 150 kHz signal in the 0° direction. A systematic error of around 15% can be observed between the results. This can be attributed to the fact that the foam core was modelled as a homogeneous isotropic material. In reality the foam has a closed cell structure and exhibits viscoelastic effects that may affect the wave propagation phenomenon. Proper modelling of these effects would have required a significant number of complicated tests which also had no guarantee of success to the thickness of the foam. Furthermore, since this work was mostly focused on the relative changes of the wave speeds with temperature, it was decided to keep the isotropic assumption. Looking at the velocity rate of change, it can be seen that the FE results match the experimental data quite well.

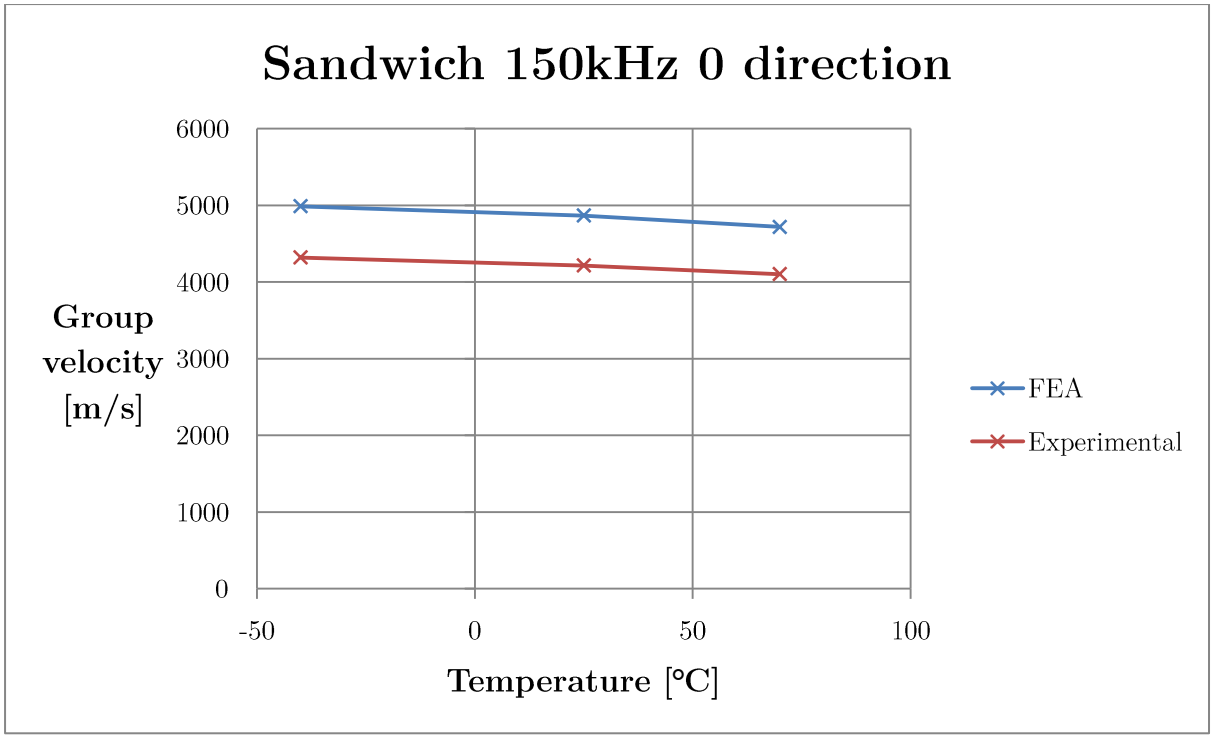

Figure 5-10: Velocity vs temperature graph for the 150 kHz signal in the 0 direction

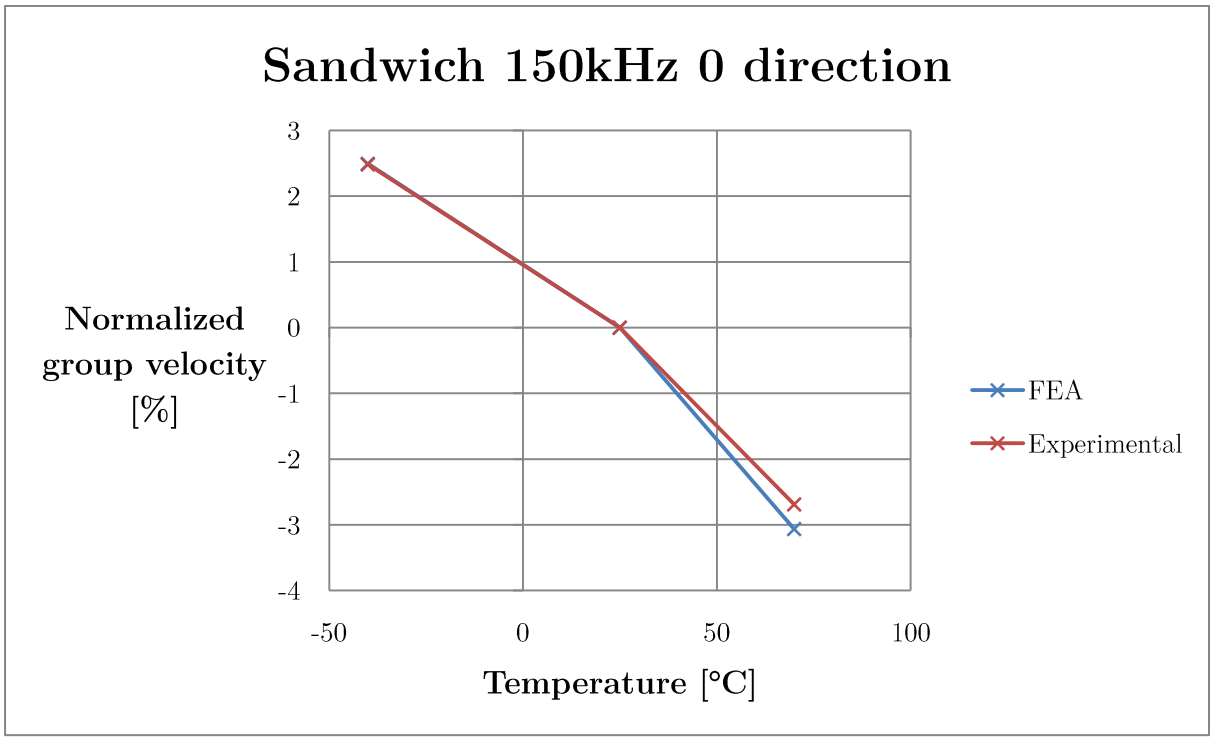

Figure 5-11: Velocity rate of change for the 150 kHz signal in the 0 direction

The results for the 45° and 90° directions are shown in Figure 5-12. The same drop in speed can be observed when compared to the laminate results. Furthermore, the variation in speed is once again higher in the 45° and 90° directions due to the larger influence of the resin. The difference between the experimental and FE results is also higher for the 70°C case most likely due to the same factors mentioned for the hybrid laminate.

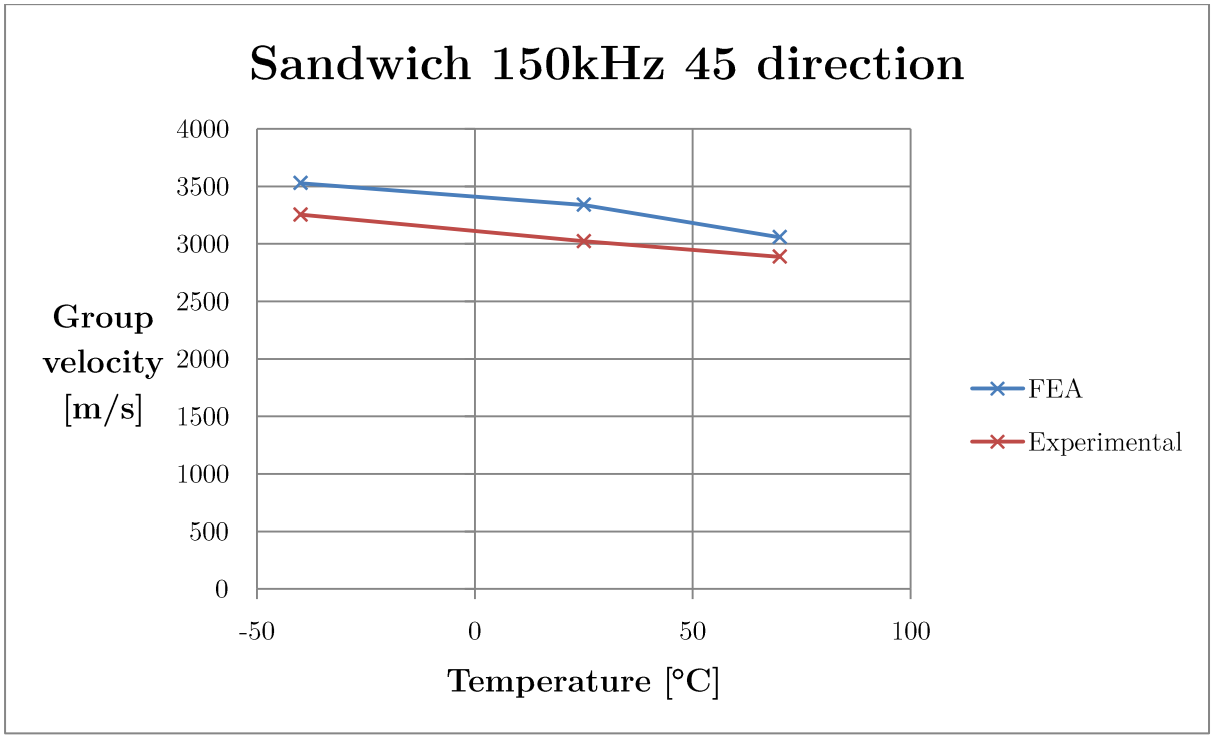

Figure 5-12: Velocity vs temperature graph for the 150 kHz signal in the 45 direction

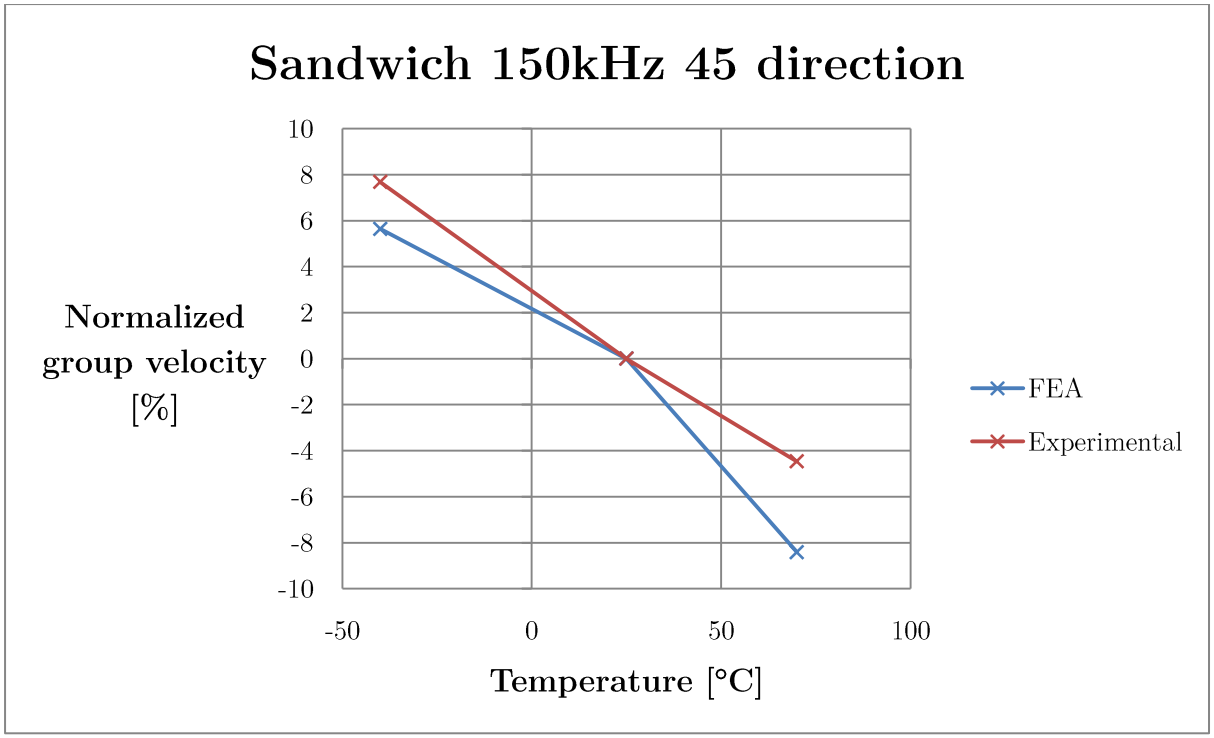

Figure 5-13: Velocity rate of change for the 150 kHz signal in the 45 direction

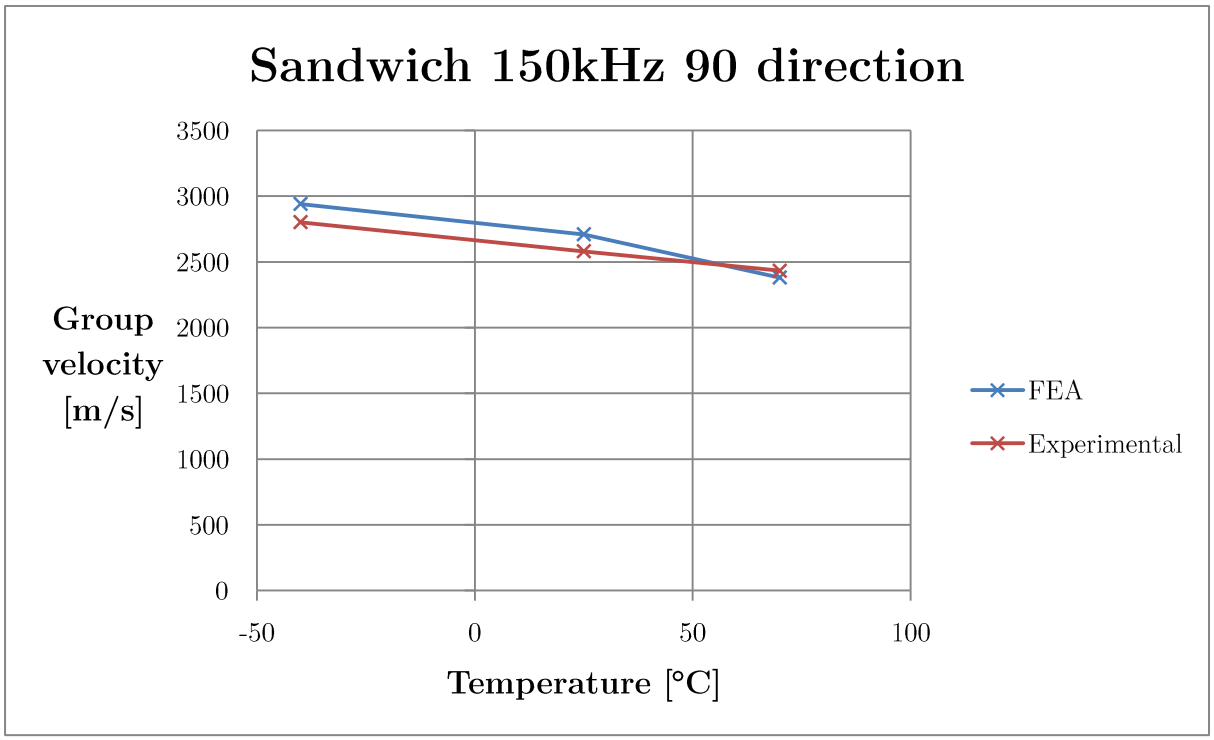

Figure 5-14: Velocity vs temperature graph for the 150 kHz signal in the 90 direction

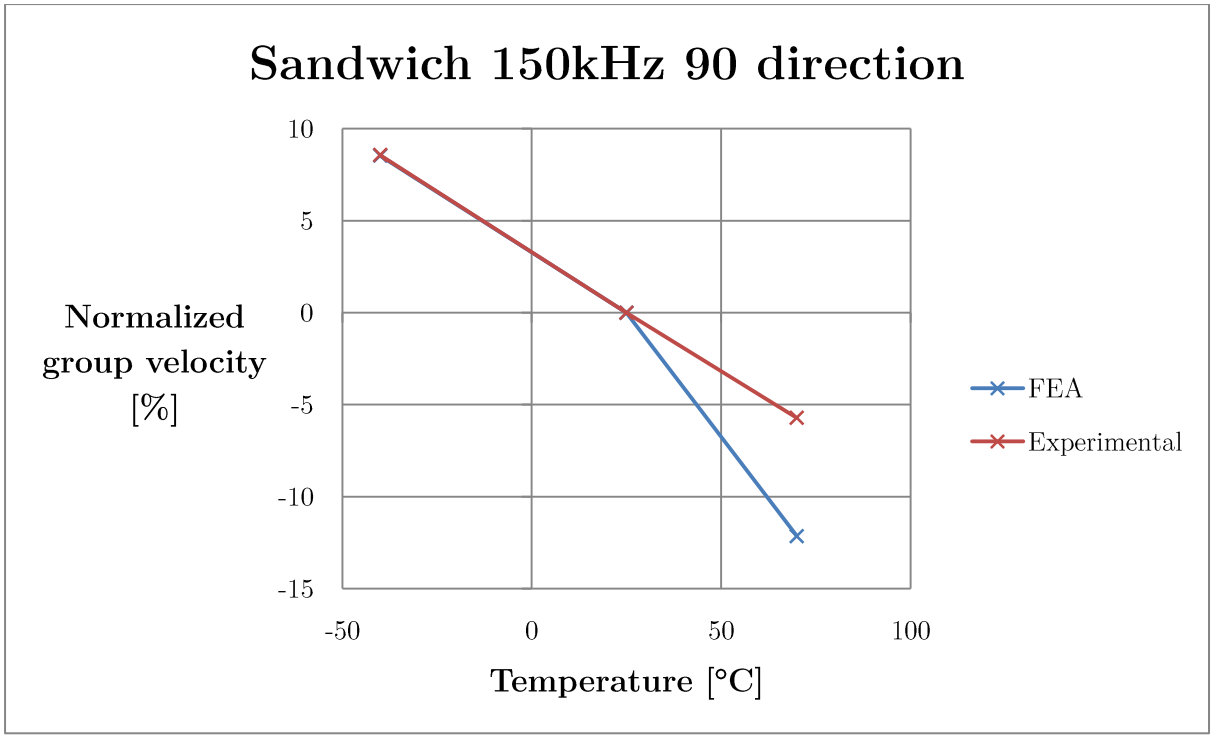

Figure 5-15: Velocity rate of change for the 150 kHz signal in the 90 direction

The results for the 300 and 400 kHz signals are shown in Appendix D – Sandwich panel 300 and 400 kHz results. The same trends can be observed for the higher frequencies, although the systematic error is larger in these cases, between 20% to 25%. This is attributed to the element size used in these analyses. Due to the large amount of computational resources needed to model the sandwich structure, the maximum element size, set using the equations mentioned in Section 4.3.4, was used. These equations were derived for shell elements and it is likely that a finer mesh is needed to achieve more accurate results for models that use solid elements.

5.2.2 Directional dependence

The directional dependence of the velocity for the sandwich panel is similar to the case of the hybrid laminate. The experimental wave speeds for the 25°C case are shown in Table 5-2. The group velocity is highest in the direction of the CF layer, while in the 45° and 90° directions the speed is slower by 39% and 63% respectively.

Table 5-2: Experimental wave speeds 25° C case

	Speed [m/s]		
Frequency [kHz]	0°	45°	90°
150	4214	3022	2580
300	4256	3016	2578
400	4267	2992	2576

The wave fronts of the S_0 and A_0 can be seen in Figure 5-16. Figure 5-16 shows a full model of the sandwich panel that was built to understand the computational load required. The results were not used because the model had a slightly coarser mesh than was required, however it does give a clearer view of the wave front.

Figure 5-16: Sandwich panel S_0 mode wave front

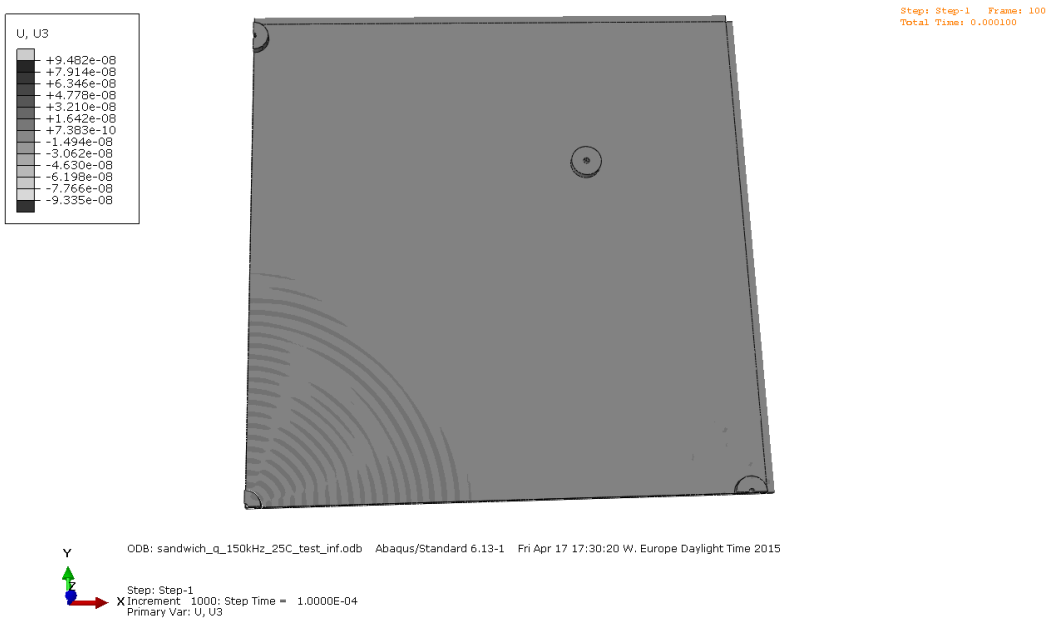

Figure 5-17: Sandwich panel A_0 mode wave front

6 Conclusions and recommendations

Operational and maintenance costs make up a significant portion of commercial aviation companies expenses. In an attempt to reduce the amount of maintenance needed to ensure structural integrity there is a desire to switch from the presently used time-based maintenance approach to the more cost-effective Condition Based Maintenance. This model requires a SHM system that can function regardless of the various conditions that the structure is exposed to (temperature, load, humidity).

AE based SHM systems have been shown to have the potential to detect and localize damage in complex structures, such as the ones on an aircraft. However further research is required in order to fully understand and predict the effects of EOC on AE based systems, especially when applied to composite materials. Thus, the objective of this thesis was: *to understand how temperature affects the propagation of guided Lamb waves in composite materials by modelling the behaviour both analytically and with FEM simulations while performing experimental verifications.*

In order to answer this question, several steps were necessary. In the first step, a literature study was performed on the subject of structural health monitoring, with a focus on the AE method, and on the propagation of acoustic waves through anisotropic media, with a focus on how this phenomenon is affected by temperature changes. The main conclusion of the literature study was that temperature changes have a significant effect on the propagation of Lamb waves, sometimes the effect can be higher than that due to damage, and that this effect can be modelled using temperature dependant material properties. Furthermore, this effect was expected to be higher for propagation in directions with matrix dominated material properties.

In the second step, the material properties of the CF-epoxy and GF-epoxy layers used in this work had to be determined. The literature study showed that the velocity with which the Lamb waves propagate depend on the mechanical properties and the density of the material. In particular, the S_0 mode depends on the modulus in the direction of the propagation and the density. Thus, a number of different laminates were manufactured using vacuum infusion, cut into samples and then tested using a Zwick 250 kN tension and compression bench. The dimensions of the samples and the methodology used in the tests followed the guidelines of the ASTM D 3039 – 08 and ASTM D 3518 – 94 standard test methods for Tensile and In-plane shear response of polymer matrix composite materials. For the CF laminate only the longitudinal and transverse moduli were determined experimentally due to difficulties associated with the infusion of a laminate that would fit the required standard.

Finally, the experimental tests were performed and the results were verified using analytical and FE models. The methodology consisted of generating results at 3 temperature steps (-40, 25 and 70°C) and 3 different frequencies (150, 300 and 400 kHz) using all of the previously mentioned

tools for the hybrid laminate case and using the experiment and FE model in the case of the sandwich. An attempt was made to use the analytical method to generate dispersion curves for the sandwich panel in order to see if the method works for such structures. However, the solution proved to be unstable and no relevant results were found. The analytical approach was developed by Pant *et al.* in order to generate dispersion curves for layered composite materials using the partial wave technique and the Global Matrix method. As some of the tests performed in this work revealed, the method is mostly suited for quasi-isotropic layups and had some difficulties predicting the group velocity in the laminates 45° direction. The results for the 0 and 90° directions were close to those found in the experiments.

The FE models were set up in order to model the experiments as closely as possible. Thus, two models were created, one for each of the two specimens. The hybrid laminate was modelled fully using shells elements, while the sandwich panel was modelled using symmetry conditions and infinite boundaries in order to reduce the computational resources needed run it. The piezoelectric transducers were modelled using piezoelectric elements available in the ABAQUS/CAE software. Only the active part of the transducers was modelled and the bonding between the specimens and the transducers was as assumed to be perfect. Furthermore, the effects of temperature variation on the piezoelectric material and on the bonding agent were not taken into account. Due to the nature of the analysis, certain restriction had to be applied to the mesh size and the time step used in these analyses. Equations determined by Chen *et al.* were used to calculate the maximum sizes of these parameters. While these equations worked well for the hybrid laminate, the results of the 300 and 400 kHz cases of the sandwich panel indicate that a finer mesh may be required to get a higher degree of accuracy in the results. This could not be investigated in this work due to the large computational requirements needed to analyse models with a finer mesh.

The experiments were performed using a setup that consisted of: an environmental chamber connected to a temperature cycling machine, the AMSY-6 AE system from Vallen Systeme, a waveform generator, amplifier, thermocouples connected to a Keithley data acquisition system and 4 broadband piezoelectric transducers. Three 5 cycle Hanning windows of 150, 300 and 400 kHz peak frequency were generated and transmitted to the actuator and the subsequent waveform was recorded using sensors located in the 0, 45 and 90° directions of the laminate. This process was performed for each sample at the three different temperature steps mentioned earlier. The same Hanning windows were also used in the FE models.

The thermal effects in both the analytical and FE models were modelled using an empirical approach developed by Tsai. This method uses a thermal degradation factor which is calculated using the glass transition temperature of the resin and the operating temperature to predict the change in material properties and parameters which are resin specific. It is important to note

that the parameters used in this work apply for epoxy resins and different parameters will apply when using other types of resin, such as non-polymeric resins.

One of the main aspects shown by the experimental results was that there was a linear dependence between the velocity of the waves and the temperature. Thus, the wave speeds decreased with increasing temperature. This effect was observed for both the hybrid laminate and the sandwich panel at all of the different frequency values tested. The variations in speed were found to be between 200 and 400 m/s between the values at -40°C and 70°C, temperatures which are representative for the conditions an aircraft structure may be exposed to during its operational life. The results showed that the change in speed was larger in the 90° directions of both the laminate and the sandwich panel. This was due to the fact that the stiffness in this direction was matrix dominated which is more sensitive to temperature changes than the fibres. This trend also predicted by both the analytical and FE models with various degrees of accuracy.

In the case of the hybrid laminate, both methods predicted the behaviour quite well for the 0° direction. The FE model was the most accurate with maximum difference of around 3% from the experimental values, while the analytical model was off by around 10%. This was also the case for the 45° direction, where the error of the values increased slightly for both models. However the analytical models error was very large in the 90° case, where it over predicted the effects by 20 to 40%. This suggests that the analytical model is not suitable for determining the speed variation in directions in which the stiffness is not fibre dominated.

The experimental results obtained from the sandwich panel were only compared with FEA results. The results showed that all of the wave speeds were lower in the sandwich panel when compared with the hybrid laminate. This was due to the presence of the foam core which had a much lower stiffness when compared with the face sheets. Otherwise, the same trends that were observed in for the hybrid laminate could be seen in the case of the sandwich. The most accurate results were obtained for the 0° directions while the 45 and 90°directions showed a slightly larger error. It should be noted that the 300 and 400 kHz analyses showed larger errors than the 150 kHz case. This is most likely due to the mesh size that was used in these cases. The results from a finer mesh could not be investigated due to the time needed to analyse such a model. This also suggests than any Lamb wave propagation studies that may involve more complex structures might have difficulties with analysing frequencies higher than 150 kHz.

The magnitude of these changes due to temperature variations suggests that the effects on an AE based localization system will be fairly small. Similar tests done for metallic structures have shown that a variation of 200 m/s due to temperature and load caused an increase in the error of a location algorithm of no more than 1 cm. Since the thermal effects found in this thesis are of similar magnitude, it is expected that any localization error will also be similar. The localization

process will be influenced far more by the directional dependence of the group velocity and the amplitude of the signals.

The experimental results for both samples showed that the wave speeds were around 40% lower in the 45° direction and 60% lower in the 90° direction. This effect must be taken into account in a localization analysis performed on these materials.

When analysing the results from the sandwich panel, it was observed that the amplitudes of the recorded signals was smaller than in the case of the hybrid. This was due to the presence of the core which had a damping effect on the signal. Due to the lower amplitude, the error in the TOA is larger due to the threshold effect that was mentioned in Section 4.1.1. The error due to this effect can be larger than the effect of temperature changes and would influence the results of a localization analysis. Considering that sandwich structures used in real applications have larger cores than the one used in this study, this effect will be even more important.

Considering all of the things mentioned in this chapter and the results of the work described earlier, the research questioned posed in the introduction can be answered as follows:

- It is possible to develop a thorough understanding of the physics governing the propagation of Lamb waves in anisotropic materials influenced by the effects of temperature.
- Analytical and FEM simulations of Lamb waves propagating in composite materials are able to predict with a good degree of accuracy the changes in wave speed for directions in which fibres are present. Considering that composite materials in most real applications have quasi-isotropic layups, this suggests that it is possible to model the thermal effects for most composite structures.
- The thermal effects described in this work have a small effect on localization algorithms, such as the one based on Geiger's method. The results of this thesis showed that effects due to the directional dependence of the group velocity and the low amplitude of the signals in sandwich structures can be larger than those due to thermal effects and may have a higher influence on the results of a localization algorithm.

Some recommendations for further research also arise from this work:

- FE modelling of the sandwich structure showed the limitations of this method when it comes to wave propagation. It is very time consuming and expensive to model higher frequencies in these structures due to the use of solid elements. Thus it would be useful to develop an analytical method of generating dispersion curves for sandwich structures.
- Develop a threshold independent method of measuring the TDOA.
- Investigate the effects of combined temperature and load in composite structures.

- Develop a localization algorithm than takes into account the directional dependence of the group velocity.

References

[1] D. Balageas, Structural Health Monitoring, Wiley, 2010.

[2] C. Boller and N. Meyendorf, "State-of-the-Art in Structural Health Monitoring for Aeronautics," in *International Symposium on NDT in Aerospace*, Fürth/Bavaria, 2008.

[3] Federal Aviation Administration, "Federal Aviation Administration," [Online]. Available: www.faa.gov. [Accessed 07 05 2015].

[4] European Aviation Safety Agency, "European Aviation Safety Agency," [Online]. Available: www.easa.europa.eu. [Accessed 07 05 2015].

[5] C. Kassapoglou, Design and Analysis of Composite Structures with Applications to Aerospace Structures, 1st ed., John Wiley & Sons, 2010.

[6] W. J. Staszewski, Mahzan S. and S. Traynor, "Health monitoring of aerospace composite structures - Active and passive approach," *Composites Science and Technology,* vol. 69, pp. 1678-1685, 2009.

[7] C. Farrar and K. Worden, "An introduction to structural health monitoring," *Philosophical transaction of The Royal Society A,* vol. 365, pp. 303-315, February 2007.

[8] M. Boldue and C. Roy, "Evaluation of Impact Damage in Composite Materials using Acoustic Emission," *Composite Materials: Fatigue and Fracture,* vol. 4, pp. 127-138, 1993.

[9] P. Y.Z. and K. V., "Toughness characterization and acoustic emission monitoring of a 2D carbon/carbon composite," *Engineering Fracture Mechanics,* vol. 68, no. 14, pp. 1557-1573, 2001.

[10] H. Sohn, "Effects of environmental and operational variability on structural health monitoring," *Philosophical Transactions of The Royal Society A,* vol. 365, pp. 539-560, 2006.

[11] P. Kudela, W. Ostachowicz and A. Zak, "Influence of temperature fields on wave propagation in composite plates," *Key Engineering Materials,* vol. 347, pp. 537-542, 2007.

[12] D. Gagar, M. Martinez, M. Yanishevski, B. Rocha, J. McFeat, P. Foote and P. Irving, "Detecting and Locating Fatigue Cracks in a Complex Wing-box Structure Using the Acoustic Emission Technique: a Verification Study," *Structural Health Monitoring,* vol. 1, pp. 65-72, 2013.

[13] S. Pant, J. Laliberte, M. Martinez and B. Rocha, "Derivation and experimental validation of Lamb wave equations for an n-layered anisotropic composite laminate," *Composite Structures,* vol. 111, pp. 566-579, 2014.

[14] D. Systems. [Online]. Available: http://www.3ds.com/products-services/simulia/portfolio/abaqus/abaqus-portfolio/abaquscae/ [Accessed 14/07/2014].

[15] P. Whitney, "Fatigue failure of the de Havilland Comet I," *Engineering Failure Analysis,* vol. 4, no. 2, pp. 147-154, 1997.

[16] SAE International, "Guidelines for Implementation of Structural Health Monitoring on Fixed Wing Aircraft," 2013. [Online]. Available: standards.sae.org [Accessed on 15-08-2014].

[17] D. Adams, Health Monitoring of Structural Materials and Components, John Wiley & Sons, 2007.

[18] C. Boller, "Structural Health Monitoring - Its Association and Use," in *New Trends in Structural Health Monitoring*, W. Ostachowicz and J. Güemes, Eds., Udine, Springer, 2013, pp. 9-35.

[19] D. Bently and C. Hatch, Fundametals of rotating machinery diagnostics, New York: ASME Press, 2003.

[20] P. Shull, Nondestructive Evaluation - Theory, Techniques, and Applications, New York: Marcel Dekker, Inc., 2002.

[21] J. Oakland, Statistical Process Control, Oxford: Butterworth Heinemann, 2003.

[22] M. Fugate, H. Sohn and C. Farrar, "Vibration-based damage detection using statistical process control," *Mechanical Systems and Signal Processing,* vol. 15, no. 4, pp. 707-721, 2001.

[23] C. Farrar and N. Lieven, "Damage prognosis: the future of structural health monitoring," *Philosophical Transaction of The Royal Society A,* vol. 365, pp. 623-632, 2007.

[24] P. Cawley and R. Adams, "The location of defects in structures from measurements of natural frequencies," *Journal of Strain Analysis for Engineering Design,* vol. 4, no. 2, pp. 49-57, 1979.

[25] A. Robinson, L. Peterson and G. James, "Health monitoring of aircraft structures using experimental flexibility matrices," in *Adaptive Structures Forum*, Salt Lake City, UT, 1996.

[26] G. Manson, K. Worden and D. Allman, "Experimental validation of a damage severity method," in *First European Workshop on Structural Health Monitoring*, Paris, 2002.

[27] G. Manson, K. Worden and D. Allman, "Experimental validation of a structural health monitoring methodology, Part II: Novelty detection on a Gnat aircraft," *Journal of Sound and Vibration,* vol. 259, no. 2, pp. 345-363, 2003.

[28] G. Manson, K. Worden and D. Allman, "Experimental validation of a structural health monitoring methodology, Part III: Damage location on an aircraft wing," *Journal of Sound and Vibration,* vol. 259, no. 2, pp. 365-385, 2003.

[29] J. Tracy and G. Pardeon, "Effect of delamination on the natural frequencies of composite laminates," *Journal of Composite Materials,* vol. 23, pp. 1200-1215, 1989.

[30] B. Lee, C. Sun and D. Liu, "An assessment of damping measurement in the evaluation of integrity of composite beams," *Journal of Reinforced Plastics and Composites,* vol. 6, pp. 114-125, 1987.

[31] W. Staszewsky, C. Boller and G. Tomlinson, Health Monitoring of Aerospace Structures - Smart Sensor Technologies and Signal Processing, John Wiley & Sons, 2004.

[32] R. Rulli, F. Dotta and P. da Silva, "Flight tests performed by EMBRAER with SHM systems," *Key Engineering Materials,* vol. 558, pp. 305-313, 2013.

[33] D. Roach, "Real time crack detection using mountable comparative vacuum monitoring sensors," *Smart Structures and Systems,* vol. 5, no. 4, pp. 317-328, 2009.

[34] M. Perterer, M. Friemel and H. Baier, "Characterization of the Mechanical Influence of Comparative Vacuum Measurement (CVM) Sensors in the Context of Structural Health Monitoring (SHM) Systems," in *6th European Workshop on Structural Health Monitoring*, Dresden, 2012.

[35] D. Roach, J. Kollgaard, S. Emery, J. Register, K. Colavito and D. Galella, "Application and Certification of Comparative Vacuum Monitoring Sensors of In-Situ Crack Detection," FAA Hughes Technical Center.

[36] K. Diamanti and C. Soutis, "Structural health monitoring techniques for aircraft composite structures," *Progress in Aerospace Sciences,* vol. 46, pp. 342-352, May 2010.

[37] J. Rose, Ultrasonic Waves in Solid Media, Cambridge University Press, 1999.

[38] W. Ostachowicz, P. Kudela, M. Krawczuk and A. Zak, Guided Waves in Structures for SHM - The Time-Domain Spectral Element Method, John Wiley & Sons, 2012.

[39] G. Bottai, N. Chrysochoidis, V. Giurgiutiu and A. Saravanos, "Analytical and Experimental Evaluation of Piezoelectric Wafer Active Sensors Performances for Lamb Waves based Structural Health Monitoring in Composite Laminates," in *Health Monitoring of Structural and Biological Systems*, San Diego, 2007.

[40] V. Giurgiutiu, "Tuned Lamb Wave Excitation and Detection with Piezoelectric Wafer Active Sensors for Structural Health Monitoring," *Journal of Intelligent Material Systems and Structures,* vol. 16, pp. 291-305, April 2005.

[41] Z. Su and L. Ye, Identification of Damage Using Lamb Waves - From Fundamentals to Applications, Berlin: Springer, 2009.

[42] S. Kessler, S. Spearing and C. Soutis, "Damage detection in composite materials using Lamb wave methods," *Smart Materials and Structures,* vol. 11, pp. 269-278, 2002.

[43] J.-B. Ihn and F.-K. Chang, "Pitch catch active sensing methods in structural health monitoring for aircraft structures," *Structural Health Monitoring, An International Journal,* vol. 7, no. 1, pp. 5-19, 2008.

[44] Z. Su, L. Ye and Y. Lu, "Detection and monitoring of hidden fatigue crack growth using a built-in piezoelectric sensor/actuator network," *Smart Materials and Structures,* vol. 13, pp. 609-620, 2004.

[45] C. Potel, P. Gatigno and J.-F. De Belleval, "Flaw Detection by Lamb Waves," in *Materials and Acoustics Handbook*, M. Bruneau and C. Potel, Eds., ISTLE Ltd and John Wiley & Sons, 2009, pp. 595-607.

[46] L. Wang and Y. F.G., "Group velocity and characteristic wave curves of Lamb waves in composites: Modeling and experiments," *Composites Science and Technology,* vol. 67, pp. 1370-1384, 2007.

[47] W. J. Staszewski, "Ultrasonic/Guided Waves For Structural Health Monitoring," *Key Engineering Materials,* Vols. 293-294, pp. 49-62, September 2005.

[48] N.-d. t. r. center. [Online]. Available: http://www.ndt-ed.org/EducationResources/CommunityCollege/Other%20Methods/AE/AE_Theory-Sources.htm [Accessed 23/06/2014].

[49] C. U. Grosse, "Introduction," in *Acoustic Emission Testing*, C. U. Grosse and M. Ohtsu, Eds., Springer, 2008, pp. 3-11.

[50] NDT Education Resource Center, "NDT Resource Center," [Online]. Available: https://www.nde-ed.org/EducationResources/CommunityCollege/Other%20Methods/AE/AE_Equipment.htm. [Accessed 07 05 2015].

[51] F. Leone, D. A. J. Ozevin and T.-M. Tan, "Detecting and locating damage initiation and progression in full-scale sandwich composite fuselage panels using acoustic emission," *Journal of Composite Materials,* vol. 47, no. 13, pp. 1643-1644, 2012.

[52] T. Kundu, S. Das, S. Martin and V. Jata, "Locating point of impact in anisotropic fiber reinforced composite plates," *Ultrasonics,* vol. 48, pp. 193-201, 2008.

[53] D. Aggelis, N.-M. Barkoula, T. Matikas and A. Paipetis, "Acoustic structural health

monitoring of composite materials: Damage identification and evaluation in cross ply laminates using acoustic emission and ultrasonics," *Composites Science and Technology,* vol. 72, pp. 1127-1133, 2012.

[54] D. Katerelos, A. Paipetis, T. Loutas, G. Sotiriadis, V. Kostopoulos and S. Ogin, "In situ damage monitoring of cross-ply laminates using acoustic emission," *Plastics, Rubber and Composites,* vol. 38, no. 6, pp. 229-234, 2009.

[55] T. Fu, Y. Liu, Q. Li and J. Leng, "Fiber optic acoustic emission sensor and its applications in the structural health monitoring of CFRP materials," *Optics and Lasers in Engineering,* vol. 47, pp. 1056-1062, 2009.

[56] C. Baldwin and A. Vizzini, "Acoustic emission crack detection with FBG," in *Smart Structures and Materials 2003: Smart Sensor Technology and Measurement Systems*, San Diego, 2003.

[57] T. Shiotani, "Parametric AE Analysis," in *Acoustic Emission Testing*, C. Grosse and M. Ohtsu, Eds., Springer, 2008, pp. 41-53.

[58] B. Lempriere, Ultrasound and Elastic Waves - Frequently Asked Questions, Academic Press, 2002.

[59] M. Ge, "Analysis of source location algorithms Part II: Iterative methods," *Journal of Acoustic Emission,* no. 21, pp. 29-51, 2003.

[60] M. Boon, D. Zarouchas, M. Martinez, D. Gagar, R. Benedictus and P. Foote, "Temperature and load effects on acoustic emission signals for structural health monitoring applications," in *EWSHM*, Nantes, 2014.

[61] A. Raghavan and C. Cesnik, "Review of Guided-wave Structural Health Monitoring," *The Shock and Vibrations Digest,* pp. 91-114, 2007.

[62] A. Srinivasan and M. Mcfarland, Smart Structures, Cambridge: Cambridge University Press, 2001.

[63] A. Raghavan and C. Cesnik, "Studies on effects of elevated temperature for guided-wave structural health monitoring," *Sensors and Smart Structures Technologies for Civil, Mechanical and Aerospace Systems,* 2007.

[64] R. Wolf and S. Trolier-McKinstry, "Temperature dependence of the piezoelectric response in lead zirconate titanate films," *Journal of Applied Physics,* vol. 95, no. 3, pp. 1397-1406, 2004.

[65] J. Sharma, D. Singh and R. Kumar, "Generalized thermoelastic waves in homogeneous isotropic plates," *THe Journal of the Acoustical Society of America,* pp. 848-851, 2000.

[66] B. Lee, G. Mason and W. Staszewski, "Environmental effects on lamb wave responses from piezoceramic sensors," *Material Science Forum,* 2003.

[67] J. Dodson, Guided Wave Structural Health Monitoring with Environmental Considerations, Blacksburg, Virginia, 2012.

[68] J. Dodson and I. D.J., "Thermal sensitivity of Lamb waves for structural health monitoring applications," *Ultrasonics,* pp. 677-685, 2013.

[69] K. Verma, "On the propagation of waves in layered anisotropic media in generalized thermoelasticity," *International Journal of Engineering Science,* vol. 40, pp. 2077-2096, 2002.

[70] M. Torres-Arredondo and C.-P. Fritzen, "Ultrasonic Guided Wave Dispersive Characteristics in Composite Structures Under Variable Temperature and Operational Conditions," in *6th European Workshop on Structural Health Monitoring*, Dresden.

[71] P. Kudela, W. Ostachowicz and A. Zak, "Influence of temperature fields on wave propagation in composite plates," *Key Engineering Materials,* vol. 347, pp. 537-542, 2007.

[72] P. Kudela, M. Krawczuk, W. Ostachowicz, M. Palacz and A. Zak, "????," in *3rd European Workshop on Structural Health Monitoring*, Madrid, 2006.

[73] C. Park and S. Jun, "Guide Wave Damage Detection in Composite Plates under Temperature Variations," *Materials and Manufacturing Processes,* vol. 25, pp. 227-231, 2010.

[74] C. Park and S. Jun, "Temperature Effects on Guided Wave Structural Damage Detection," *Advanced Materials Research,* pp. 129-132, 2008.

[75] S. Salamone, I. Bartoli, F. Di Scalea and S. Coccia, "Guided-wave Health Monitoring of Aircraft Composite Panels under Changing Temperature," *Journal of Intelligent Material Systems and Structures,* vol. 20, pp. 1079-1090, 2009.

[76] R. Kumar and T. Kansal, "Propagation of Lamb waves in transversely isotropic thermoelastic diffusive plate," *International Journal of Solids and Structures,* pp. 5890-5913, 2008.

[77] K. Schubert, T. Block, C. Brauner and A. Herrmann, "A Compensation Method to Accound for Environmental Effects on Active Lamb-Wave Based SHM," in *Non-Destructive Testing in Aerospace*, Augsburg, 2012.

[78] D. Chronopoulos, M. Ichchou, B. Troclet and O. Bareille, "Thermal effects on the sound transmission through aerospace composite structures," *Aerospace Science and Technology,* pp. 192-199, 2013.

[79] S. Mall, "Laminated Polymers Matrix Composites," in *Composites Engineering Handbook*, CRC Press, 1997, pp. 811-891.

[80] I. Varma and V. Gupta, "Thermosetting Resin - Properties," in *Comprehensive Composite Materials - Volume 2*, Elsevier, 2000, pp. 1-51.

[81] v. D. Krevelen and t. K. Nijenhuis, Properties of Polymers, Elsevier, 2009.

[82] C. Chamis, "Simplified Composite Micromechanics Equations for Hygral, Thermal and Mechanical Properties," *SAMPE Quarterly,* vol. 15, no. 3, pp. 14-23, 1984.

[83] S. Tsai, Composite design, Dayton: Think composites, 1988.

[84] R. Augustinus, J. Chang, J. van Gorcum, M. Koot, H. Ubbens, C. Cakiroglu, M. Estrada, B. Groenenboom, A. Naruta and M. Wassenaar, "Solad Powered Amphibious Unmanned Aerial Vehicle (UAV) - Final Report," Delft, 2013.

[85] SGL Group, "SGL Group - The Carbon Company," [Online]. Available: http://www.sglgroup.com/cms/international/home/index.html?___locale=en. [Accessed 19 03 2015].

[86] Hexcel, "Hexcel - Fabrics Data Sheets," [Online]. Available: http://hexply.com/hexforce/database/web/front/main/. [Accessed 19 03 2015].

[87] P. Martinez Bueno, "Structural Design, FEM Analysis and Manufacturing of a Composite Optic Fibre Instrumented UAV Wing," Delft, 2014.

[88] Hexion, [Online]. Available: http://www.swiss-composite.ch/pdf/t-Hexion-Harz-EPR04908.pdf. [Accessed 19 03 2015].

[89] Marbocote Release Technology, "Marbocote Release Technology," [Online]. Available: http://www.marbocote.co.uk/. [Accessed 07 05 2015].

[90] ASTM International, *Standard Test Method for Tensile Properties of Polymer Matrix Composite Materials,* ASTM International, 2008.

[91] ASTM International, *Standard Test Method for In-Plane Shear Response of Polymer Matrix Composite Materials by Tensile Test of a ±45 Laminate,* ASTM International, 2007.

[92] Hexcel Corporation, *HexForce 7581 Fiber Glass Fabric - Product Data,* Seguin, TX: Hexcel Corporation.

[93] M. P. Bueno, "Structural Design, FEM Analysis and Manufacturing of Composite Optic Fibre Instrumented UAV Wing - Final Report," Delft, 2014.

[94] R. Blackman and J. Tukey, “Particular Pairs of Windows,” in *The Measurement of Power Spectra, From the Point of View of Communications Engineering*, New York, Dover, 1959, pp. 98-99.

[95] G. Springer, Environmental effects on Composite Materials - Volume I, Westport: Technomic Publishing Company, 1981.

[96] M. Randall, “Fast programs for layered half-space problems,” *Bulletin of the Seismic Society of America,* vol. 51, pp. 1299-1316, 1967.

[97] S.-H. Rhee, J.-K. Lee and J.-J. Lee, “The group velocity variation of Lamb wave in fiber reinforced composite plate,” *Ultrasonics,* vol. 47, pp. 55-63, 2007.

[98] Noliac Group, “Noliac Group,” [Online]. Available: www.noliac.com. [Accessed 15 04 2015].

[99] L. Chen, Y. Dong, Q. Meng and W. Liang, “FEM Simulation for Lamb Wave evaluate the defects of plates,” in *2012 International Workshop on MMWCST*, Chengdu, 2012.

[100] Vallen Systeme, *Vallen AMSY-6 Handbook - System Description,* Icking: Vallen Systeme, 2013.

[101] URSA Insulation, “URSA XPS D N-III-I,” URSA Insulation, [Online]. Available: http://www.ursa.de/de-de/produkte/ursa-xps/ursa-xps-d-n-iii-i/Seiten/informationen.aspx. [Accessed 16 04 2015].

[102] Clima Temperatur Systeme, “CTS Environmental Simulation,” Clima Temperatur Systeme, [Online]. Available: http://www.cts-umweltsimulation.de/english/index_eng.html. [Accessed 16 04 2015].

[103] J. L. Peterson, “Petri Nets,” *ACM Computing Surveys,* vol. 9, no. 3, pp. 223-252, September 1977.

[104] R. Fehling, “A concept of hierarchical Petri nets with building blocks,” *Lecture Notes in Computer Science,* vol. 674, pp. 148-168, 1993.

[105] R. Millner, A Calculus of Communicating Systems, Springer, 1982.

[106] D. Taubner, “Finite representations of CCS and TCSP programs by automata and Petri nets,” *Lecture Notes In Computer Science,* vol. 369, p. 168, 1989.

[107] J. M. Fernandes, “VHDL generation from hierarchical petri net specifications of parallel controllers,” *IEE Proceedings: Computers and Digital Techniques,* vol. 144, no. 2, pp. 127-137, March 1997.

[108] M. J. Morley, Modelling British Rail's Interlocking Logic: Geographic Data Correctness,

] LFCS Report Series: ECS-LFCS-91-186, Dept. Computer Science, University of Edinburgh, 1991.

[109 J.-P. Monchalin, "Laser-Ultrasonics: Principles and Industrial Applications," in *Ultrasonic and Advanced Methods for Nondestructive Testing and Material Characterization*, C. H. Chen, Ed., World Scientific Publishing, 2007.

[110 R. Grimberg, D. Premel, A. Savin, Y. Le Bihan and D. Placko, "Eddy current holography evaluation in carbon epoxy composites," *Insight,* vol. 43, no. 4, pp. 260-271, 2001.

[111 K. Hoffmann, An Introduction to Measurements usign Strain Gages, Hottinger Baldwin Messtechnik GmbH, 1989.

[112 C. Boller, F.-K. Chang and Y. Fujino, Encyclopedia of structural health monitoring, John Wiley & Sons, 2009.

[113 B. P. C. Rao, T. Jayakumar and B. Raj, "Electromagnetic NDE techniques for materials characterization," in *Ultrasonic and Advanced Methods for Nondestructive Testing and Material Characterization* , C. H. Chen, Ed., World Scientific Publishing, 2007.

[114 W. Ostachowicz and G. J.A., New Trends in Structural Health Monitoring, Udine: Springer, 2013.

[115 C. Meola and G. Carlomagno, "Recent advances in infrared thermography," *Measurement Science and Technology,* vol. 15, pp. 27-58, 2004.

[116 J. Kurz, S. Köppel, L. Linzer, B. Schechinger and C. Grosse, "Source Localization," in *Acoustic Emission Testing*, C. Grosse and M. Ohtsu, Eds., Springer, 2008, pp. 101-149.

[117 G. Liu, J. Tani, K. Wananabe and T. Ohyoshi, "Lamb wave propagation in anisotropic laminates," *Journal of Applied Mechanics,* vol. 57, no. 4, pp. 923-929, 1990.

[118 A. Nayfeh, Wave propagation in layered anisotropic media with applications to composites, New York: Elsevier, 1995.

[119 M. Lowe, "Matrix techniques for modeling ultrasonic waves in multilayered media," *IEEE Trans Ultrason Ferroelectr Freq Control,* vol. 42, no. 4, pp. 525-542, 1995.

[120 A. Nayfeh, "The general problem of elasti wave propagation in multilayered anisotropic media," *J Acoust Soc Am,* vol. 89, no. 4, pp. 1521-1531, 1991.

[121 V. Giurgiutiu, Structural health monitoring with piezoelectric wafer sensors, Burlington: Elsevier, 2008.

[122 M. Sharma, "Wave propagation in Anisotropic Generalized Thermoelastic Media," *Journam*

] *of Thermal Stresses,* pp. 629-642, 2006.

[123] S. Momon, M. Moevus, N. Godin, M. R'Mili, P. Reynaud, G. Fantozzi and G. Fayolle, "Acoustic emission and lifetime prediction during static fatigue tests on ceramic-matrix-composite at high temperature under air," *Composites: Part A,* vol. 41, pp. 913-918, 2010.

[124] R. Dhaliwal and H. Sherief, "Generalized thermoelasticity for anisotropic media," *Q. Appl. Math.,* vol. 38, pp. 1-8, 1980.

[125] V. systeme. [Online]. Available: www.vallen.de [Accessed: 15/07/2014].

[126] J. Vinson and S. R.L., The Behavior of Structures Composed of Composite Materials, Dordrecht: Kluwer Academic Publishers, 2002.

[127] G. Konstantinidis, B. Drinkwater and P. Wilcox, "The temperature stability of guided wave structural health monitoring systems," *Smart Materials and Structures,* pp. 967-976, 2006.

[128] M. Ge.

Appendix A

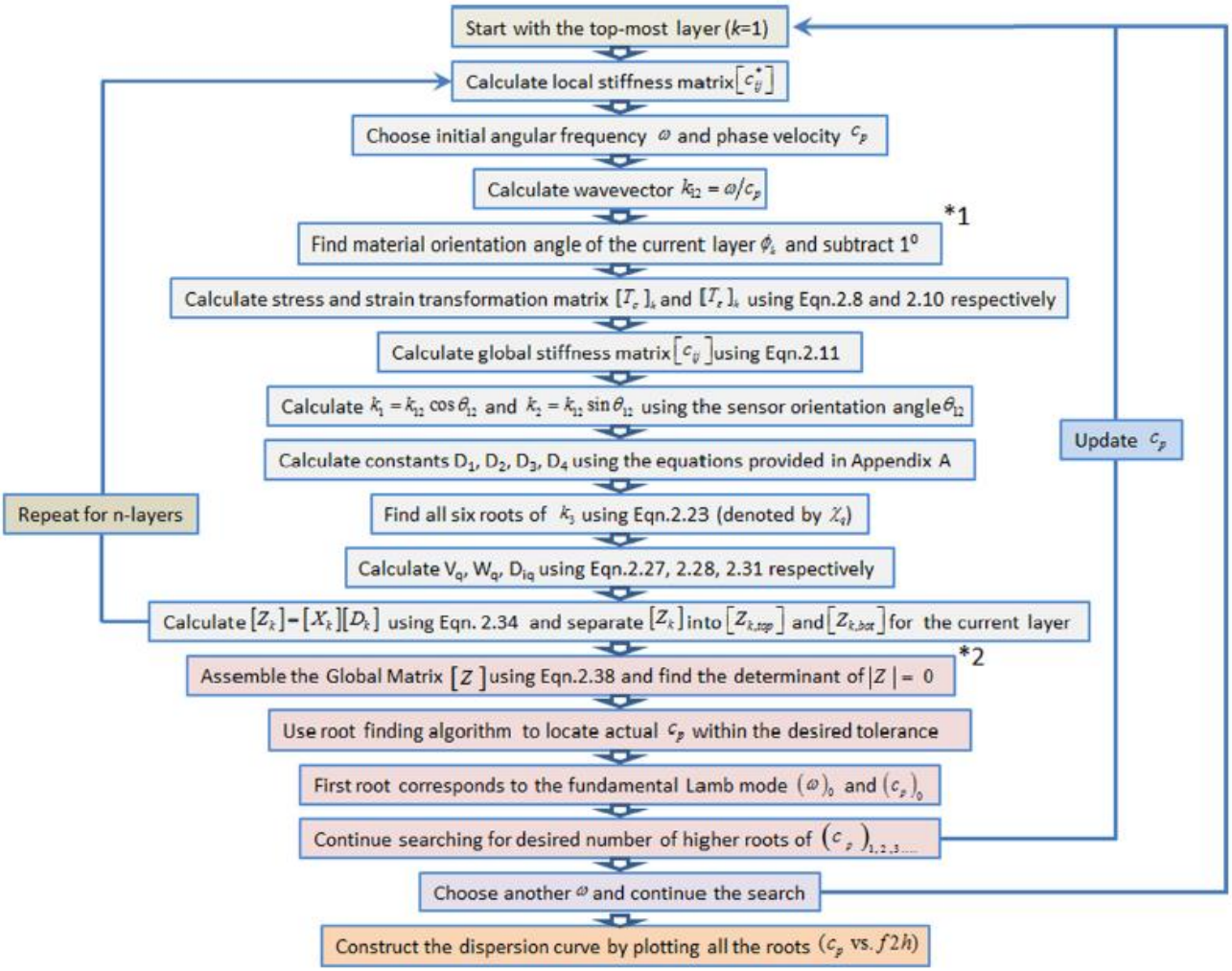

Process used by Pant *et al* [13] to numerically solve the Lamb wave equations

Appendix B – NCE51 datasheet

PIEZO MATERIALS

NCE51 - extended specification

1. The presented data are determined on standardized specimens in the form of small-signal measurements according to European Standard EN 50324 and IEC Publication 483.
2. The standardized specimens are manufactured using a standard production powder and a standard production technology.
3. The data given represents nominal values which were determined 24 hours after poling process at an ambient temperature 23°C +/- 2°C.
4. Standard Tolerances: Electrical properties ± 10 %. Mechanical Properties ± 5 %. Piezoelectric properties ± 5 %.

Properties	Symbol	Unit	
ELECTRICAL PROPERTIES			
Dielectric dissipation factor	tan δ	$[10^{-4}]$	150
Relative permittivity	$\varepsilon^T_{33}/\varepsilon_0$	[1]	1900
	$\varepsilon^S_{33}/\varepsilon_0$	[1]	823
	$\varepsilon^T_{11}/\varepsilon_0$	[1]	1940
	$\varepsilon^S_{11}/\varepsilon_0$	[1]	906
Curie Temperature	T_c	[°C]	360
Mechanical Properties			
Poisson's ratio	σ^E	[1]	0.32
Density	ρ	$[kg.m^{-3}]$	7850
PIEZOELECTRIC PROPERTIES			
Frequency Constants			
Planar	N_p	[Hz.m]	1925
Thickness shear	N_{t5}	[Hz.m]	1180
Transverse	N_{31}	[Hz.m]	1370
Longitudinal	N_{33}	[Hz.m]	1320
Thickness	N_t	[Hz.m]	2000
COUPLING FACTORS			
Planar	k_p	[1]	0.650
Thickness shear	k_{15}	[1]	0.730
Transverse	k_{31}	[1]	0.380
Longitudinal	k_{33}	[1]	0.740
Thickness	k_t	[1]	0.500
Charge Constant	d_{33}	$[10^{-12}C/N]$	443
Voltage Constant	g_{33}	$[10^{-3}V.m/N]$	26.3
Mechanical Quality Factor	Q_m	[1]	80
STABILITY			
Temperature Coefficient			
Range 20 - 80 °C	$\alpha_{permittivity}$	$[10^{-6}K^{-1}]$	4000
	α_{kp}	$[K^{-1}]$	0
Aging Rates	c_ε	[%] per decade	-1.40
	c_{Np}	[%] per decade	0.25
	c_{kp}	[%] per decade	0.10

PIEZO MATERIALS

NCE51 - complete coefficient matrix

Elastic Properties

ELASTIC COMPLIANCE MATRIX E					
s^E	$[10^{-12}m^2/N]$				
17.0	-5.36	-8.69	0	0	0
-5.36	17.0	-8.69	0	0	0
-8.69	-8.69	21.3	0	0	0
0	0	0	48.9	0	0
0	0	0	0	48.9	0
0	0	0	0	0	44.6

ELASTIC COMPLIANCE MATRIX D					
s^D	$[10^{-12}m^2/N]$				
14.5	-7.81	-3.22	0	0	0
-7.81	14.5	-3.22	0	0	0
-3.22	-3.22	9.64	0	0	0
0	0	0	22.9	0	0
0	0	0	0	22.9	0
0	0	0	0	0	44.6

ELASTIC STIFFNESS MATRIX E					
c^E	$[10^{10}N/m^2]$				
13.4	8.89	9.09	0	0	0
8.89	13.4	9.09	0	0	0
9.09	9.09	12.1	0	0	0
0	0	0	2.05	0	0
0	0	0	0	2.05	0
0	0	0	0	0	2.24

ELASTIC STIFFNESS MATRIX D					
c^D	$[10^{10}N/m^2]$				
13.2	8.76	7.34	0	0	0
8.76	13.2	7.34	0	0	0
7.34	7.34	16.2	0	0	0
0	0	0	4.37	0	0
0	0	0	0	4.37	0
0	0	0	0	0	2.24

Piezoelectric Properties

CHARGE CONSTANT MATRIX					
d	$[10^{-12}C/N]$				
0	0	0	0	669	0
0	0	0	669	0	0
-208	-208	443	0	0	0

e	$[C/m^2]$				
0	0	0	0	13.7	0
0	0	0	13.7	0	0
-6.06	-6.06	17.2	0	0	0

VOLTAGE CONSTANT MATRIX					
g	$[10^{-3}Vm/N]$				
0	0	0	0	38.9	0
0	0	0	38.9	0	0
-12.4	-12.4	26.3	0	0	0

h	$[10^8V/m]$				
0	0	0	0	17.0	0
0	0	0	17.0	0	0
-8.31	-8.31	23.5	0	0	0
0	0	0	38.9	0	0
-12.4	-12.4	26.3	0	0	0

PIEZO MATERIALS

Dielectric properties

PERMITTIVITIES [10^{-8}F/m]					
ε_{11}^T	1.72		ε_{11}^S	0.802	
ε_{22}^T	1.72		ε_{22}^S	0.802	
ε_{33}^T	1.68		ε_{33}^S	0.729	

RELATIVE PERMITTIVITIES [1]					
ε_{11r}^T	1940		ε_{11r}^S	906	
ε_{22r}^T	1940		ε_{22r}^S	906	
ε_{33r}^T	1900		ε_{33r}^S	823	

YOUNG MODULUS MATRIX					
Y^E	[10^{10}N/m^2]				
5.9	-18.6	-11.5	0	0	0
-18.6	5.9	-11.5	0	0	0
-11.5	-11.5	4.69	0	0	0
0	0	0	2.05	0	0
0	0	0	0	2.05	0
0	0	0	0	0	2.24

YOUNG MODULUS MATRIX					
Y^D	[10^{10}N/m^2]				
6.9	-12.8	-31.1	0	0	0
-12.8	6.9	-31.1	0	0	0
-31.1	-31.1	10.4	0	0	0
0	0	0	4.37	0	0
0	0	0	0	4.37	0
0	0	0	0	0	2.24

Matrix

Z_{ab} Z - Property
a - direction
b - direction

	1	2	3	4
1	Z_{11}	Z_{12}	Z_{13}	→b
2	Z_{21}	Z_{22}	Z_{23}	
3	Z_{31}	Z_{32}	Z_{33}	
4	↓a			

Appendix C – Hybrid laminate 300 and 400 kHz results

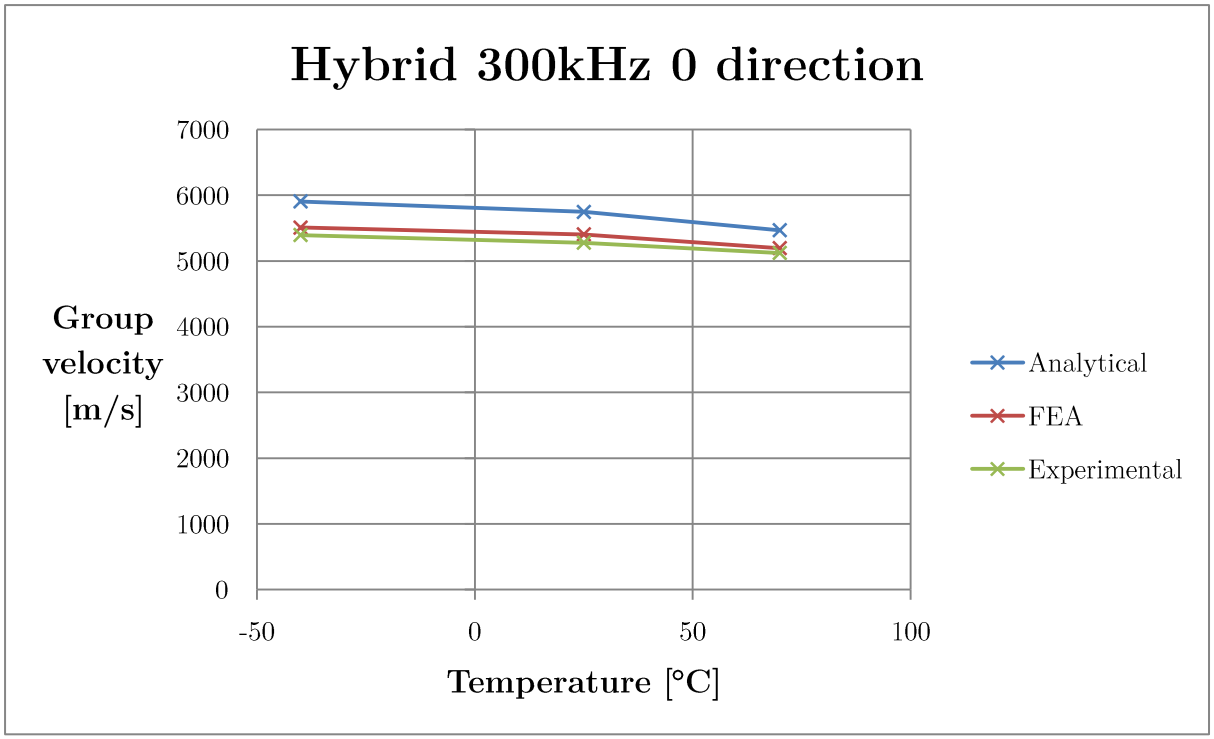

Velocity vs temperature graph for the 300 kHz signal in the 0 direction

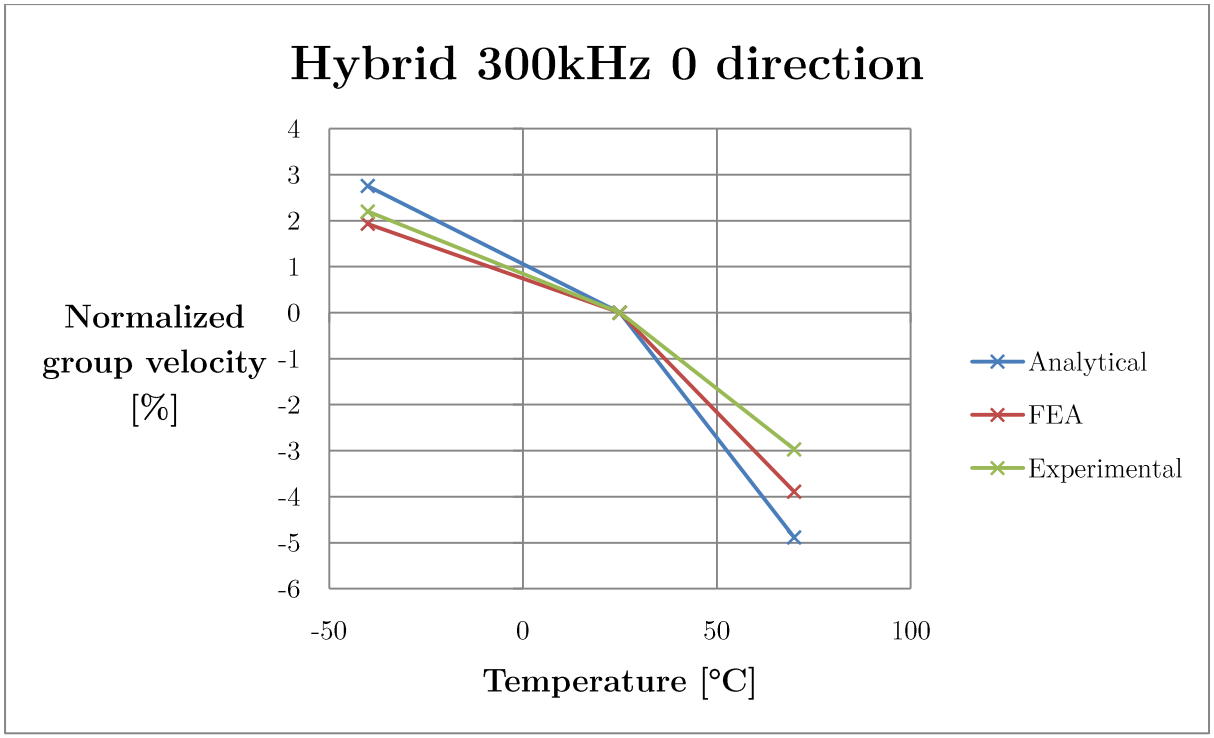

Velocity rate of change for the 300 kHz signal in the 0 direction

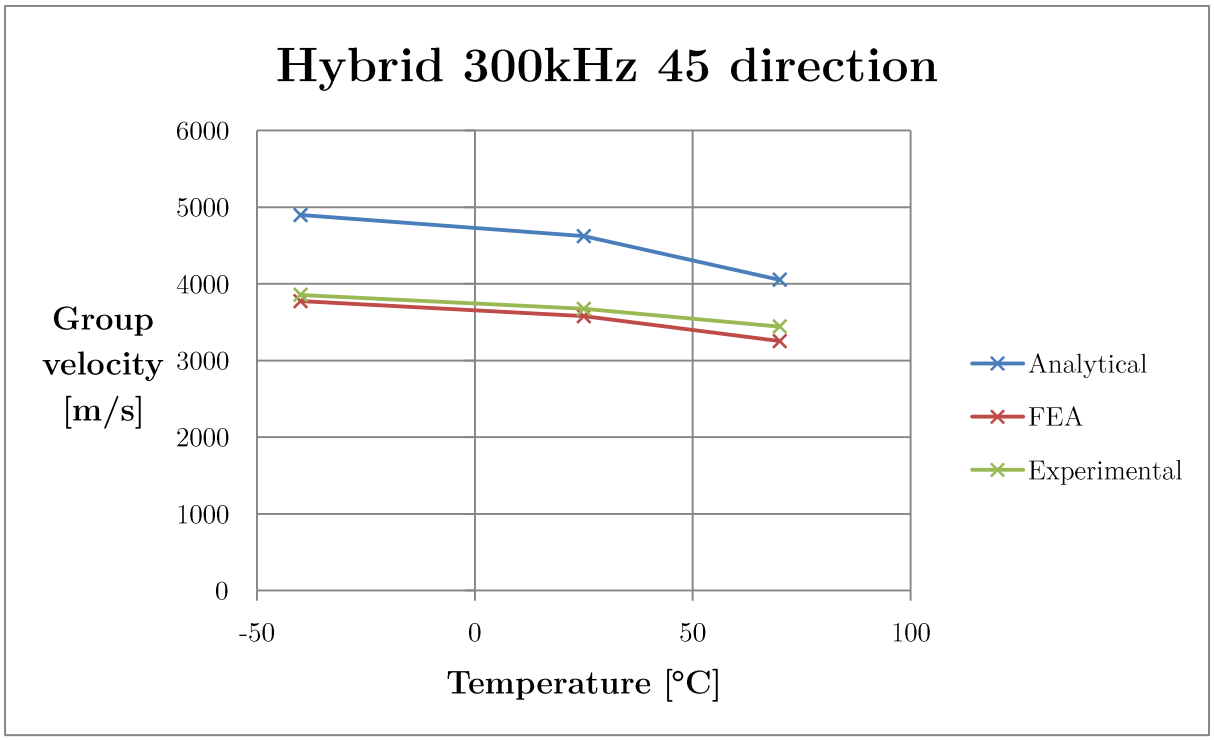

Velocity vs temperature graph for the 300 kHz signal in the 45 direction

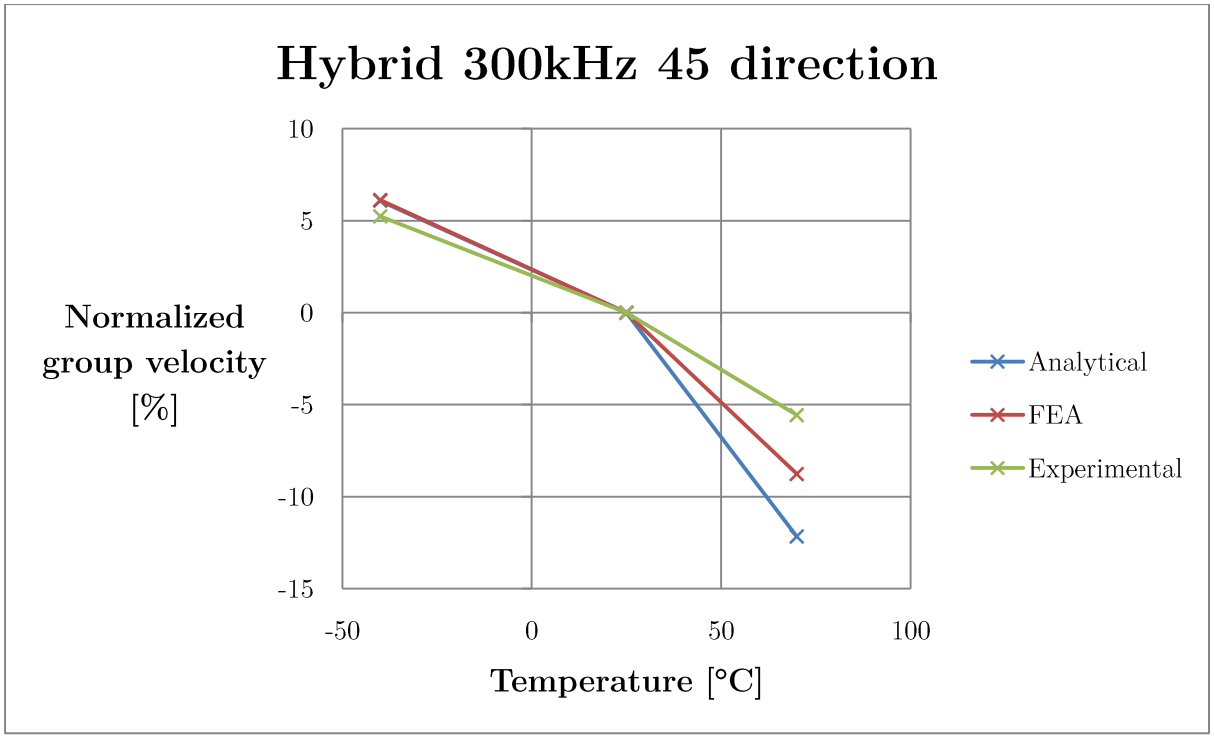

Velocity rate of change for the 300 kHz signal in the 45 direction

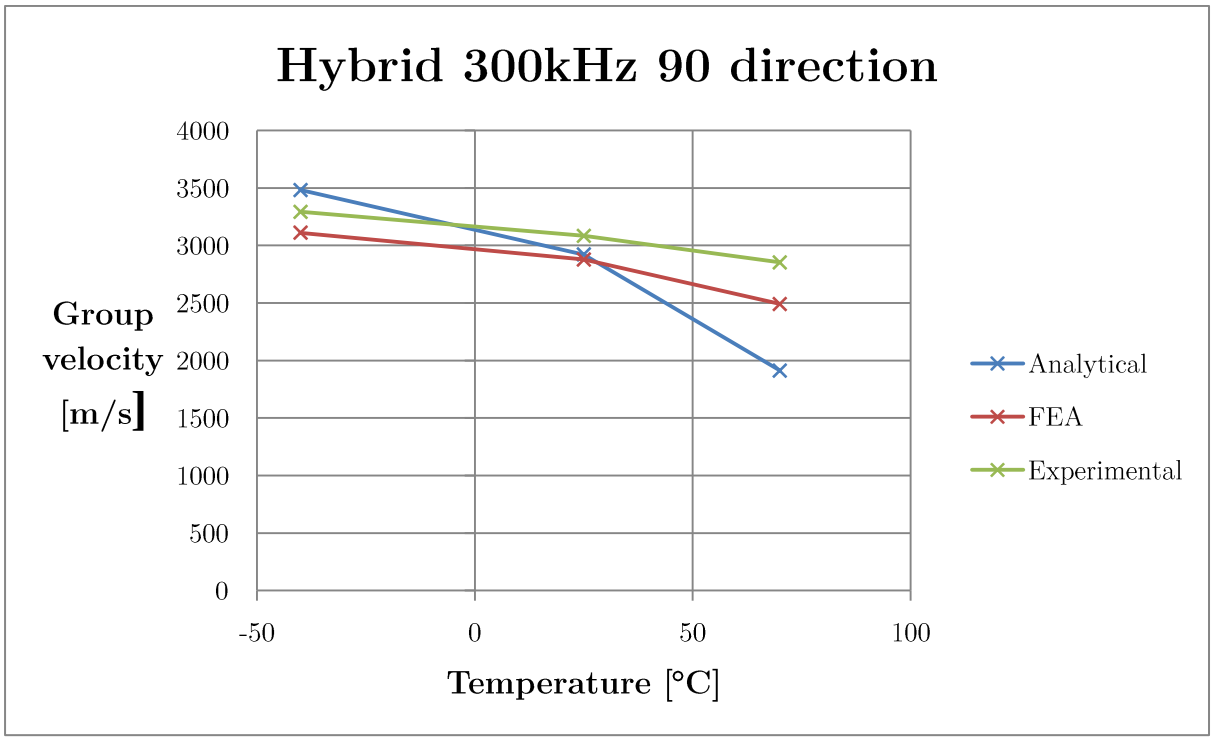

Velocity vs temperature graph for the 300 kHz signal in the 90 direction

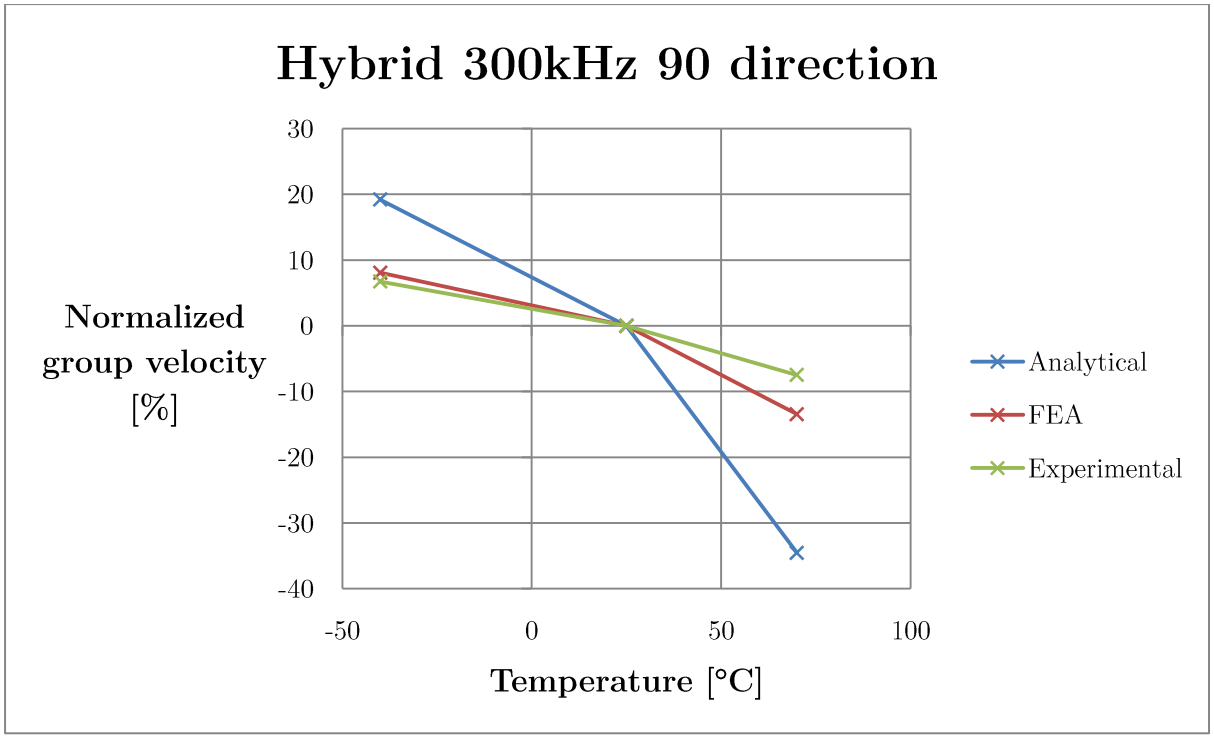

Velocity rate of change for the 300 kHz signal in the 90 direction

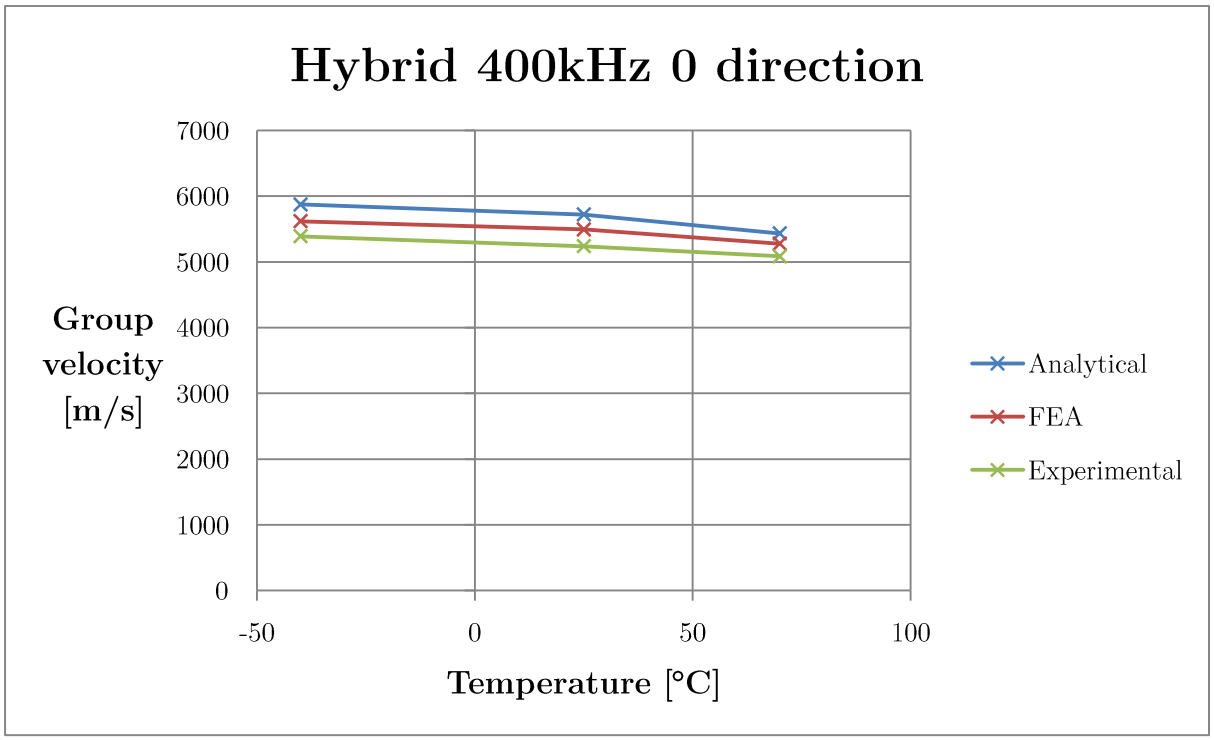

Velocity vs temperature graph for the 400 kHz signal in the 0 direction

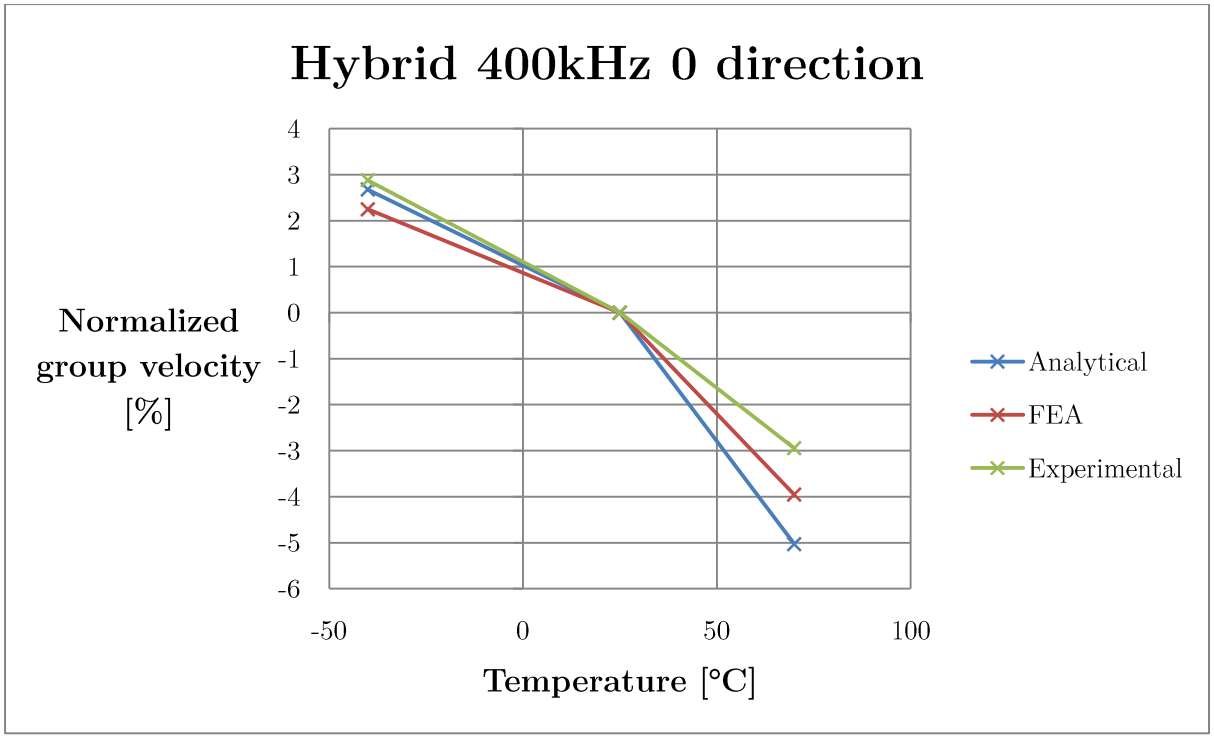

Velocity rate of change for the 400 kHz signal in the 0 direction

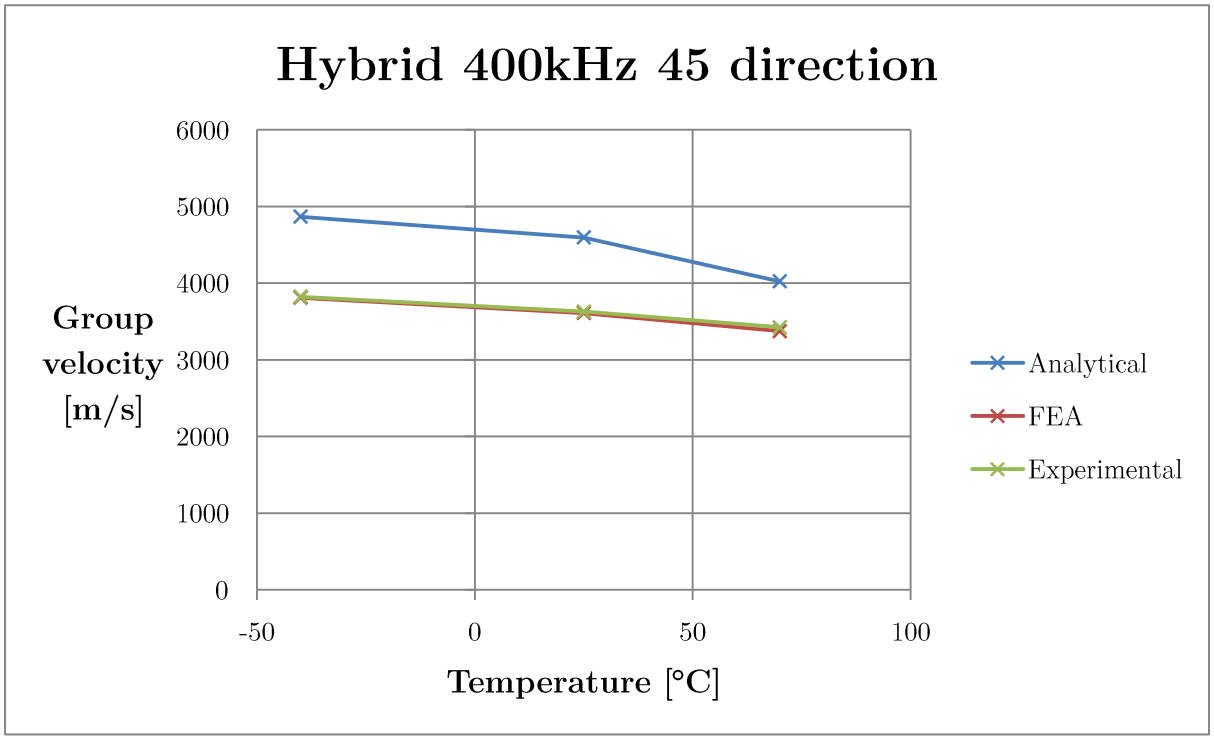

Velocity vs temperature graph for the 400 kHz signal in the 45 direction

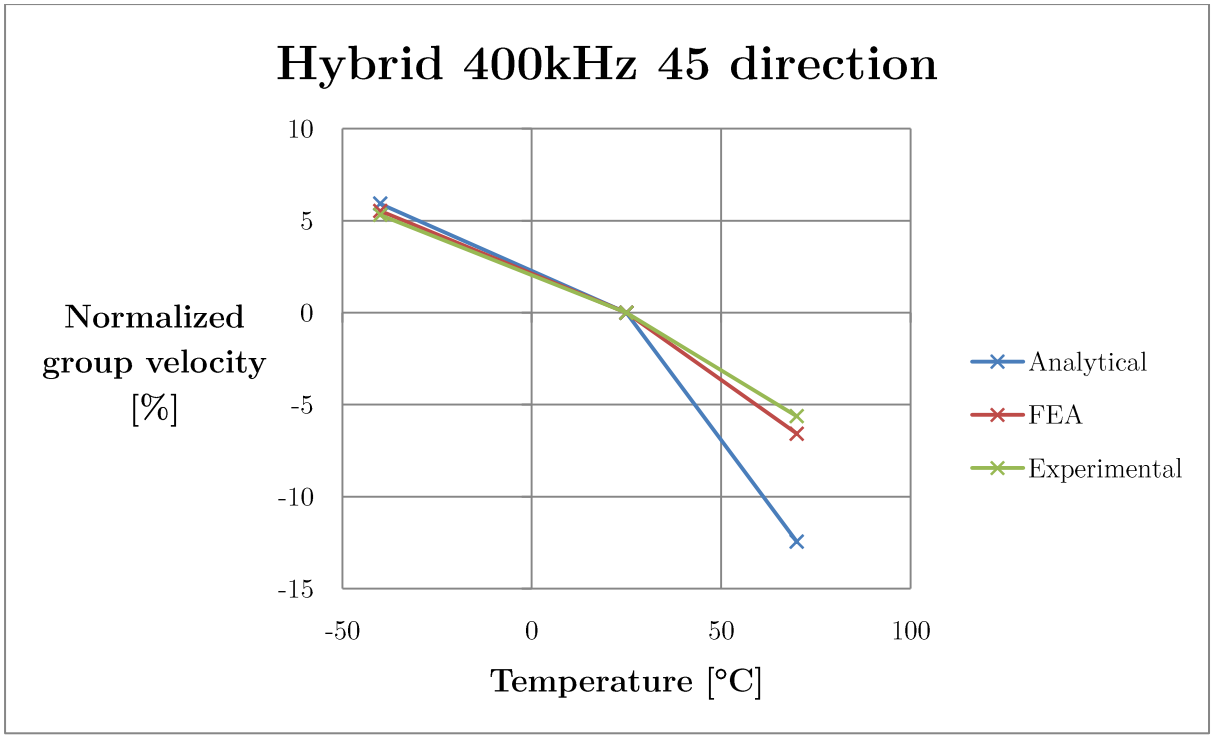

Velocity rate of change for the 400 kHz signal in the 45 direction

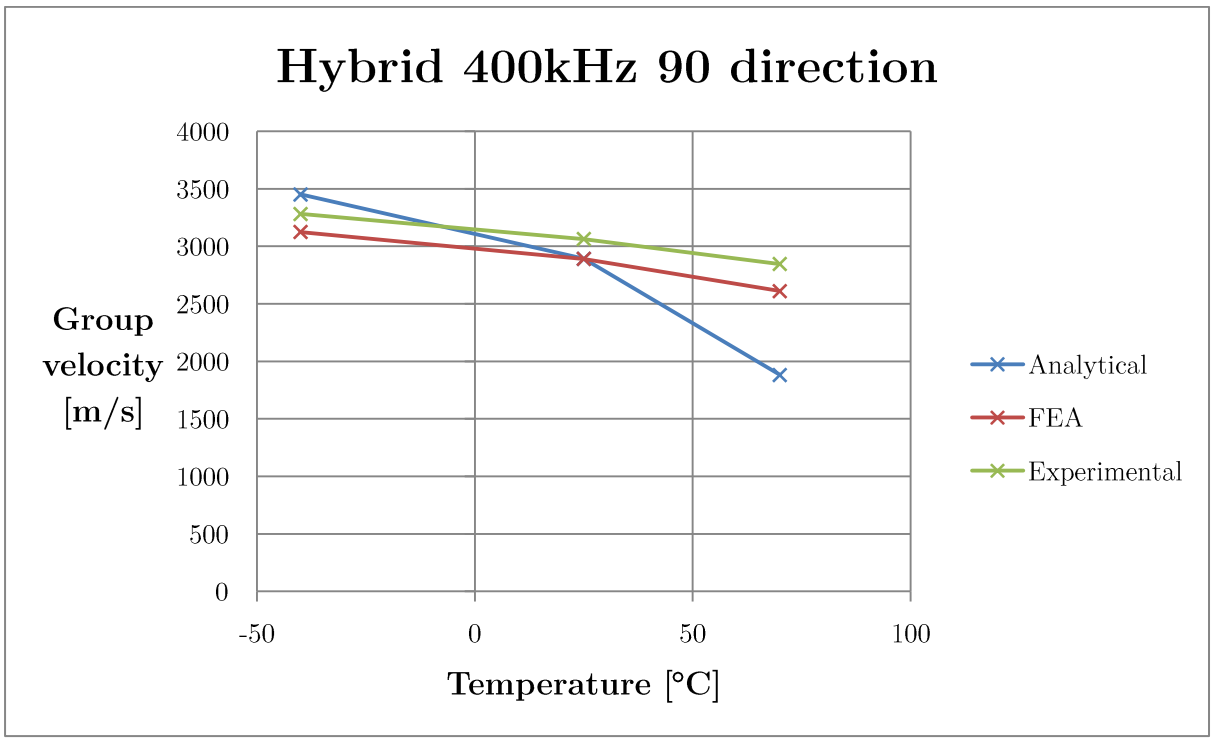

Velocity vs temperature graph for the 400 kHz signal in the 90 direction

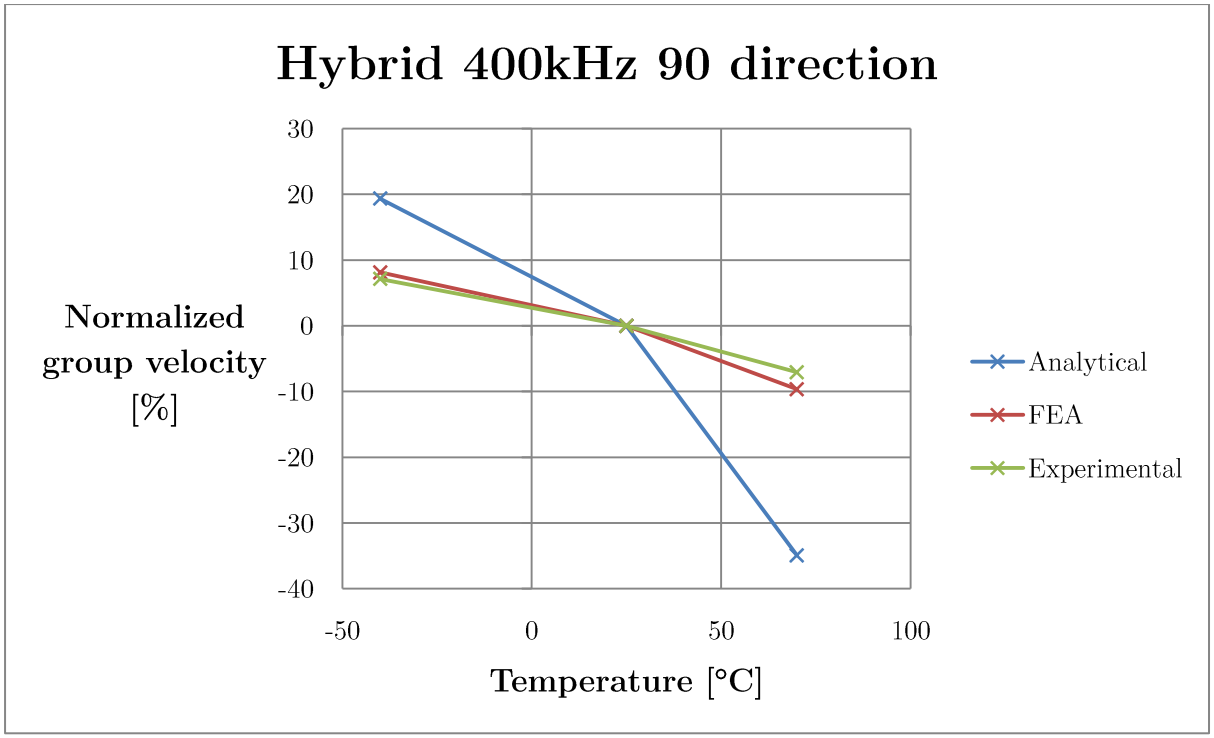

Velocity rate of change for the 400 kHz signal in the 90 direction

Appendix D – Sandwich panel 300 and 400 kHz results

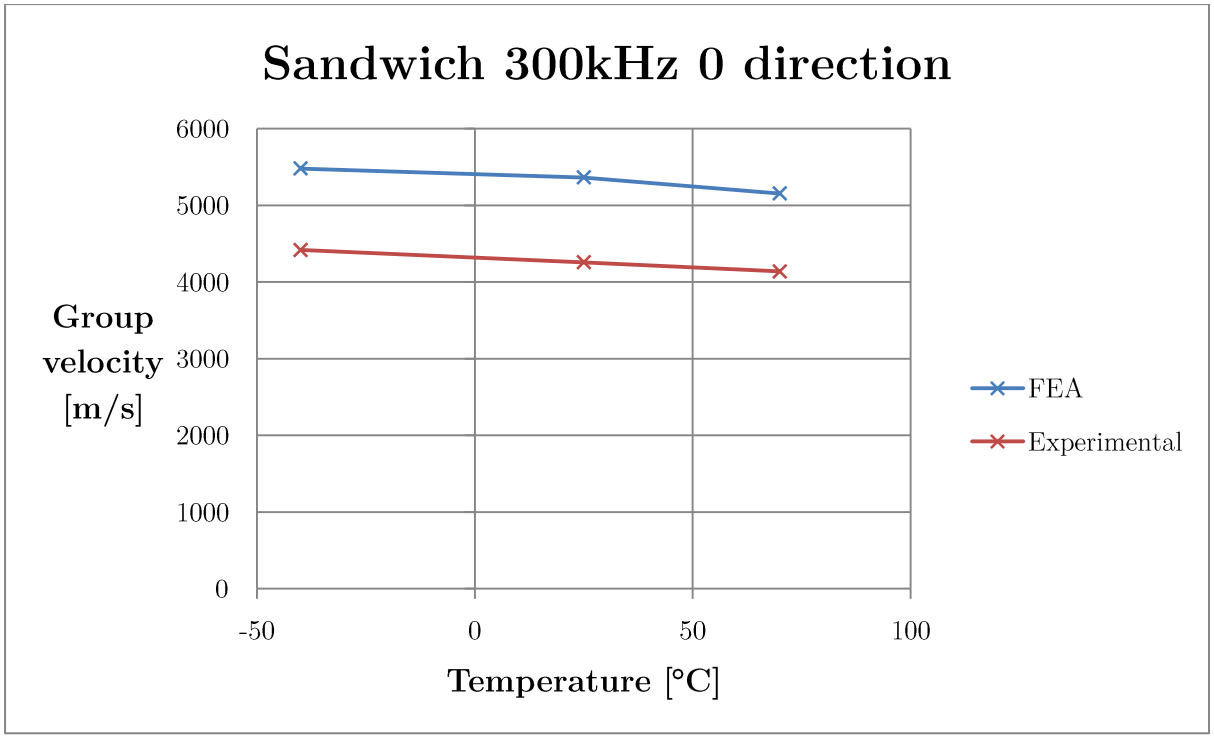

Velocity vs temperature graph for the 300 kHz signal in the 0 direction

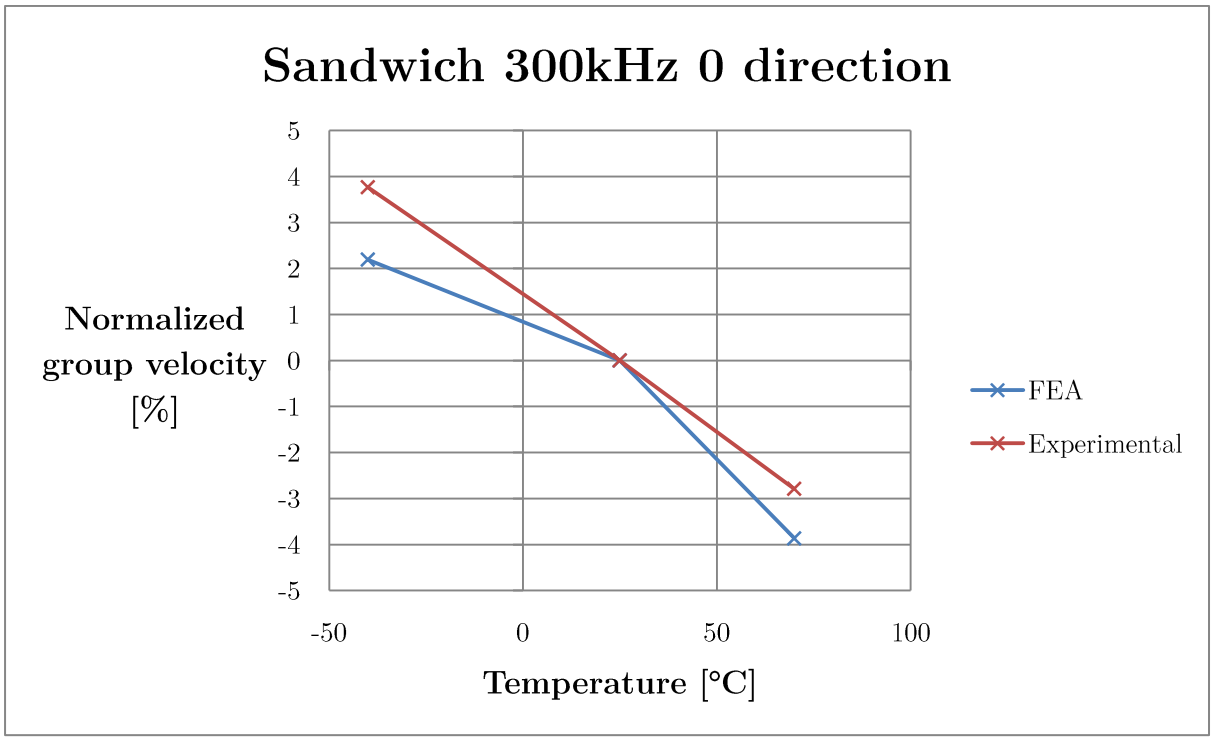

Velocity rate of change for the 300 kHz signal in the 0 direction

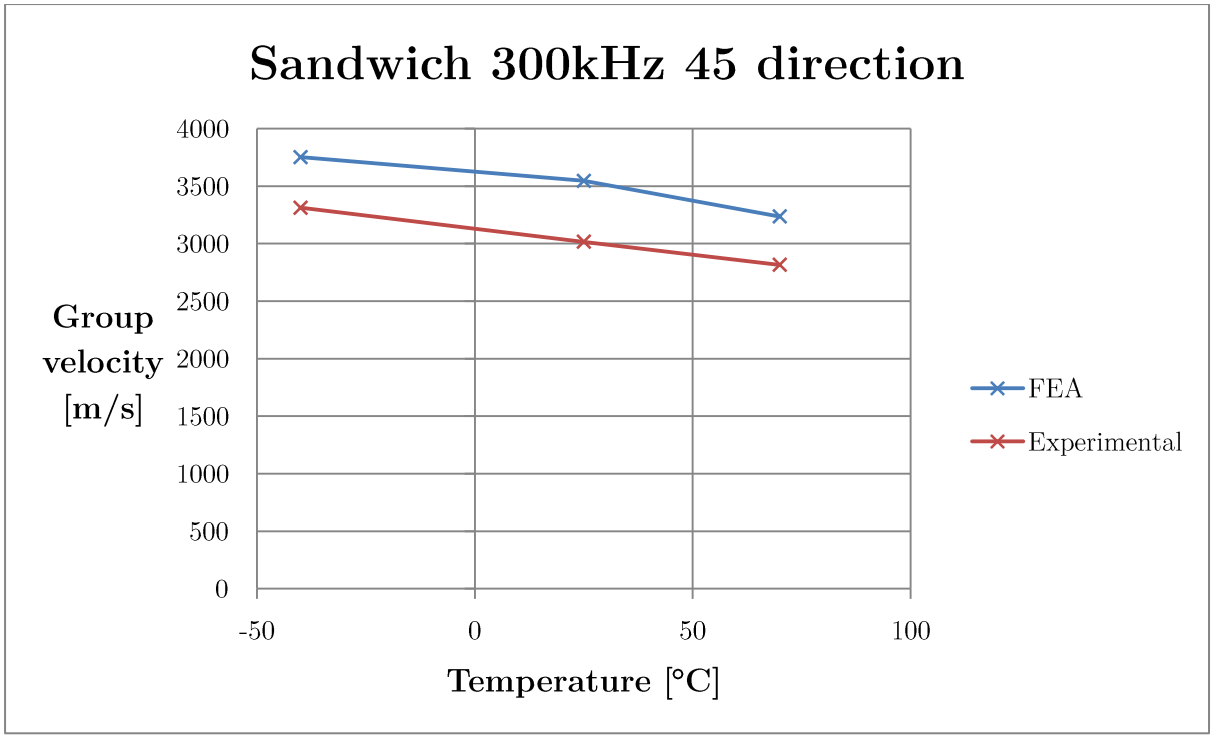

Velocity vs temperature graph for the 300 kHz signal in the 45 direction

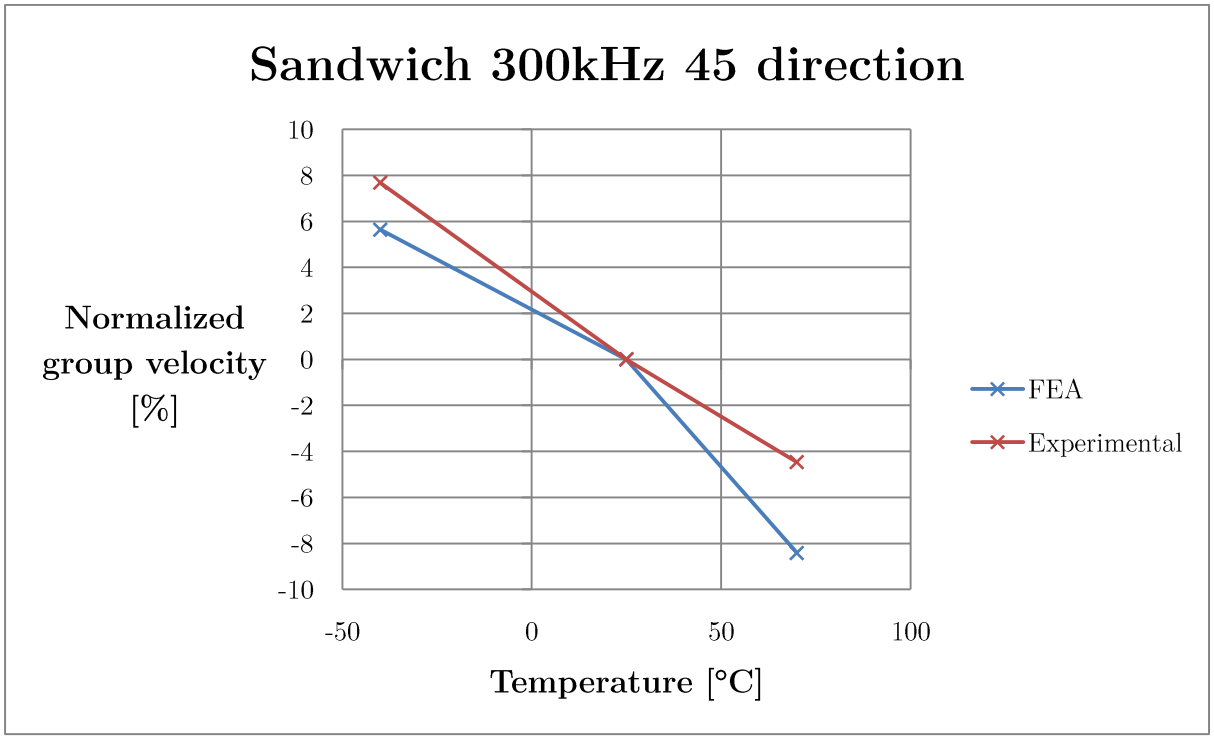

Velocity rate of change for the 300 kHz signal in the 45 direction

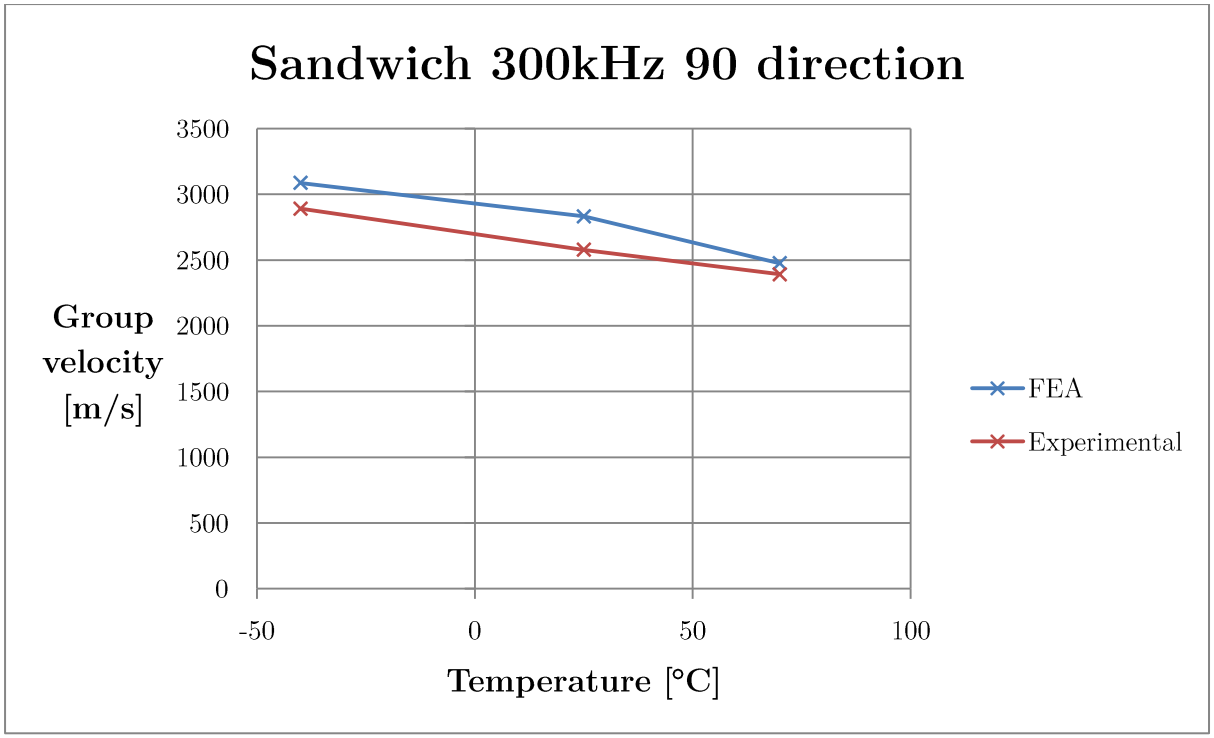

Velocity vs temperature graph for the 300 kHz signal in the 90 direction

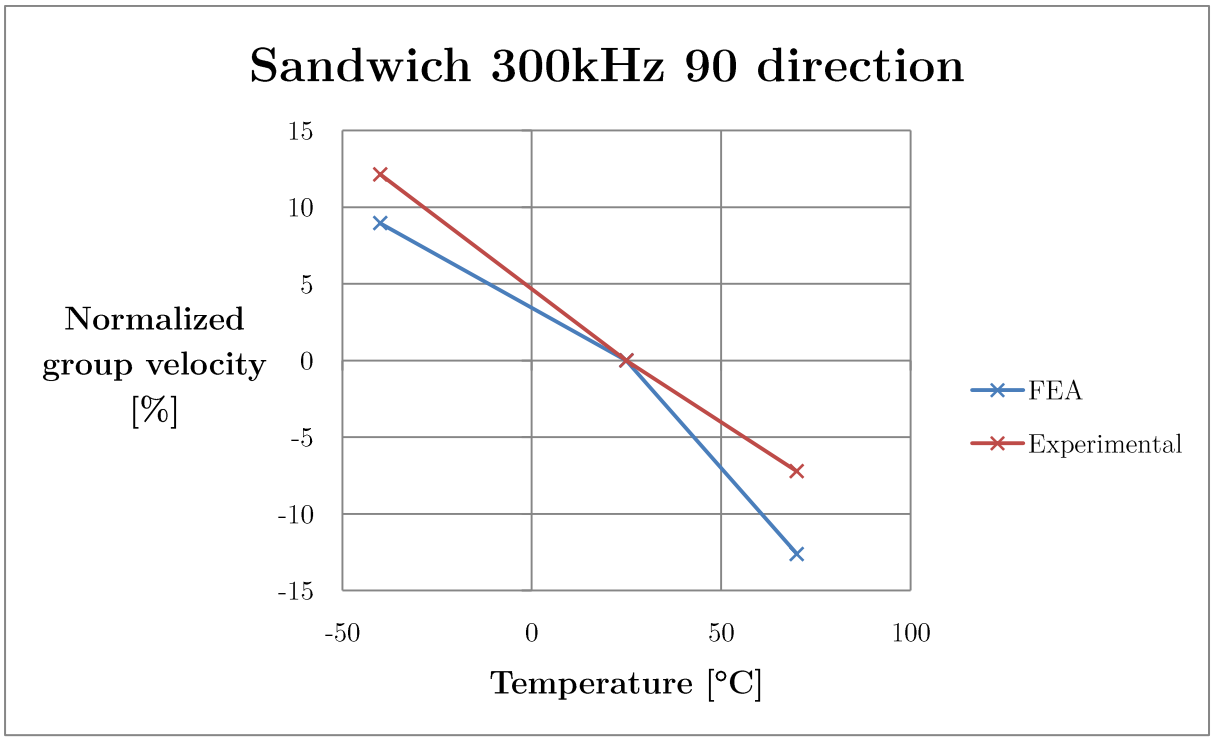

Velocity rate of change for the 300 kHz signal in the 90 direction

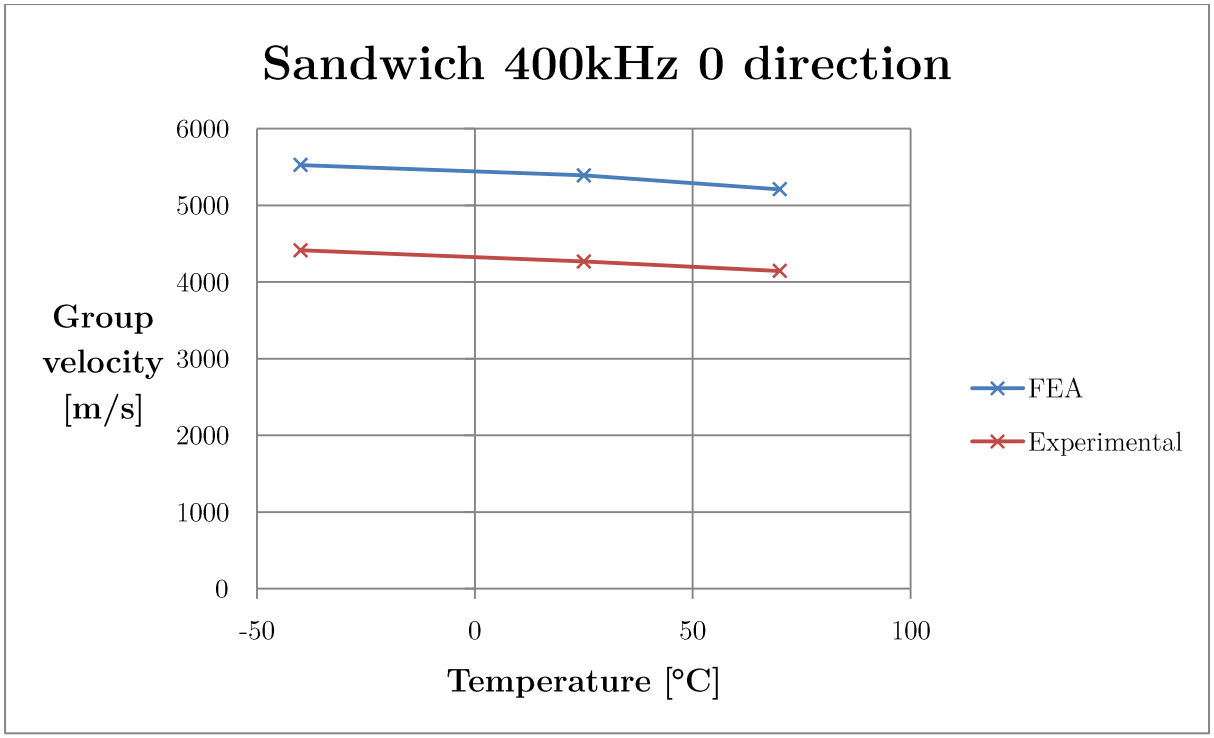

Velocity vs temperature graph for the 400 kHz signal in the 0 direction

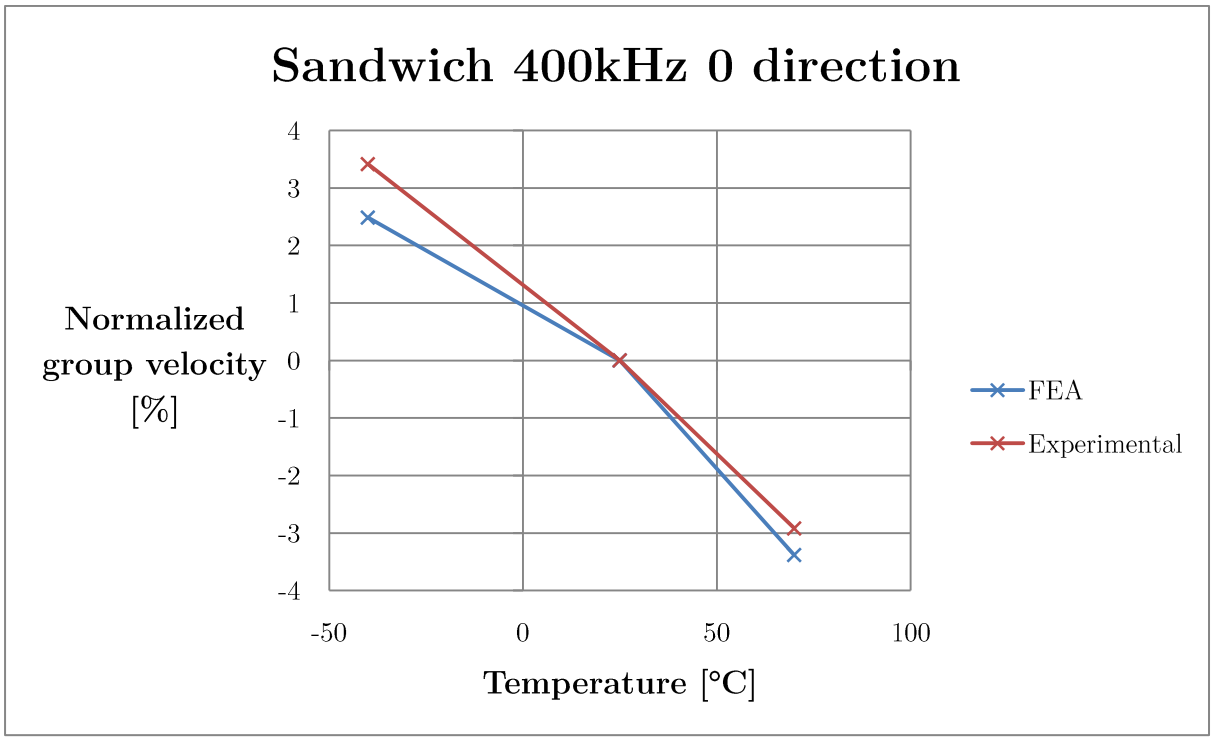

Velocity rate of change for the 400 kHz signal in the 0 direction

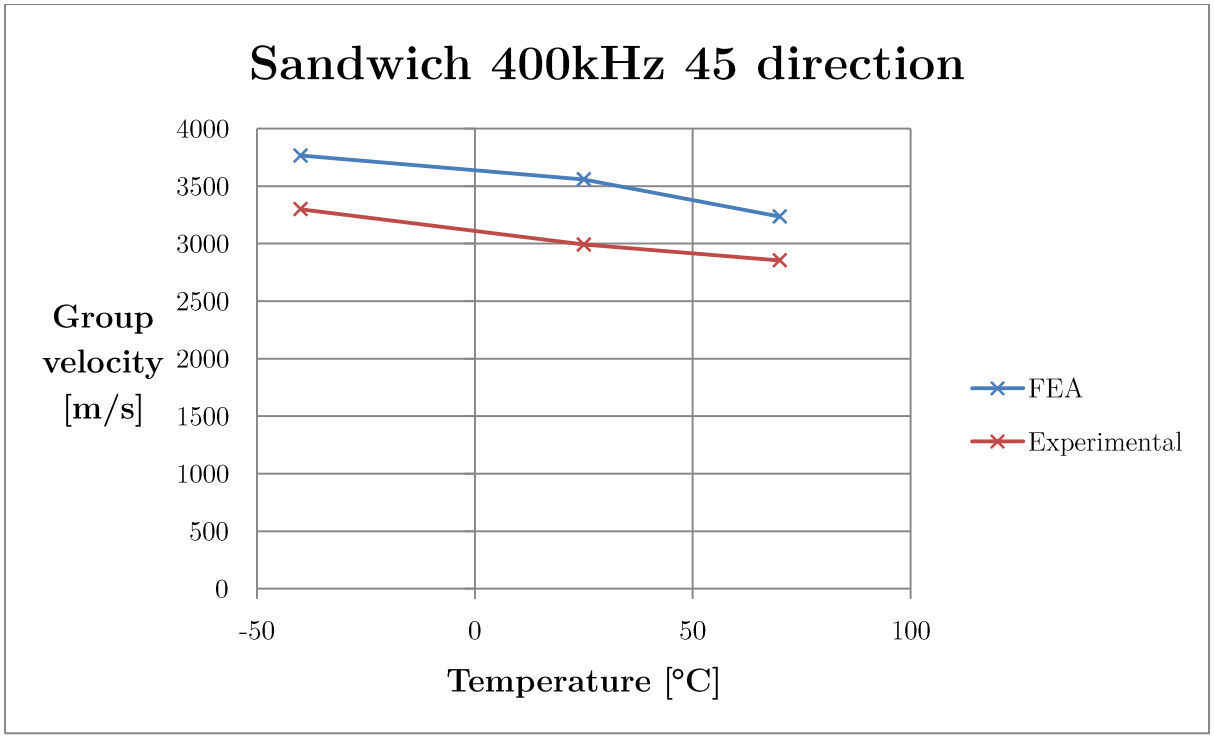

Velocity vs temperature graph for the 400 kHz signal in the 45 direction

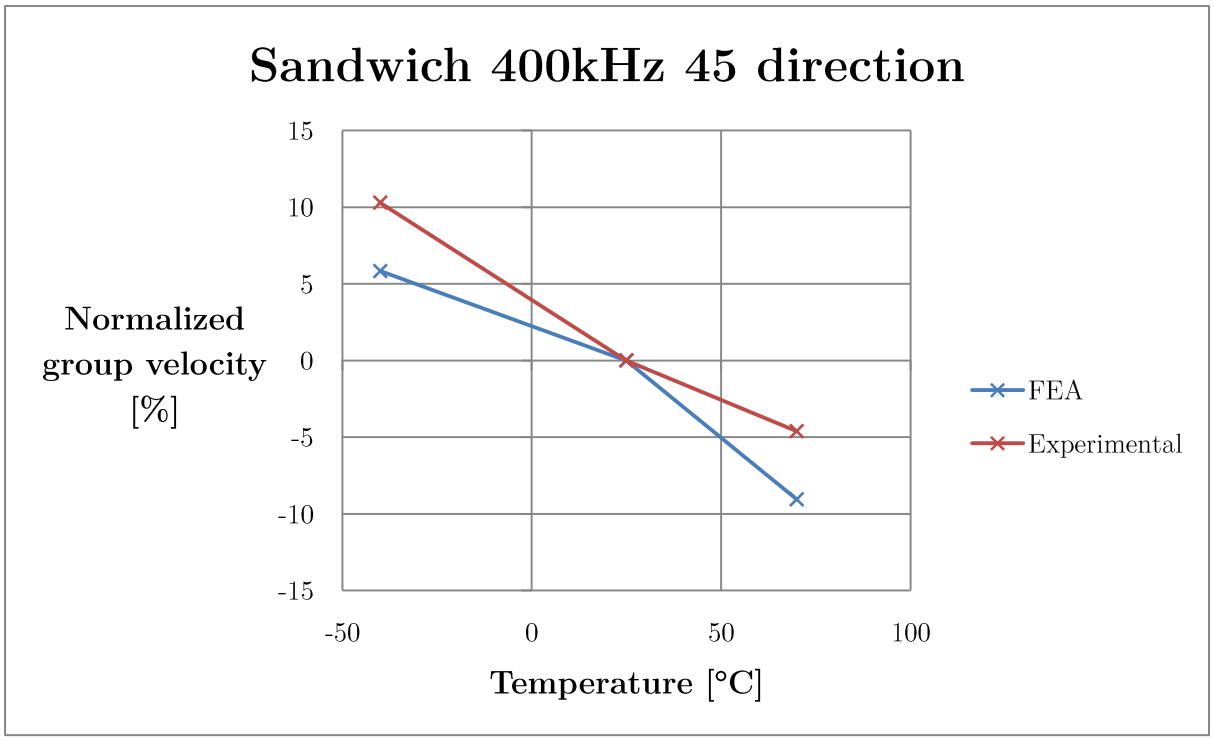

Velocity rate of change for the 400 kHz signal in the 45 direction

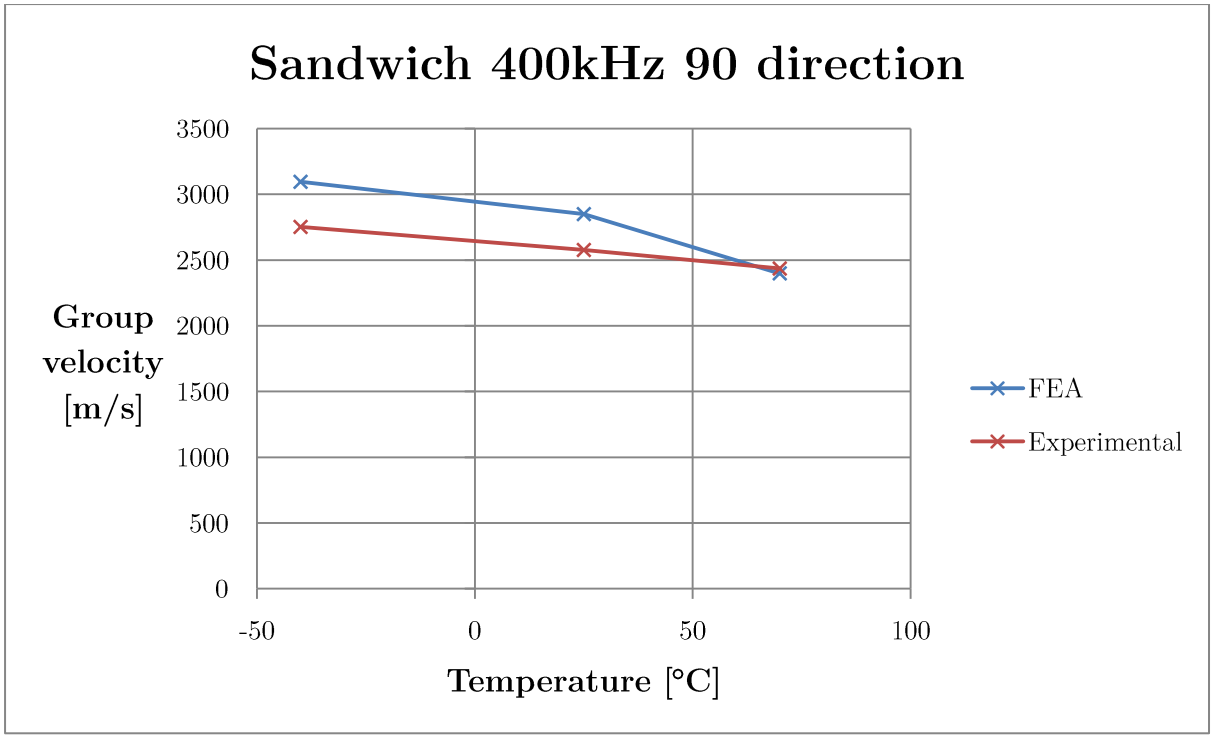

Velocity vs temperature graph for the 400 kHz signal in the 90 direction

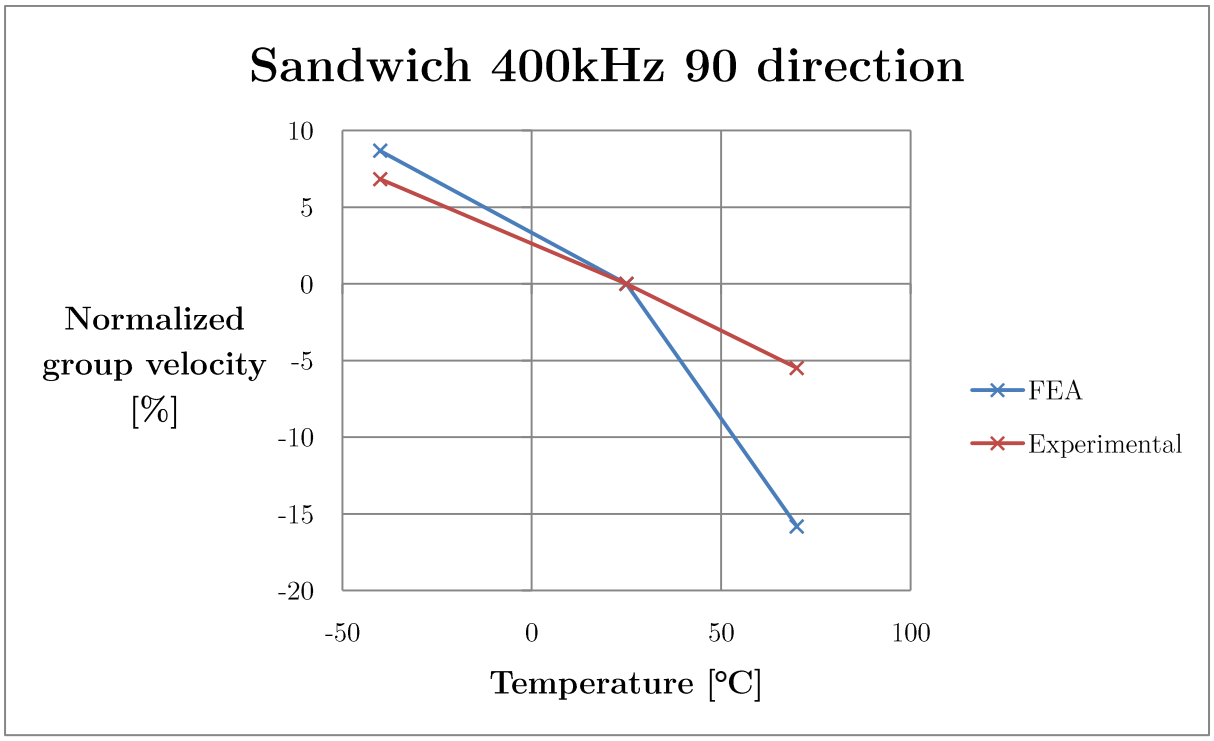

Velocity rate of change for the 400 kHz signal in the 90 direction